INVESTIGATIONS OF MAGNETIC NANOSTRUCTURES FOR PATTERNED MEDIA

MOJTABA RANJBAR
B. Sc. Applied Physics (Hons.), Shiraz University, Iran

A THESIS SUBMITTED FOR THE DEGREE OF
DOCTOR OF PHILOSOPHY

DEPARTMENT OF ELECTRICAL AND COMPUTER ENGINEERING

NATIONAL UNIVERSITY OF SINGAPORE

ADVISORS:
PROFESSOR CHONG TOW CHONG
DR. S. N. PIRAMANAYAGAM
DR. RACHID SBIAA

SINGAPORE INTERNATIONAL AWARD (SINGA)
DATA STORAGE INSTITUTE
AGENCY FOR SCIENCE, TECHNOLOGY AND RESEARCH (A*STAR**)**

August 2012

Declaration

I hereby declare that this thesis is my original work and it has been written by me in its entirely. I have duly acknowledged all the sources of information which have been used in the thesis.

This thesis has also not been submitted for any degree in any university previously.

IN THE NAME OF GOD
THE MOST GRACIOUS, THE MOST MERCIFUL.

DEDICATED TO THE SPIRIT of MY BELOVED BROTHER

"**HAMID REZA RANJBAR**"

(1986-2012)

Acknowledgements

Many thanks to my God, Allah, who has continuously showed me the right way, and facilitated and motivated me to pave the path.

First and foremost I would like to thank and acknowledge Dr. S. N. Piramanayagam (Prem) and Dr. Rachid Sbiaa, who have led me into this wonderful field of nanoscience. Without their guidance, inspiration and encouragement, accomplishment of this thesis would not have been possible. They showed me an excellent example of successful scientists working diligently and smartly along with their charming personality.

I would acknowledge all of the support from Professor Chong Tow Chong, as my primary Ph.D. advisor. I would like to express my sincerest gratitude to Dr. Wong Seng Kai for his support, guidance and help during my experiments.

I owe special thanks to my friends; Mojtaba Rhimabadi, Z.T, Amir Tavakkoli K.G., Taiebeh Tahmasebi, Nikita Gaur, Lisen, Mehdi, Mohammad, Saied, and Mohsen Rahmani for fruitful discussions and all memorable moments we have had together.

I want to thank Dr. Tan Kim Piew who helped me in using Advance Recording Modeling software and shared his experience with this program package.

I wish to thank Dr. Randall Law Yaozhang, Lim Boon Chow, Kay Ywe Seng Anthony, Tan Hang Khume, and Dr. Allen Poh Wei Choong for their valuable and great scientific guidance, for sharing the knowledge in this field or research, for the steady discussion of forthcoming work and for the warm hearted cooperation. I would like to thank my thesis advisory committee members, Professor Yihong Wu and Professor Ding Jun for their useful and constructive technical comments.

Finally, I would like to express gratitude from the A*STAR-SINGA graduate scholarship program for their financial support, DSI and IMRE staff for their help and friendship.

Last but not least, I present the thesis to my beloved family for their endless and unwavering support throughout my life.

Table of Content

Abstract

Continuing increases in areal density of hard disk drives will be limited by transition noise and superparamagnetic effect. The transition noise arises from random zig-zag domain walls between bits in granular media. Alternatively, superparamagnetic limit in which the individual grain and boundary sizes in the magnetic recording medium become small that they are not stable enough in opposition to thermal fluctuation. These conditions are not desirable as the stored data in hard disk drives may be lost in period of a short time frame. To address above problems, bit patterned media (BPM) technology is considered as one of the most promising candidates to enable recording densities above 1 Terabits/inch^2.

In bit patterned media, a periodic array of magnetic bits is defined lithographically on a magnetic substrate. In such scheme, each bit is stored in a single magnetic island, which can help to eliminate transition noise between the bits. However, BPM is not without problem either. Fabrication of 10 nm nanostructures over a large area at a high throughput with cheaper cots is an immense challenge for the manufacturing. Moreover, writability and synchronization of patterned islands are other challenges for recording system. One of the fundamental issues associated with BPM is the element to element variation in intrinsic magnetic properties resulting in the widening of switching field distributions (SFD).

Therefore, the main focus of this dissertation is trying to understand and minimize the SFD of patterned magnetic media and its correlation with different structures. Two approaches such as Antiferromagnetically coupled (AFC) perpendicular configurations and Capped bit patterned media (CBPM) are used to study and minimize the SFD of patterned media.

In the first approach, AFC patterned magnetic medium reduces dipolar interaction without scarifying writability and thermal stability. In order to observe AFC at remanence state after

patterning to reduce the SFD, it is necessary to have a structure where the inter layer exchange coupling field (H_{ex}) is higher than coercivity of thinner layer. Therefore, with this focus in mind, the effect of granularity, different magnetic anisotropy constants such as (CoPt, Co, CoPd, CoCrPt) for stabilizing layer and also effect of low and high exchange coupling fields (15 kOe and less than 1000 Oe) were studied to minimize the SFD.

We showed low exchange AFC field when the Co/Pd multilayers with 10 repeats were antiferromagnetically coupled with $(Co_t/Pd)_3$. The interesting result was the observation of perpendicular magnetic anisotropy for Co/Pd multilayers even when the Co sublayers thickness was 1 nm. In addition, other type of AFC structures were fabricated in which the $(Co/Pd)_{\times 15}$ multilayers were coupled with thin Co layer. A high exchange field (15 kOe) was observed while the Co layer thickness was 0.75 nm. This obtained high exchange coupling in our work (observed for the first time) may shed light on AFC bit patterned media and in magnetic tunnel junction (MTJ) devices with an antiferromagnetically coupled (AFC) free layer.

In the second approach, we study the role of a small exchange coupling between isolated single-domain magnetic dots through a thin continuous film on SFD of patterned media. This design is called capped bit patterned media (CBPM). It was observed that the SFD can be reduced when hard patterned magnetic island is coupled with a thin film layer. CBPM also exhibit writability advantage at higher densities, indicating their potential application as bit-patterned media. In summary, this thesis indicates that both approaches (AFC and CBPM) open a new pathway to reduce SFD of patterned structures by optimizing magnetic layer structures and a proper fabrication technique.

List of Tables

List of Figures

List of Publications

Publications in peer-reviewed journals

1. S. N. Piramanayagam, M. Ranjbar, R. Sbiaa, and T.C. Chong, "Magnetic and First-Order Reversal Curve Investigations of Antiferromagnetically Coupled Nanostructures of Co/Pd Multilayers", to be published in IEEE transaction on Magnetics (2012).

2. A. Tavakkoli K. G., M. Ranjbar, H. K. Tan, Allen Poh W. C., R. Sbiaa, and T. C. Chong, "Reverse Imprint Lithography for Fabrication of Nanostructures", Nanoscience and Nanotechnology Letters **4**, 835(2012).

3. M. Ranjbar, S. N. Piramanayagam, R. Sbiaa, T. C. Chong, and I. Okamoto, "Advanced Magnetic Force Microscopy Tips for High Resolution magnetic imaging", Nanoscience and Nanotechnology Letters, **4,** 628 (2012).

4. M. Ranjbar, S. N. Piramanayagam, R. Sbiaa, T. C. Chong, "Magnetic properties of antidots in conventional and spin-reoriented antiferromagnetically coupled layers", Journal of Applied Physics, **111**, 07B921 (2012).

5. S. N. Piramanayagam, M. Ranjbar, H. K. Tan, Allen Poh W.C., R. Sbiaa, and T. C. Chong, "Magnetic Properties of Antiferromagnetically Coupled Antidots of Co/Pd Multilayers", Journal of Applied Physics, **111**, 07B916 (2012).

6. S. N. Piramanayagam, and M. Ranjbar, "Influence of magnetic viscosity on the first order reversal curves of antiferromagnetically coupled perpendicular recording media", Journal of Applied Physics, **111**, 07B728 (2012).

7. S. N. Piramanayagam, M. Ranjbar, R. Sbiaa, A. Tavakkoli KG, and T. C. Chong, "Characterization of high-density bit patterned media using ultra-high resolution magnetic force microscopy", Journal of Physica status solidi (RRL) - Rapid Research Letters, **6**, 141(2012), **DOI 10.1002/pssr.201105537**.

8. Mohsen Rahmani, Dang Yuan Lei, Vincenzo Giannini, Boris Lukiyanchuk, Mojtaba Ranjbar, Thomas Yun Fook Liew, Minghui Hong, and Stefan A. Maier, " Subgroup Decomposition of Plasmonic Resonances in Hybrid Oligomers: Modeling the Resonance Lineshape", Nano Letters, dx.doi.org/10.1021/nl3003683, (2012).

9. M. Ranjbar, S. N. Piramanayagam, S. K. Wong, R. Sbiaa, and T. C. Chong, "Anomalous Hall effect measurements on capped bit-patterned media", Applied Physics Letters, **99**, 142503 (2011).

10. M. Ranjbar, A. Tavakkoli K.G., S. N. Piramanayagam, K. P. Tan, R. Sbiaa, S. K. Wong, and T. C. Chong, "Magnetostatic interaction effects in switching field distribution of conventional and staggered bit patterned media", J. Phys. D: Appl. Phys. **44**, 265005 (2011).

11. M. Ranjbar, S. N. Piramanayagam, S. K. Wong, R. Sbiaa, W. Song, H. K. Tan, L. Gonzaga, and T. C. Chong, "Origin of anomalously high exchange field in antiferromagnetically coupled magnetic structures: Spin reorientation versus interface anisotropy", Journal of Applied Physics, **110**, 093915 (2011).

12. M. Ranjbar, S. N. Piramanayagam, R. Sbiaa, K. O. Aung, Z. B. Guo, and T. C. Chong, "Ion Beam Modification of Exchange Coupling to Fabricate Patterned Media", Journal of Nanoscience and Nanotechnology, **11**, 2611 (2011).

13. S. N. Piramanayagam, M. Ranjbar, E. L. Tan, R. Sbiaa, and T. C. Chong, " Enhanced Resolution in Magnetic Force Microscopy using Tips with Perpendicular Magnetic Anisotropy", Journal of Applied Physics, **109**, 07E326 (2011).
One of the Highlighted Articles from the Proceedings of the 55th Annual Conference on Magnetism and Magnetic Materials: http://jap.aip.org/about/55th MMM conference.

14. S. N. Piramanayagam, H. K. Tan, M. Ranjbar, S. K. Wong, R. Sbiaa, and T. C. Chong, "Magnetic Interaction in Perpendicular Recording Media with Dual Synthetic Nucleation Layers", Applied Physics Letters, **98**, 152504 (2011).

15. A. Tavakkoli K.G., S. N. Piramanayagam, M. Ranjbar, R. Sbiaa, and T. C. Chong, "A path to achieve Sub-10 nm half-pitch using electron beam lithography", Journal of Vacuum science and technology B, **29**, 011035-1 (2011).
One of the top 20 most downloaded articles in JVSTB:
http://avspublications.org/jvstb/top_20_most_downloaded

16. M. Ranjbar, S. N. Piramanayagam, D. Suzi, K.O. Aung, R. Sbiaa, and T. C. Chong, "Antiferromagnetically Coupled Patterned Media: Potential And Challenges", IEEE transaction on Magnetics, **46**, 1787 (2010).

17. R. Sbiaa, S. J. Wong, M. Ranjbar, S. N. Piramanayagam, and T. C. Chong, "Domain structure and magnetic reversal in (Co/Pd) multilayers with different aspects", Journal of Applied physics, **107**, 103901 (2010).

18. M. H. Farzad, M. Ranjbar, and H. Mazaheri Far, "Nano fiber with a metal clad", Journal of Computational and Theoretical Nanoscience, **7**, 1108 (2010).

Conference Presentations

1. S.N. Piramanayagam, M. Ranjbar, R. Sbiaa and T.C. Chong, "First-order reversal curve analysis of antiferromagnetically coupled Nanostructures of Co/Pd Multilayers", INTERMAG conference, Vancouver, Canada (2012).

2. M. Ranjbar, S. N. Piramanayagam, S. K. Wong, R. Sbiaa, and T. C. Chong, "Reduction of Switching Field Distribution in Bit-Patterned Media", 56th Annual Conference on Magnetism and Magnetic Materials (MMM), Arizona, USA (2011).

3. S. N. Piramanayagam, and M. Ranjbar, "Influence of Magnetic Viscosity on the First Order Reversal Curves of antiferromagnetically Coupled Perpendicular Recording Media", 56th Annual Conference on Magnetism and Magnetic Materials (MMM), Arizona, USA (2011).

4. S. N. Piramanayagam, M. Ranjbar, H. K. Tan, Allen Poh W.C, R. Sbiaa, and T. C. Chong, "Magnetic Properties of Antiferromagnetically Coupled Antidots of Co/Pd Multilayers", 56th Annual Conference on Magnetism and Magnetic Materials (MMM), Arizona, USA (2011).

5. M. Ranjbar, S. K. Wong, R. Sbiaa, S. N. Piramanayagam, H. K. Tan, L. Gonzaga, and T. C. Chong, "Investigation of Spin Reorientation in Complex Multilayer Systems using Anomalous Hall Effect", INTERMAG conference, Taiwan (2011).

6. M. Ranjbar, S. N. Piramanayagam, R. Sbiaa, and T. C. Chong, "Advanced Magnetic Force Microscopy Tips for High Resolution magnetic imaging", International Conference on Materials for Advance Technology (ICMAT), Singapore (2011).
(This paper has won the best poster Award).

7. A. Tavakkoli K. G., M. Ranjbar, H. K. Tan, Allen Poh W. C., R. Sbiaa, and T. C. Chong, "Reverse Imprint Lithography for Fabrication of Nanostructures", International Conference on Materials for Advance Technology (ICMAT), Singapore (2011).

8. M. Ranjbar, S. N. Piramanayagam, S. K. Wong, R. Sbiaa, and T. C. Chong, "Control of Switching Field Distribution of Bit Patterned Media", 2nd Annual poster competition on magnetism for students, Singapore (2011). (This paper has won the best poster Award).

9. M. Ranjbar, S. N. Piramanayagam, R. Sbiaa, and T. C. Chong, "Overcoming resolution limit of high density bit patterned media", 2nd Annual poster competition on magnetism for students, Singapore (2011).

10. M. Ranjbar, A. Tavakkoli K. G., S. N. Piramanayagam, R. Sbiaa, and T. C. Chong, "Influence of Antiferromagnetic Coupling on the switching field distribution of patterned nanostructures", Joint MMM-INTERMAG Conference, Washington, D. C., USA (2010).

11. M. Ranjbar, S. N. Piramanayagam, D. Suzi, K. O. Aung, R. Sbiaa, and T. C. Chong, "Antiferromagnetically Coupled Patterned Media: Potential and Challenges", Joint MMM-INTERMAG Conference, Washington, D. C., USA (2010).

12. S. N. Piramanayagam, E. L. Tan, M. Ranjbar, R. Sbiaa, and T. C. Chong, "Enhanced Resolution in Magnetic Force Microscopy using Tips with Perpendicular Magnetic Anisotropy", 55th Annual Conference on Magnetism and Magnetic Materials (MMM), Atlanta, Georgia, USA (2010).

13. M. Ranjbar, A. Tavakkoli K. G., S. N. Piramanayagam, K. P. Tan, R. Sbiaa, S. K. Wong, and T. C. Chong, "Effect of antiferromagnetically coupling configurations on switching field distribution of bit patterned media", 55th Annual Conference on Magnetism and Magnetic Materials (MMM), Atlanta, Georgia, USA (2010).

14. M. Ranjbar, S. N. Piramanayagam, R. Sbiaa, and T. C. Chong, "First Order Reversal Curves Studies of Perpendicularly Antiferromagnetically coupled ferromagnetic layers", Perpendicular Magnetic Recording Conference (PMRC), Sendai, Japan (2010).

15. M. Ranjbar, S. N. Piramanayagam, R. Sbiaa, K. O. Aung, Z. B. Guo, and T. C. Chong, "Ion Beam Modification of Exchange Coupling to Fabricate Patterned Media", International Conference on Materials for Advance Technology (ICMAT), Singapore (2009).

16. M. Ranjbar, M. H. Farzad, and H. Mazaheri Far, "Nano fiber with a metal clad", Asia Optical Fiber Communication & Optoelectronic Exposition & Conference (AOE-Shanghai), China (2008).

List of Symbols

a	Bit length
a_i	Different cosines of M with respect to crystal axes
β	Stability factor
E_d	Demagnetization Energy
E_{ze}	Zeeman Energy
H_a	Applied field
h_b	Ratio factor
H_r	Reversal field
H_u	Interaction distribution
h	Planck's constant
H_c	Coercivity
H_d	Dipolar field
H_{ex}	Effective surface exchange energy density
H_{ext}	External field
H_{in}	In-plane magnetic field
H_{out}	Out-of-plane magnetic field
H_p	Pinning field
J	Antiferromagnetic interlayer exchange energy
K	Planar-Hall coefficient
K_b	Volume anisotropy energy density
k_B	Boltzmann constant
K_{int}	Interface anisotropy density
K_u	Anisotropy constant
M	Magnetization

μ	Magnetic moments of MFM tip
μ_B	Bohr magneton
m_e	Mass of the electron
m_i	Unit vector of moment
M_r	Remanent magnetization
M_s	Saturation magnetization
N	The shape –dependent demagnetization factor
N	Number of grains per bit
q	Charge of electron
R_H	Ordinary Hall coefficient
R_S	Anomalous Hall coefficient
S	Spin vectors
S*	Coercive squareness
σ_{Ms}	Standard deviations in saturation magnetization
σ_{Hk}	Standard deviations in anisotropy field
t	Layer thickness
T	Absolute temperature
τ	Periodic attempt
δ	Media thickness
ΔH^e	Experimental switching field distribution
ΔH^s	Simulated switching field distribution
θ	Acute angle between the applied field and the easy axis
ϕ	Angle between the positive field direction and the magnetization
V	Volume
z_0	Height above the top surface

List of Abbreviations

AFC	Antiferromagnetically coupled
AFM	Atomic Force Microscopy
AHV	Anomalous Hall voltage
AGM	Alternating gradient magnetometer
AHE	Anomalous Hall effect
APM	Advanced Recording Model
BPM	Bit patterned media
CBPM	Capped bit patterned media
CGC	Coupled granular/continuous
D.C	Direct current
DCD	Direct current demagnetization
DTM	Discrete track recording media
EBL	E-beam lithography
EBR-9	Acrylate based resist
FIB	Focus ion beam
FORC	First order reversal curve
FWHM	Full-width at half-maximum
HAMR	Heat assisted magnetic recording
hcp	Hexagonal-closed-packed
HDD	Hard Disk Drive
HE	Hall effect
HSQ:XR-541	Hydrogen silsesquioxane
IBM	International business machine

kfci	Kilo-flux cycles per inch
ktpi	Kilo-tracks per inch
LMR	Longitudinal magnetic recording
LTEM	Lorentz transmission electron microscopy
MFM	Magnetic force microscopy
MIBK	Methyl isobutyl ketone
MR	Magnetoresistance controller
MRFM	Magnetic resonance force microscopy
NIL	Nano imprint lithography
nm	Nanometer
PBS	Poly butene-1-sulphone
PHV	Planar Hall voltage
PMA	Perpendicular magnetic anisotropy
PMMA	Poly methyl methacrylate
PMR	Perpendicular magnetic recording technology
RAMAC	Random Access Methods of Accounting Control
RKKY	Ruderman-Kittel-Kasuya-Yosida
RL	Recording layer
SEM	Scanning electron microscopy
SEMPA	Scanning electron microscopy with polarization analysis
SFD	Switching field distributions
S-FIL	Step-and-flash imprint lithography
SL	Stabilizing layer
SNR	Signal to noise ratio
SPLEEM	Spin-polarized low-energy electron microscopy

SQUID	Superconducting quantum interference device
STXM	Scanning transmission X-ray microscopy
SUL	Soft under layer
Tbpsi	Terabits per square inch
TMAH	Tetramethylammonium hydroxide
VSM	Vibrating Sample Magnetometer
XRD	X-ray diffractometer
ZEP	A copolymer of α -chloromethacrylate and α -methylstyrene

Chapter 1. Introduction

Magnetic recording technology, in the form of hard disk drives, has completed more than five decades of their presence. This technology has dominated over other competing technologies because of the possibility of large capacity storage at cheaper costs. It has maintained its competitive edge by scaling aggressively and overcoming the challenges by constantly innovating. As far as the read sensors are concerned, the technology has made significant technological migrations when moving from inductive heads to thin film heads, thin film heads to magnetoresistive (MR) heads, and later to giant magnetoresistive (GMR) and tunnelling magnetoresistance (TMR) heads. In the case of recording media, the starting point was a humble spray-paint of ferrite particles. Later, the media technology used thin films and granular films for longitudinal recording. The advent of perpendicular recording technology saw the use of granular films with several layers including soft magnetic underlayers. In order to extend the magnetic recording technology, alternatives such as heat-assisted magnetic recording (HAMR) and bit-patterned media are considered.

This chapter provides an overview of the principles and basic scheme of conventional recording technologies and addresses the issues in extending the areal density. Moreover, patterned media technology with its associated challenges is discussed as an advanced technology for ultrahigh density magnetic data storage. A detailed discussion is presented on switching field distribution in patterned media. In the last part of this chapter the scope, motivation and organization of thesis are addressed.

1.1 History of magnetic recording technology

Magnetic recording technology was invented 100 years ago. From tape recording to disk drives, the magnetic recording technology has come a long way. They have become an indispensable tool especially in electrical equipment such as personal computers, laptops, and MP3 players. They have also played a crucial role in development of data storage systems. Hard Disk Drive (HDD) currently is the key part of data storage industry, and this role is continually increasing due to decreasing price per gigabyte, improved performance and storage capacity. After the invention of the original Random Access Methods of Accounting Control (RAMAC) as first hard disk drive by International business machine (IBM) in 1956, a variation of scaling laws have been used to increase the areal density of HDD [1-5].

The tremendous growth of the data storage industry and storage capacities have been made possible by the increase in areal density due to the scaling down of head and media dimensions, as well as the flying height. This downward scaling is possible because of the improvement in performance of the read and write heads, media, electronics, signal processing and mechanical design. The conventional magnetic recording technologies can be categorized in to perpendicular and longitudinal recording system. The recording technology, based on in-plane magnetization (longitudinal recording) was dominant for about five decades. Perpendicular magnetic recording technology (PMR) has been proposed in the late of 1970s as an alternative to longitudinal recording [6, 6].

However, it took more than three decades to utilize the PMR commercially in hard disk drives. It is because the industries did not want to invest the time, money, equipment for a new technology which needed a lot of optimizations. Until recently, longitudinal magnetic recording (LMR) well satisfied the demands of recording areal density increasing in HDD [6, 7].

1.2 Principle of magnetic recording

Magnetic recording is based on two simple principles. First, magnets produce a magnetic field at the poles and this field is used for reading information. Second, the polarity of the magnets in the recording can be changed by applying external fields. This is generated by electromagnets by changing the direction of current in the coil, which provides a possibility of writing information. Basically, magnetic recording technology can be divided into categories such as longitudinal and perpendicular recording technologies [4-6].

1.2.1 Longitudinal recording

In longitudinal recording, where the magnetization of the bits are in the direction parallel to the media, the demagnetizing field from one bit opposes the magnetization direction of the next bit. This affects the sharpness of the transition negatively and consequentially, the maximum possible recording density [4, 5]. A schematic of longitudinal recording is shown in figure 1.1. It can be seen that a particular section of the media is magnetized by the fringing field from the recording head (inductive head) as the head passes through the media. The magnetization will either be pointing in the positive or negative longitudinal direction, creating either a transition or no transition between two bits. The presence or absence of the transition is used to determine whether the written bit is zero or one.

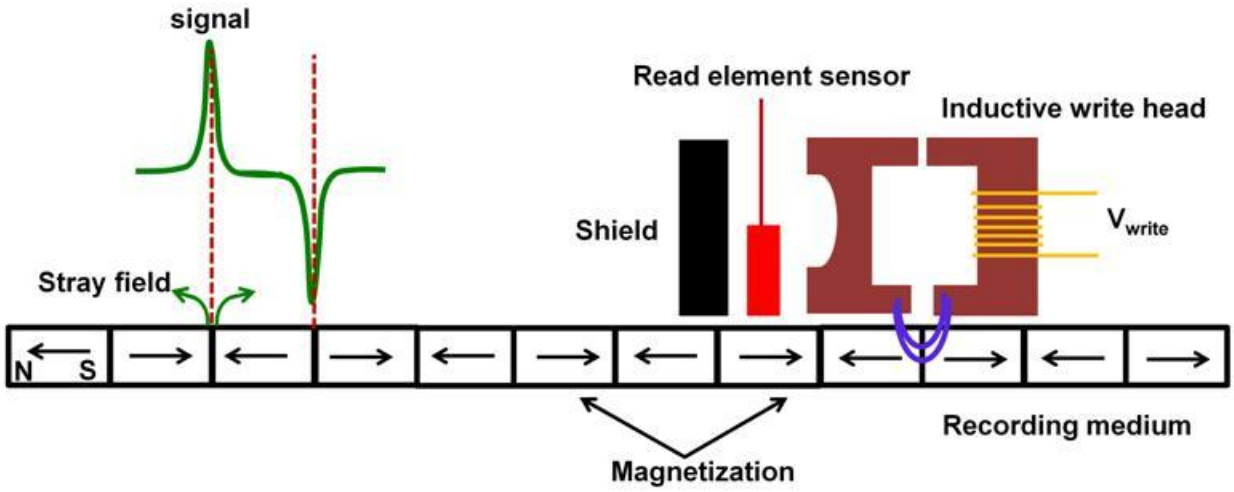

Figure 1.1. Recording a bit in longitudinal recording and Transition between two opposing magnetization.

For reading, the read head (MR Head) will pass over the medium and measure the flux emerging from the medium and the resultant voltage is compared. Where there is a transition during a read-window, the flux emitted will be large and the bit will be registered as a "1". In cases where there is no transition during a read window, a "0" will be registered. In conventional longitudinal recording, media thickness is limited by transition noise, which increases the transition parameter, and the effective head-media spacing, which lowers the writing field and writing field gradient in the media. Also, a bit boundary in longitudinal recording forms a charged domain wall, which generates strong destabilising fields that widen transitions, a problem that increases with areal density.

1.2.2 Perpendicular recording

Perpendicular magnetic recording (PMR) has been proposed to increase areal density of data storage [6] as an alternative to longitudinal recording. While the recording principle may differ slightly from that of the conventional longitudinal recording, switching to perpendicular recording required modification of almost all components of the drive design, including the head and the detection channel. For perpendicular recording, the easy axis of

magnetization is perpendicular to film plane as shown in figure 1.2. The recording layer is deposited on a soft under layer (SUL), which helps to guide the flux from the write pole to the collector pole. The SUL can be thought to be acting as a mirror image of write pole such that the medium is effectively inside the 'gap' of the write head. This results in a writing field that is nearly doubled

The hassle of making the transition to perpendicular recording as well as the success gained in optimizing the performance of longitudinal recording resulted in the delay of perpendicular recording in commercial products.

Figure 1.3 shows the schematic illustration of three important layers for PMR media, respectively. It can be seen that a magnetic recording layer (RL), a soft magnetic under layer, and intermediate layer are essential layers for PMR technology. Co-based granular media with oxide-rich grain boundaries have been used widely for recording layer. The intermediate layer has an essential role to control the structure of recording layer.

In order to sustain the continuous growth in areal density, the grain size of PMR media must be reduced. Recently, several approaches have been studied to reduce the grain size with controlling sputtering conditions, the amount of oxide in magnetic layer and engineering the intermediate layer under recording layer [7-15].

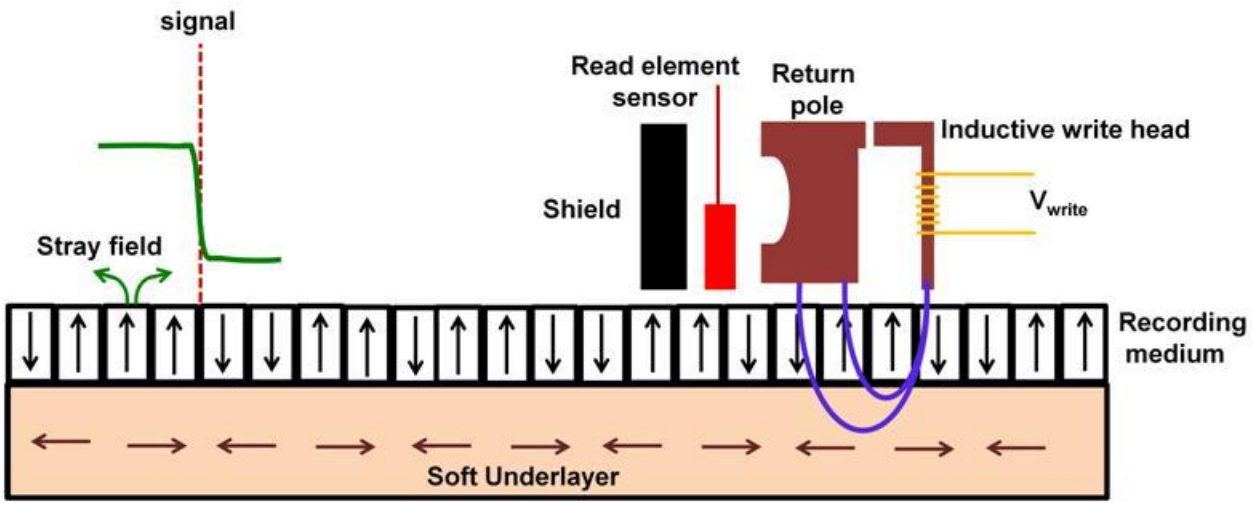

Figure 1.2. Orientation of the magnetic moment of bits in perpendicular recording media.

In chapter 4, the effects of granularities were employed to induce superparamagnetic state in stabilizing layer in contrast with advantages of granularity effect in perpendicular magnetic recording.

The use of perpendicular recording has several advantages over the traditional longitudinal recording. Firstly, higher writing field can be used in perpendicular recording. This is due to the single pole head working in conjunction with the SUL. The writing field is effectively doubled hence allowing grains of higher anisotropy to be used ensuring higher thermal stability.

Secondly, perpendicular media are strongly oriented, resulting in less DC noise and hence a sharper recorded transition. The highly oriented grains are due to its natural anisotropy perpendicular to the film plane direction.

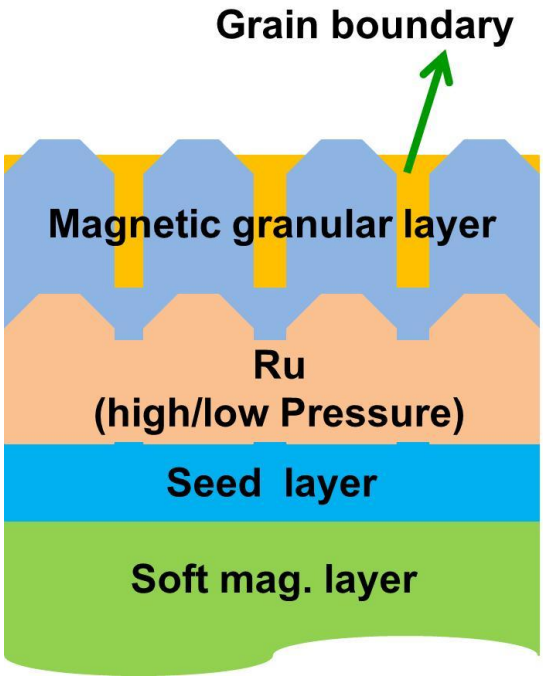

Figure 1.3. The illustration of schematic perpendicular media structure.

Lastly, demagnetization field is small at transition. Narrow transition (smaller transition length) can be written and this improves thermal stability of high-density data pattern. Non-linear transition shift in the perpendicular medium are less critical, compared to longitudinal recording [16].

1.3 Magnetic recording media trilemma and superparamagnetic effect

The increase in the areal density of hard disk drives will be limited by the trilemma (thermal stability vs. writability and signal to noise ratio (SNR)) of granular thin film media used in current magnetic recording technology as shown in figure 1.4 [17].

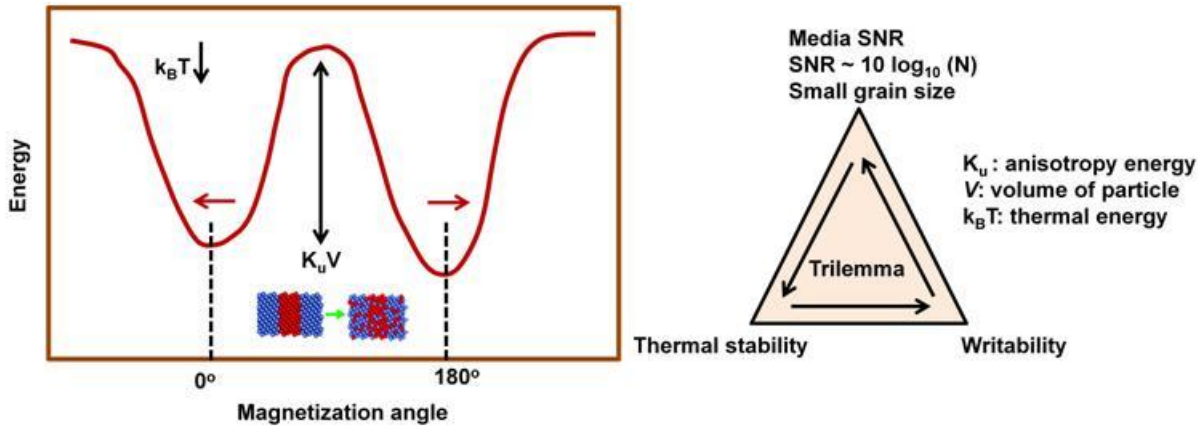

Figure 1.4. Trilemma of granular media.

It can be seen that, to achieve high signal to noise ratio for higher areal density which is relating to number of grains per bit (N), there is a need to increase number of grain per bits. So, grain size should be decreased. However, by decreasing size of grain and its volume (V) and it can reduce the thermal stability of grains. The thermal stability factor is measured with Arhennius equation. The Arhennius equation (Equation 1.1) relates to the time it takes for decay in magnetization in a magnetic media.

$$\tau = \tau_0 \exp\left(\frac{K_u V}{k_B T}\right) \quad (1.1)$$

τ_0 is the periodic attempt for magnetic reversal which has a value of about 10^{-9} s. V is the volume of the particle under consideration. T is the absolute temperature in Kelvin and K_u is anisotropy constant. k_B is the Boltman constant, 1.38× 10^{-23} J/K. From research done so far regarding magnetic media, it has been stated that the value of $\frac{K_u V}{k_B T}$ which refers to the stability factor must be in the range of 40 to 60 for a single bit to remain stable for a period of 10 years.

If the value of the stability factor is too low, τ in equation 1.1 will be very low, indicating a reversal time of the bit to be very fast. This would mean that the bit will lose its

magnetization very fast and superparamagnetic effect becomes a major problem. It means that without applying external magnetic field the magnetization direction will fluctuate and it can result in a loss of data. Naturally, a very high stability factor is desirable because it would make the decay time to be very long and hence enabling archival ability for the information stored. Nevertheless, there is also a limitation as to how high the stability factor should be. A stability factor too high will affect writability of the media because the head field might not be strong enough to be able to magnetize the grains [18-20]. Therefore, it is necessary to consider novel technologies to delay superparamagnetic effect. Nowadays, there are two important technologies for this objective such as Energy assisted recording [21, 22], and patterned media. Heat assisted recording has the potential to circumvent the superparamagnetic limit by making use of high anisotropy materials. Bit patterned media is another technology that has been studied as one of the most promising candidates for extending the recording density with sustained stability. [19-21]

1.4 Bit-patterned Media (BPM)

A patterned recording medium consist of periodic arrays of magnetic elements, as shown in figure 1.5, where each element has a uniaxial magnetic anisotropy and will store one bit [18-20]. The easy axis could be either parallel or perpendicular to the substrate, although the latter is more common in today's research. Unlike the thin film media, grain within each patterned media element are preferred to be strongly coupled so that the entire element can behave as a single magnetic domain.

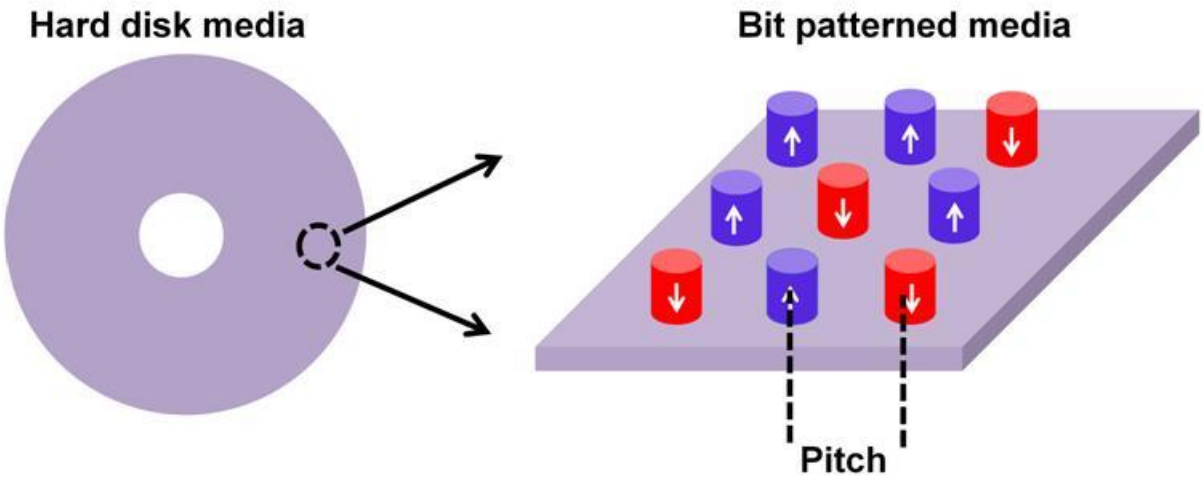

Figure 1.5. An illustration of bit patterned media.

Shew *et al.* in 1963 recognized the advantages of patterning recording media. They illustrated that discrete patterned tracks on a hard disk platter could reduce the cross-talk and noise problems associated with head positioning errors and allow increased tracking tolerances [23]. Lambert *et al*, have used patterned magnetic films to explore narrow track recording [24]. It was shown that patterned magnetic medium can be used to provide feedback information to a head servomotor.

The first studies of regular islands of sub-micron patterned magnetic islands were presented in a series of papers by Smyth et al. [25]. The group studied the collective switching properties of lithographically defined permalloy (NiFe) islands, and compared their results with micro-magnetic calculations.

1.4.1 Advantages of bit patterned medium

Patterned media scheme has several advantages. First, it is desirable to avoid grain boundaries within the magnetic element. It means that the transition noise is eliminated because the bits are now defined by the physical location of the elements and not by the boundary between two oppositely magnetized (but physically in contact) regions of a thin film media. Second, very high data densities can be achieved because the thermal stability

criterion now refers to the volume and anisotropy of the entire magnetic element, not to the individual grains comprising the conventional granular media. In addition, the grain size can be as large as the isolated element, which is around 10 nm for Tbit/in^2.

1.4.2 Bit patterned media Challenges

Figure 1.6 shows the major challenges for patterned media. They have to be optimized in which this technology becomes commercialized.

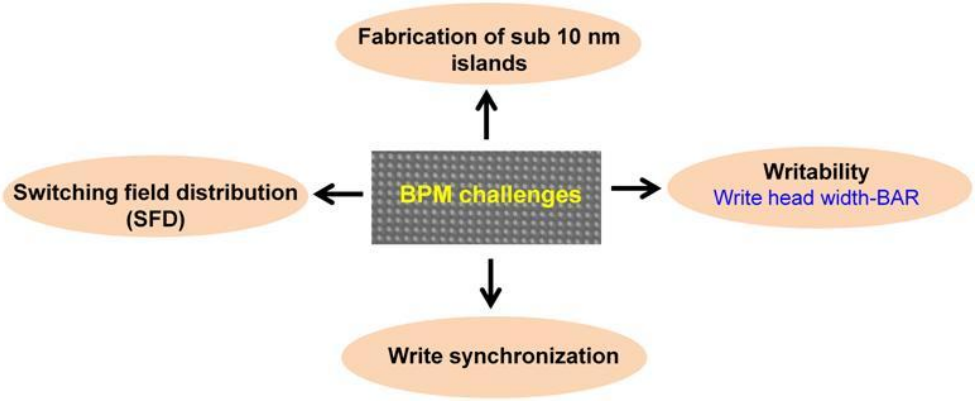

Figure 1.6. Obstacles of Bit patterned media (BPM).

One of the challenges in patterned media recording is the manufacturing of the sub 10 nm patterned media. Fabrication procedures such as electron beam lithography, ion beam lithography, immersion lithography, and nanoimprinting [26-31] have been investigated for high-resolution patterned media. Yang et al. fabricated bit-patterned media using high-resolution electron beam lithography followed by the deposition of a magnetic film in order to avoid resolution degradation due to etching or lift off. They have demonstrated a 5.1 Gb/mm² (3.3 Tb/in²) areal density [32]. In addition to the difficulties of disk fabrication, writing must be synchronized so that the write field is coincident with the location of patterned bits. This adds huge challenges to the development of patterned media technology [32].

For patterned media to be viable, the information must be read at a higher data density level than that of conventional hard drive. The higher data density is completely determined by fabrication resolution. As it is shown in table 1.1 to achieve 1, 4 and 10 Tbit/in^2 recording density, the center to center spacing (pitch) has to be 25, 12.5 and 8 nm respectively. This limit is well beyond the conventional optical lithography. Moreover, another limitation of BPM is the difficulty of realizing a low-cost and high-throughput fabrication process. However, improvement in resolving this problem will result in the realization of bit-patterned media (BPM) in the near future.

Table 1. 1. Pitch (center to center) and bit area requirements for different areal densities. The BAR is defined as the track pitch/bit pitch [33].

Density (Gb/in^2)	Bit area (nm^2)	Center-to-center distance (nm). Along track (BAR=1)	Center-to-center distance (nm). Along track (BAR=4)
500	1290	35.9	18
750	860	29.3	14.7
1000	625	25.4	12.7
2500	258	16.1	8
5000	129	11.4	5.7
10000	64.5	8	4

Another fundamental issue associated with patterned media is the element to element variation in intrinsic magnetic properties resulting in the widening of switching field distribution (SFD) [19-21, 34, 35] as shown in figure 1.7, which will cause an increase in write-in-error. The write-in-errors occurs when the information cannot be written at all or the writing cannot be performed in the time window necessary (figure 1.7b) to ensure synchronization between the head position and the bit location. In order to record on to each individual bit reliably without disturbing the surrounding neighbors, a narrow SFD is required (figure 1.7a).

The broadening of SFD has been attributed to several sources such as, grain orientation and/or grain boundary variations within nanodots [36], lithographic variations between nanodots [37], and distributions of the anisotropy field [20]. Shaw et al [34], in their recent work showed that the switching filed distribution in patterned Co/Pd multilayers is a direct result of material properties. They found that the origin of SFD is due to an intrinsic material property of Co/Pd multilayer. The broadest SFD is observed while the Pd as seed layer. However the Ta is used as a seed layer, the SFD reduced to below 5%.

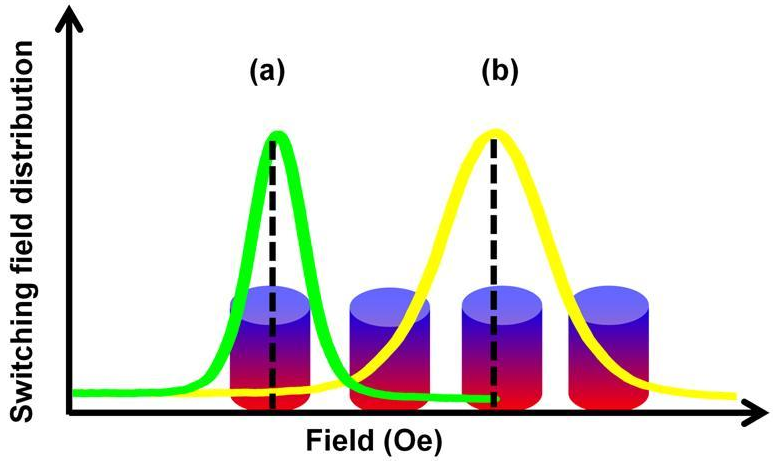

Figure 1. 7. a) A narrow vs b) wide switching field distributions.

O. Hellwig *et al* [38], studied the effect of pattern uniformity on switching field distribution. They fabricated patterned islands with three different methods such as: i) direct electron beam lithography [39], ii) copolymer self-assembly method [39] and iii) combination of electron beam lithography and block copolymer [41]. Uniform patterned dots with narrowest switching field distributions were achieved with the combination of electron beam registration and block copolymer elf-assembly. These results indicated that not only magnetic properties of media designs [40, 42] contribute to the SFD but also the placement uniformity and bit size distribution are critical to obtain a narrow SFD.

In another study from O. Hellwig *et al*.[43], they investigated the coercivity tuning to adjust reversal field in high perpendicular magnetic anisotropy (Co/Pd) multilayer based bit patterned media. They have studied two approaches to minimize the switching field distribution (SFD). The first approach, effect of increasing individual Co thickness to change magnetic anisotropy, and the second approach is combining the soft material $(Co/Ni)_{8-N}$ which have low anisotropy with hard material $(Co/Pd)_N$ to maintain narrow normalized switching field distribution. Data collected show that it is suitable to use a laminated hard/soft layer approach in order to minimize coercivity and smaller increase in switching field distribution in bit patterned media based on Co/Pd multilayer structures. They mentioned this can be happening because of narrower c-axis distribution, uncorrelated averaging over hard and soft layer SFD and strong exchange coupling of soft layer to hard layer. These results are significant for research and high areal density industry beyond of $1Tb/in^2$, because it focuses in SFD which is one of crucial problems in bit patterned media to exact addressability of bits without over writing adjacent bits. However, the requirement of a thick soft layer for such a composite structure poses more fabrication challenges and large head keeper spacing, which reduce the head writing capability. It also introduces issues such a large demagnetization fields and strong dependence on the exchange coupling strength.

The study with T. Hauet *et al.* [42], the role of reversal incoherency is investigated to reduce the SFD for new design of patterned media. They used the heterogeneous systems called exchange coupled composite **(**ECC) media [44, 45] consist of at least two coupled layers with low (soft) and high (hard) magnetic anisotropies. During the reversal mechanism the layer with low anisotropy starts reversing first and helps to hard layers moment to follow via the interlayer exchange coupling integrations. The torque produced with the soft layer moment allows decreasing the switching field of the hard layer stack, while conserving

thermal stability. This method can also improve the perpendicular magnetic recording writability.

More recently, Hauet *et al.* [46] reported the effect of light He+ ion irradiation as a method to tune the switching field and SFD in patterned Co/Pd multilayers. They observed that the irradiation has a strong influence on the Co/Pd interface anisotropy, inducing a reduction in the coercivity on patterned islands. Moreover, the normalized SFD is increased dramatically, which can be realized from the enhanced relative impact of misorientated grains as the interlayer anisotropy is lowered with increasing ion dose. This approach might be used to reduce the SFD of high anisotropy FePt patterned islands.

Demagnetization field between the patterned islands has an important role to have wide switching filed distributions. Piramanayagam *et al.* [47], proposed the antiferromagnetically coupled (AFC) patterned media to reduce the demagnetization effects in patterned medium. By this approach without changing the saturation magnetization, the magnetic remanet moment of media can be reduced and consequently magnetostatic interactions between dots can be tailored. In order to achieve the AFC after pattering, it is necessary that the coercivity of thinner layer be smaller than the exchange coupling field. Therefore, the suitable material design is essential to provide this criterion.

1.5 Scope and motivation

In this thesis, understanding and control of switching filed distribution (SFD) is considered as one of the main gaps for bit patterned media. Therefore, the main focus of this thesis lies in understanding the switching field distribution of patterned magnetic media and its correlation with different structures. In order to investigate the SFD of bit patterned media, Antiferromagnetically coupled (AFC) media and Capped bit patterned media (CBPM) based on experimental and simulation works are employed to minimize the SFD.

The continuous films were patterned into different pitches such as (400 nm, 100 nm and 50 nm) using E-beam lithography (EBL) and Nano imprint lithography (NIL) methods. Magnetic force microscopy (MFM), Anomalous Hall effect (AHE) measurement and Alternating gradient magnetometer (AGM) were used to study of magnetic properties of bit patterned media.

1.6 Organization of the Dissertation

The thesis is organized in the following way:

In chapter 1, a brief introduction of background information and the research motivation with thesis organization were delivered. In addition, principle of magnetic recording technology was addressed in the first part. Afterward, longitudinal and perpendicular recording technologies with their challenges (media trilemma) and superparamagnetic limits were presented, and possible solutions were proposed. More understanding of physics for novel recording technologies to further extend the limit of recording areal density was discussed. In the last part of this chapter, a review of patterned media with its challenges especially switching field distribution was addressed. In addition dipolar interaction was discussed in this chapter, as an important factor to have a wide switching field distribution in bit patterned media.

In chapter 2, the fabrication and characterization methods particularly anomalous Hall effect measurements and magnetic force microscopy tip with perpendicular magnetic anisotropy (PMA) are discussed for thin films and pattern islands.

Chapter 3 focuses on a quantitative study on the effect of dipolar interactions on SFD of patterned media based on simulation, modeling and experimental works. The SFD is

compared in the square and staggered bit patterned media with 50 nm pitch and 30 nm dot diameters, from a fundamental point view. Moreover, antiferromagnetically coupled bit patterned media with its main criteria to achieve AFC state after patterning is introduced to reduce the SFD.

In chapter 4, AFC patterned media is studied in two schemes with emphasis placed on the effect of the top layer coercivity, which will determine the remanent moment (M_r) and hence the dipolar interaction. In the first part of this chapter, the effect of patterning is discussed on stabilizing layer with different granularities. In the second part, the effect of patterning on the stabilizing layers with different magnetic anisotropy constant such as CoPt and CoCr:SiO_2 layers have been studied to achieve AFC state at remanent magnetization.

Chapter 5 focuses on basic and fundamental of two kinds of patterned AFC structures with low and high exchange coupling field. After then, the effect of these exchange coupling fields are discussed on SFD of patterned islands based on obtained full hysteresis loops.

In chapter 6, the second approach to reduce the SFD of patterned dots based on capped bit-patterned media is addressed.

Chapter 7, the highlights of the thesis and few suggested future works are summarized.

The main body of this dissertation is based on 17 published papers in several journals during the PhD period which are provided in publication list and vita.

Summary

In summary**,** in this chapter we have reviewed briefly magnetic recording principles, conventional recording technologies, media trilemma, magnetic properties and challenges of BPM. We understood that fabrication of sub 10 nm magnetic islands over a large area with

high throughput at cheaper costs is huge challenges for manufacturing of bit patterned media. Moreover, writability, synchronization and switching field distribution are other main concerns of bit-patterned media. Several works minimized some of the limitations of BPM but SFD of patterned structures has not studied extensively. In this thesis, switching filed distributions is considered as a main gap of bit patterned media. Therefore, antiferromagnetically coupled structure and Capped bit patterned media are investigated to minimize the SFD. It is necessary to understand the basic mechanism of thin/patterned films fabrications and characterization methods before studying the magnetic properties of patterned media. Therefore, in next chapter the fabrication methods and characterization techniques for thin films and patterned structures are discussed.

References

1. H. N. Bertram, "Theory of Magnetic Recording", Cambridge University Press (1994).
2. S. N. Piramanayaganm and T. C. Chong, "Developments in Data Storage: Materials Perspective", Wiley-IEEE Press (2012).
3. K. Ise, K. Yamakawa, K. Ouchi, H. Muraoka, Y. Sugita and Y. Nakamura , IEEE Trans. Magn., **36**, 2520 (2000).
4. H. J. Richter, E. Champion and Q. Peng, IEEE Trans Magn. **39**, 697 (2003).
5. H. J. Richter, J. Phys. D: Appl. Phys., **40**, R149 (2007).
6. S. Iwasaki, Y. Nakamura, IEEE Trans. Magn., **13**, 1272 (1977).
7. Y. Ikeda, Y. Sonobe, G. Zeltzer, B.K. Yen, K. Takano, H. Do, E.E. Fullerton, P. Rice, IEEE Trans. Magn. **37**, 1583(2001).
8. K. Hayashi, M. Hayakawa, H. Ohmori, A. Okabe, K. Aso, J. Appl. Phys, **67**, 5175 (1990).
9. T. Hikosaka, T. Komai, Y. Tanaka, IEEE Trans. Magn., **30**, 4026 (1994).

10. T. Oikawa, M. Nakamura, H. Uwazumi, T. Shimatsu, H. Muraoka, Y. Nakamura, IEEE Trans. Magn., **38**, 1976 (2002).
11. H. Uwazumi, K. Enomoto, Y. Sakai, S. Takenoiri, T. Oikawa, S.Watanabe, IEEE Trans. Magn., **39**, 1914(2003).
12. E. Girt, S. Wu, B. Lu, G. Ju, T. Nolan, S. Harkness, B. Valcu, A. Dobin, J.D. Risner, M. Munteanu, R. Thangaraj, C.-H. Chang, T. Tran, X. -Wu, O. Mryasov, D. Weller, S. Hwang, J. Appl. Phys., **99**, 08E715(2006).
13. S.H. Park, S.O. Kim, T.D. Lee, H.S. Oh, Y.S. Kim, N.Y. Park, D.H. Hong, J. Appl. Phys, **99**, 08E701(2006).
14. I. Takekuma, R. Araki, M. Igarashi, H. Nemoto, I. Tamai, Y. Hirayama, Y. Hosoe,J. Appl. Phys., **99**, 08E713(2006).
15. S.N. Piramanayagam, J. Appl. Phys., **102**, 011301(2007).
16. A.Moser, K.Takano, D.T. Margulies, M.Albrecht, Y.Sononbe, Y.Ikeda, S. Sun, E. E. Fullerton, J.Appl. Phys., **35**, R157 (2002).
17. W. F. Brown, Phys. Rev., **130**, 1677 (1963).
18. B. D. Terris and T. Thomson, J. Phys. D., **38**, R199 (2005).
19. T. Thomson, G. Hu, and B.D. Terris, Phys. Rev. Lett., **96**, 257204 (2006).
20. C. Ross, Annu. Rev. Mater. Res., **31**, 203 (2001).
21. M. H. Kryder, E. C. Gage, T. W. McDaniel, W. A. Challener, R. E. Rottmayer, G. Ju, Y.-T. Hsia and M. F. Erden, Proceedings of the IEEE, **96**, 1810 (2008).
22. O. Hellwig, A. Berger, T. Thomson, E. Dobisz, H. Yang, Z. Bandic, D. Kercher, and E. E. Fullerton, Appl. Phys. Lett., **90**, 162516 (2007).
23. L. F. Shew, *IEEE Trans. Broadcast and TelevisionReceivers,* **56,** *BTR-9, (*1963).
24. S. E. Lambert, I.L.S., A. M. Patlach, M. T. and M. Krounbi, IEEE Trans. Mag., **23**,3690 (1987).

25. J. F. Smyth, S. Schultz, D. R. Fredkin, D. P. Kern, S. A. Rishton, H. Schmid, M. Cali, and T. R. Koehler, J. Appl. Phys., **69**, 5262 (1991).

26. A. Moser, K. Takano, D. T. Margulies, M. Albrecht, Y. Sonobe, Y. Ikeda, S. H. Sun and E. E. Fullerton, J. Phys. D: Appl.Phys., **35**, R157 (2002).

27. D. Weller and A. Moser, IEEE Trans. Magn., **35**, 4423 (1999).

28. H. J. Richter, J. Phys. D: Appl. Phys., **32**, R147 (1999).

29. S. H. Charap, P. L. Lu and Y. J. He, IEEE Trans. Magn., **33**, 978 (1997).

30. J. Lohau, A. Moser, C. T. Rettner, M. E. Best and B. D. Terris, Appl. Phys. Lett., **78**, 990 (2001).

31. B. D. Terris, J. Magn. Magn. Mater. **321**, 512 (2009).

32. J. K. W. Yang, Y. Chen, T. Huang, H. Duan, N. Thiyagarajah, H. K. Hui, S. H. Leong and V. Ng, Nanothecnology., **22**, 385301 (2011).

33. Y. Shiroishi, K. Fukuda, I. Tagawa, H. Iwasaki, S. Takenoiri, H. Tanaka, H. Mutoh and N. Yoshikawa, IEEE Trans. Magn., 45, 3816 (2009).

34. J.M. Shaw, W.H. Rippard, S.E. Russek, T. Reith, and C.M. Falco, J. Appl. Phys., **101**, 023909 (2007).

35. R. Sbiaa, C.Z. Hua, S.N. Piramanayagam, R. Law, K.O. Aung, and N. Thiyagarajah, J. Appl. Phys., **106**, 023906 (2009).

36. C. Haginoya, S. Heike, M. Itabashi, K. Nakamura, and K. Koike, J. Appl. Phys., **85**, 8327 (1999).

37. Y. Kitade, H. Komoriya, and T. Maruyama, IEEE Trans. Magn., **40**, 2516 (2004).

38. O. Hellwig, J. K. Bosworth, E. Dobisz, D. Kercher, T. Hauet, G. Zeltzer, J. D. Risner-Jamtgaard, D. Yaney, and R. Ruiz, Appl. Phys. Lett., **96**, 052511 (2010).

39. O. Hellwig, T. Hauet, T. Thomson, E. Dobisz, J. D. Risner-Jamtgaard, D. Yaney, B. D. Terris, and E. E. Fullerton, Appl. Phys. Lett., **95**, 232505 (2009).

40. K. W. Guarini, C. T. Black, and S. H. I. Yeuing, Adv. Mater., **14**, 1290 (2002).

41. R. Ruiz, H. Kang, F. A. Detcheverry, E. Dobisz, D. S. Kercher, T. R. Albrecht, J. J. de Pablo, and P. F. Nealey, Science, **321**, 936 (2008).

42. T. Hauet, E. Dobisz, S. Florez, J. Park, B. Lengsfield, B.D. Terris and O. Hellwig, Appl. Phys. Lett., **95**, 262504 (2009).

43. O. Hellwig, A. Moser, E. Dobisz, Z. Bandic, H. Yang, D. S. Kercher, J. D. Risner-Jamtgaard, D. Yaney, and E. E. Fullerton, Appl. Phys. Lett., **93**, 192501 (2008).

44. R. H. Victora and X. Shen, IEEE Trans. Magn., **41**, 537 (2005).

45. D. Suess, T. Schrefl, S. Fähler, M. Kirschner, G. Hrkac, F. Dorfbauer, and J. Fidler, Appl. Phys. Lett., **87**, 012504 (2005).

46. T. Hauet, O. Hellwig, S.-H. Park, C. Beigné, E. Dobisz, B. D. Terris, and D. Ravelosona, Appl. Phys. Lett., **98**, 172506 (2011).

47. S. N. Piramanayagam, K. O. Aung, S. Deng, and R. Sbiaa, J. Appl. Phys., **105**, 07C118 (2009).

Chapter 2. Fabrication and characterization methods

In the following chapter, the fabrication methods and characterization techniques of thin films and patterned islands under our study are discussed with details. The new kind of magnetic force microscopy (MFM) tip sputtered material with perpendicular magnetic anisotropy (PMA) constant is explored to observe the switching mechanism of magnetic islands. In addition, anomalous Hall effect (AHE) measurement is explained in order to measure full hysteresis loop of magnetic nanostructures.

2.1 Sputtering for thin film deposition

Sputtering is one of the suitable vacuum deposition technique used by manufacturers of Hard disk drives, semiconductors, and optical devices. Sputtered films show very good homogeneity, density, adhesion and purity. With sputtering method, it is possible to deposit alloys of precise composition, or oxides. The magnetic layers for this study were deposited using DC magnetron sputtering. The basic principle of sputtering method is shown schematically in figure 2.1

Sputtering is a physical vapour deposition method, and it occurs by bombarding a target with energetic ions, typically Ar in a highly vacuumed condition. During sputtering, the materials are removed as atoms from a target collided with energetic Ar ions. By applying a high DC or RF voltage between the target (also known as the cathode), and the substrate (the anode), energetic atoms from the target form transferring to stick on substrate.

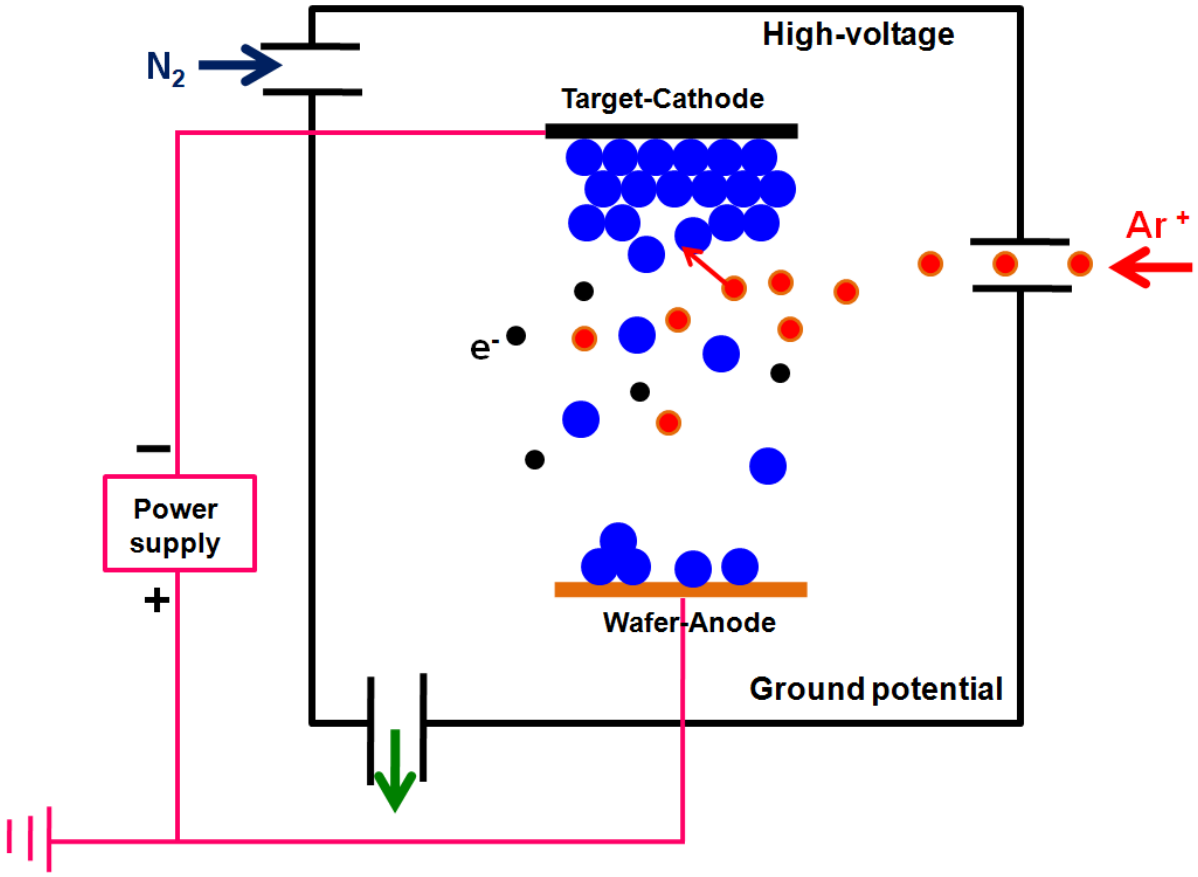

Figure 2.1.schematic of sputtering process.

2.2 Alternating Gradient Magnetometer (AGM)

Alternating gradient magnetometer (AGM) belongs to a group of magnetometers that measures the force exerted on a magnetized sample in a magnetic field gradient. Another group of magnetometers measures the voltage induced by changing magnetic flux such as Vibrating Sample Magnetometer (VSM).

The AGM is used to obtain magnetic properties of magnetic samples. The advantage of the AGM is that it is able to measure the hysteresis loop of magnetic samples with small magnetic moments. A schematic of AGM system is shown in figure 2.2. The sample must first be cut to a dimension of 3 mm by 3 mm. Grease is then applied to the sample before sticking it to the sample probe. The probe is then placed onto the adjustable bracket or the

sample holder. Finally, it must be ensured that there is no swaying before the start of calibration.

Basically, a sample placed in a magnetic field is vibrated at a fixed frequency via an electro-mechanical transducer. AGM system uses an alternating gradient field to produce a periodic force on a sample placed in a static direct current (D.C) or variable D.C field. The sample is mounted on an extension rod attached to a piezoelectric element. The alternating field gradient exerts an alternating force on the sample proportional to the magnitude of the gradient field and the magnetic moment of the sample.

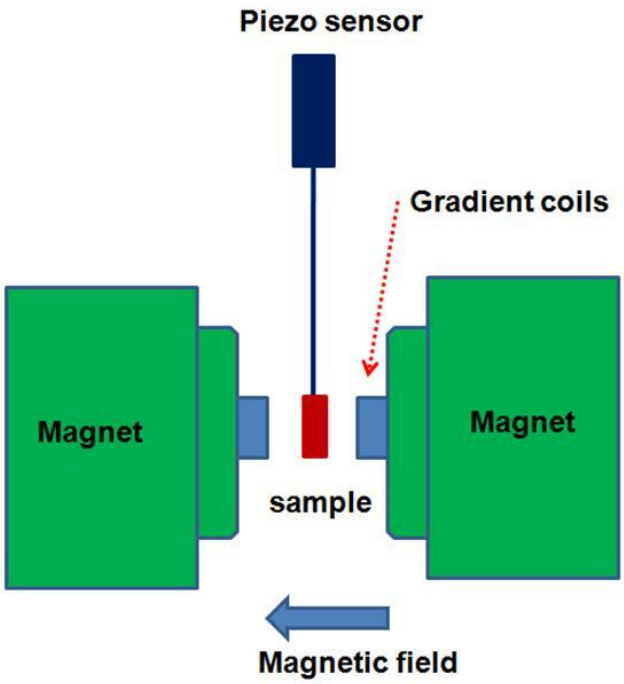

Figure 2.2. Schematic of AGM system to characterize magnetic properties of magnetic layers.

The resulting deflection of the extension is transmitted to the piezoelectric sensing element. The output signal from the piezoelectric element is synchronously detected at the operating frequency of the gradient field. The signal developed by the piezoelectric element is greatly

enhanced by operating at or near the mechanical resonant frequency of the assembly. A built-in software function automatically determines mechanical resonance and sets the appropriate operating frequency for the sample under study and the electromagnet can induce magnetic fields up to 20 kOe.

2.3 Electron Beam Lithography (EBL)

In Electron beam lithography (EBL), a beam of electrons are used as the exposure source, and electron beam has a very high resolution and good depth of focus on resist. Because of smaller spot diameter of the electrons beam compare to optical lithography, which is limited by the wavelength of light used for exposure, EBL is one of the best techniques for creating extremely fine patterns down to sub 10 nm. Direct write electron beam lithography systems are the most common EBL systems. Most direct write systems use a small electron beam spot which is moved with respect to the wafer to expose the wafer one pixel at a time. Direct write systems can be categorized as raster scan or vector scan, with either fixed or variable beam geometry. Electron beam resist is an essential part of this method for exposure [1, 2].

Electron beam resists are the recording and transfer medium for e-beam lithography. The usual e-beam resists are polymers that dissolve in a liquid solvent. After baking out the casting solvent, electron exposure modifies the resist. Basically, there are two kinds of electron beam resists: positive tone and negative tone. In case of usage of positive resists, the resist is washed away at exposed regions whereas in the case of negative resist the exposed region remains after development. The negative electron beam resists act based on formation of interchain linkages during radiation procedure, which is insoluble. The schematic of E-beam lithography for negative and positive resists is shown in figure 2.3.

Some of the positive e-beam resists are: EBR-9 (acrylate based resist), PMMA (Poly methyl methacrylate), PBS (Poly butene-1-sulphone), ZEP (a copolymer of α -chloromethacrylate and α -methylstyrene), and some of the negative tone e-beam resists are: Hydrogen silsesquioxane (HSQ: XR-1541), COP and Shipley SAL which has 3 components, a base polymer, an acid generator, and a cross linking agent.

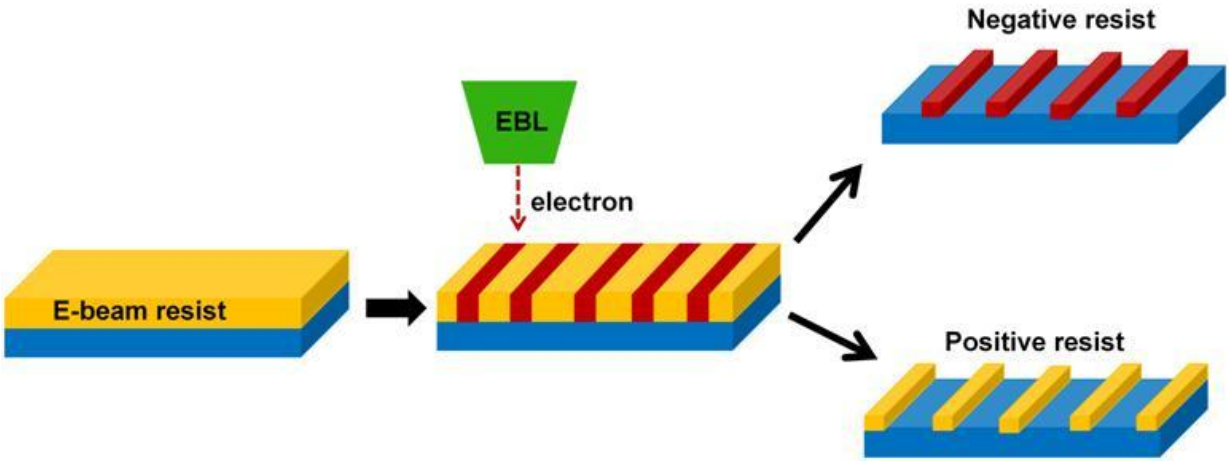

Figure 2.3. Schematic illustration of E-beam lithography for negative and positive resist.

Unfortunately, EBL has a severe problem with throughput. Making disk samples using EBL will take several weeks depending on the density. Therefore, this method is only suitable for R&D or as a method for making a mold. The molds can be imprinted onto magnetic layers to make disks in mass-production.

In our works, high resolution electron beam lithography was carried out on negative resist Hydrogen silsesquioxane (HSQ: XR-1541) purchased from Dow Corning. HSQ was diluted with methyl isobutyl ketone (MIBK) with concentration ratio of (1:2) to achieve about 50-55 nm thickness of resist under identical spin coating conditions [3]. Figure 2.4 shows the pattern fabrication process using EBL. Magnetic layers such as single layer CoPt and AFC thin films were spin coated with HSQ at speeds of 6000 rpm for 60 s. The thickness of the

spin coated HSQ was measured with an ellipsometer at a wavelength of 632.8 nm and a fixed refractive index of 1.386 [4].

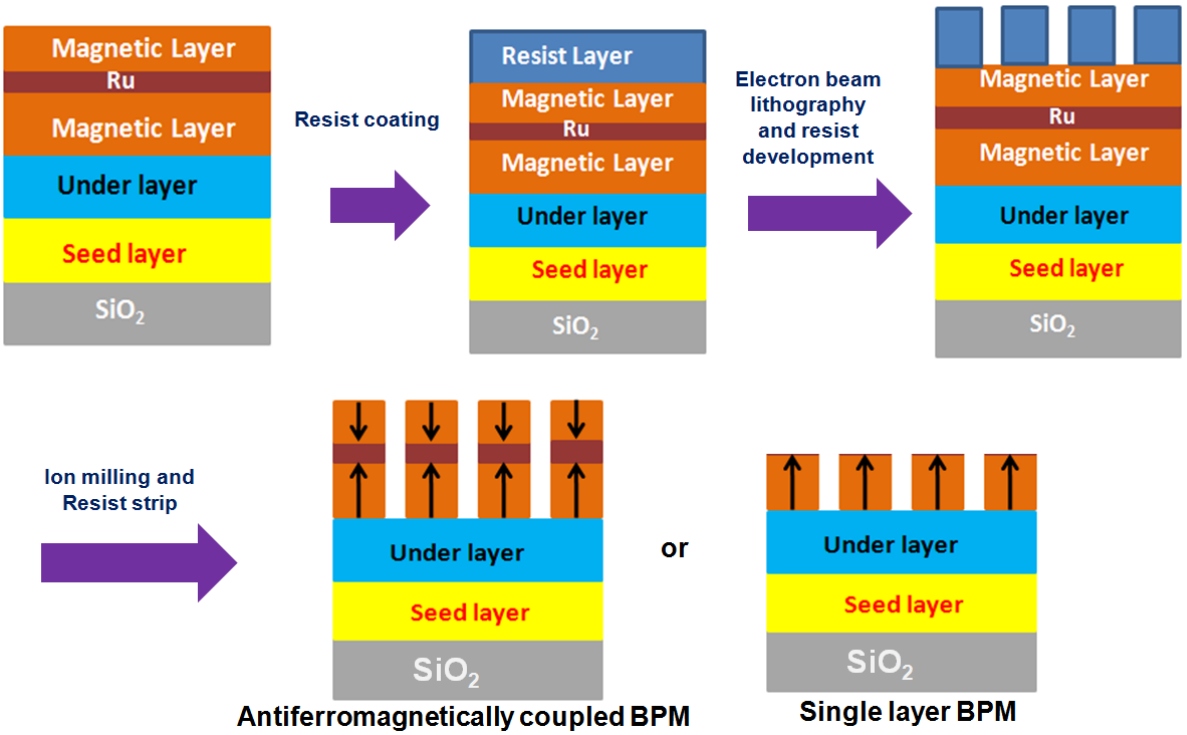

Figure 2.4. Patterned islands fabrications by using EBL.

Subsequent to spin coating, samples were pre baked on an oven at 150 °C for 2 min followed by another baking at 200 °C for an additional 2 min. The resist was exposed in Elionix ELS-7000 EBL system at 100 kV acceleration voltage and 500 pA beam current to obtain nanodots.

After exposure, samples were developed by immersion in 25% tetramethylammonium hydroxide (TMAH) developer at room temperature for 30 s, rinsed in 2.5% TMAH for 15 s followed by a rinse in de-ionized water for another 15 s. Then, by ion milling process (using Ar ion) patterns are transferred to magnetic layers from resist level.

2.4 Nanoimprint Lithography (NIL)

Nano-imprint lithography (NIL) is a process in which a mold is pressed into a thin polymer film on a substrate to create sub-25 nm trenches in polymers, as shown by Stephen Chou et. al. [5] in the mid-1990s. Their work found that nano-structures imprinted in the polymers conform completely to the geometry of the mold.

Nano-imprint lithography is a paradigm-shift method that has shown sub-10 nm resolution, high throughput and low cost. Based on the mechanical embossing principle, nano-imprint technique and its variants can achieve pattern resolutions beyond limitations set by the light diffractions or beam scatterings in other conventional techniques. This patterning technique was successfully applied to the fabrication of silicon nano-devices and since then has been applied to fabrication of numerous electrical, optical and magnetic devices. Nano-imprint lithography has a working principle fundamentally different from conventional lithography. Nano-imprint creates features by mechanical deformation of the resist shape using a mold. During the deformation, a nano-imprint resist (made of thermal plastic or a curable material) is in a liquid flow able state and becomes solidified after the deformation.

To imprint a surface, three basic components are required. These are: (1) a stamp with suitable feature sizes. (2) The material to be printed, usually a layer of polymer of a few nanometers' thickness with suitable glass transition temperature and molecular weight, spun on substrate and (3) equipment for printing with adequate control of temperature, pressure and control of parallelism between the stamp and substrate.

Figure 2.5 shows a schematic illustration of the NIL process steps which was used to fabricate the magnetic nanostructure in this thesis. The first part of the process involves making a flexible daughter mold from the master mold using thermal imprinting and second part involves making patterned resist on a magnetic (or other desired) substrate by using UV-

NIL method. Figure 2.5a shows daughter mold fabrication process based on hot-embossing over a polymer sheet, as an example. A daughter mold produced in this way (or other methods) may be spin-coated with UV-sensitive resist followed by a baking step. The spin-coating has to be optimized to achieve deep and uniform coverage of the resist over the mold. The spin-coating thickness determines the residual layer thickness. If the spin-coating thickness is too large, the residual layer thickness will also be larger which will invalidate the advantage of this method. The advantages of using the first part of the process steps are in the ability to decrease the fabrication cost and damage of the master mold and in making the process of separation (demolding) easier [6]. The daughter mold, which is fabricated in this part of processing step, can be used several times and hence there is no need to repeat the first part of the process again.

In the second step, magnetic layers are spin coated with a commercial UV resist (STU from Obducat). Then daughter mold is transferred to the STU resist in the form of patterned resist at a low temperature and pressure by exposure under UV light (Figure 2.5b). After the transfer of the resist, the flexible daughter mold can be released easily. The resist pattern, thus formed, can be used for pattern transfer to magnetic layer of hard disk media or other desired substrates. The details of NIL process are as following. Nano-imprinting was done using an Obducat system. For the hot-embossing process, a pressure of 30 bar was applied on the polymer sheet at a temperature of 160 ºC for a time period of 180 s as has been described by E. L. Tan *et al*. [7]. The magnetic material was then coated with UV resist by spin-coating at a speed of 6000 rpm for 60 s, followed by a baking step at 95 ºC for 3 min. This yields a resist thickness of about 58 nm. The resist on the polymer sheet was transferred on substrate in the form of patterned resist at molding temperature and pressure of 65 ºC and 10 bar respectively and exposed under UV light for 5 s.

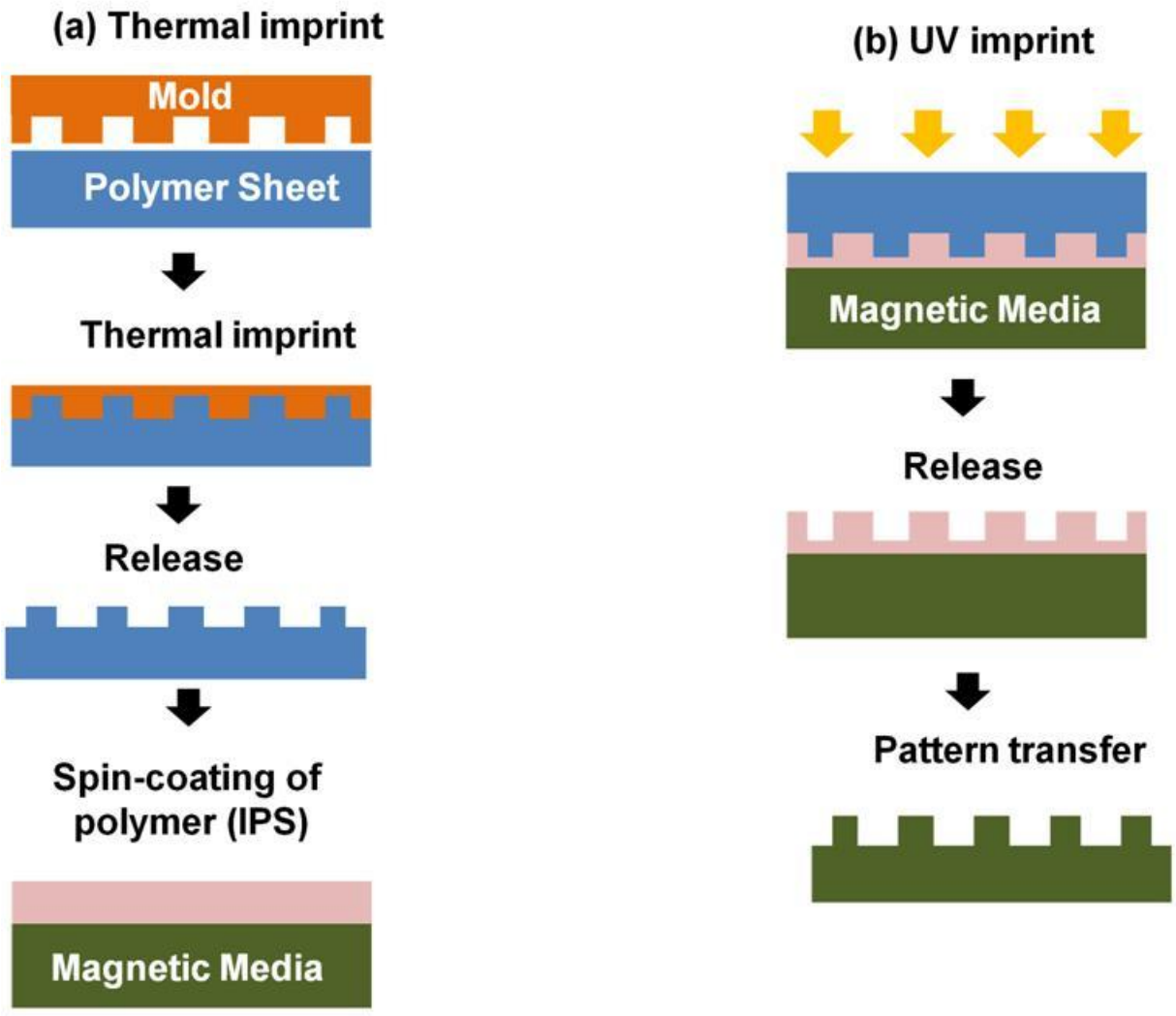

Figure 2.5. a) Thermal imprint process to make daughter mold, b) UV imprint process and transfer the patterned structures from daughter mold to magnetic layer.

2.5 Atomic and Magnetic Force Microscopy (AFM/MFM) measurement

In this session, we describe basic principle of atomic force microscopy (AFM) measurement and later magnetic force microscopy tip with perpendicular magnetic anisotropy (PMA) is discussed. Moreover, PMA-MFM tip based on modeling and simulation results are addressed.

2.5.1 Atomic Force Microscopy (AFM)

The Atomic Force Microscope (AFM) is a powerful tool based on the Nobel prize-winning invention by Binning, Quate and Gerber in 1986 [8]. It has proved to be extremely useful in the process of characterizing features on various kinds of surfaces from the micrometer scale to the nanometer scale. Besides its capabilities as a nanoscale characterizer, the AFM can also be used as a nanoscale robot, i.e. for modifying surfaces or manipulation structures such as nanoparticles and nano-rods [9, 10].

2.5.1.1 Principle of AFM measurement

The AFM consists of a cantilever with a sharp tip at its end, as shown in figure 2.6. The tip scanned over a sample at distances on the order of a few nanometers. Inter-atomic forces occurred between the tip and the sample, which is less than 10^{-9} N. This small force is sensed by the cantilever, whose deflection is measured by a laser and a photodetector. As the tip scans the surface of the sample, moving up and down with the contour of the structure, the laser beam is deflected off the attached cantilever into a quad-photodetector. The photodetector measures the difference in light intensities between the upper and lower photodetector, and then converts to voltage. Feedback from the photodiode difference signal, through software control from the computer, enables the piezoelectric scanner to move the sample for further control.

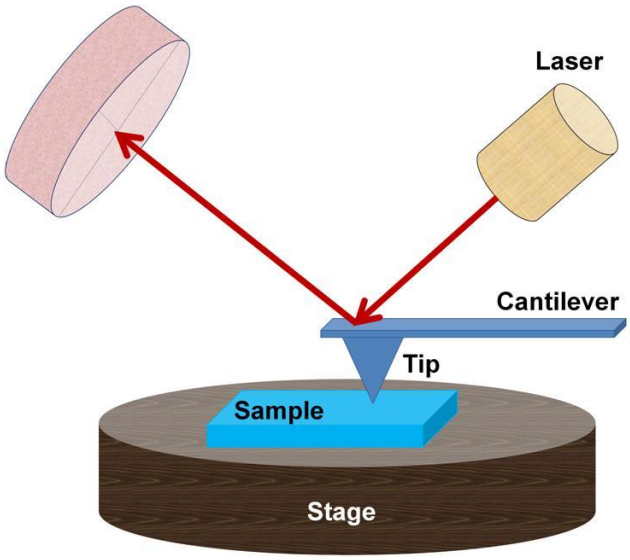

Figure 2.6. Illustration of atomic force microscopy measurement.

2.5.1.2 The Common AFM Working Modes

The AFM scans on either Tapping Mode or Contact Mode. Each mode should be selected according to the specimen to be scanned and the kind of results desired. The three types of AFM modes are: 1) The contact mode; 2) the non-contact mode and 3) the tapping mode (or intermittent contact). In the contact regime, the cantilever is held less than a few angstroms from the sample surface, and the interatomic force between the cantilever and the sample is repulsive, as shown in figure 2.7. In the non-contact regime, the cantilever is held on the order of tens to hundreds of angstroms from the sample surface, and the interatomic force between the cantilever and sample is attractive (largely a result of the long-range van der Waals interactions). In the tapping mode, the cantilever makes the intermittent contact with the sample. In this thesis, tapping mode was used to obtain AFM images.

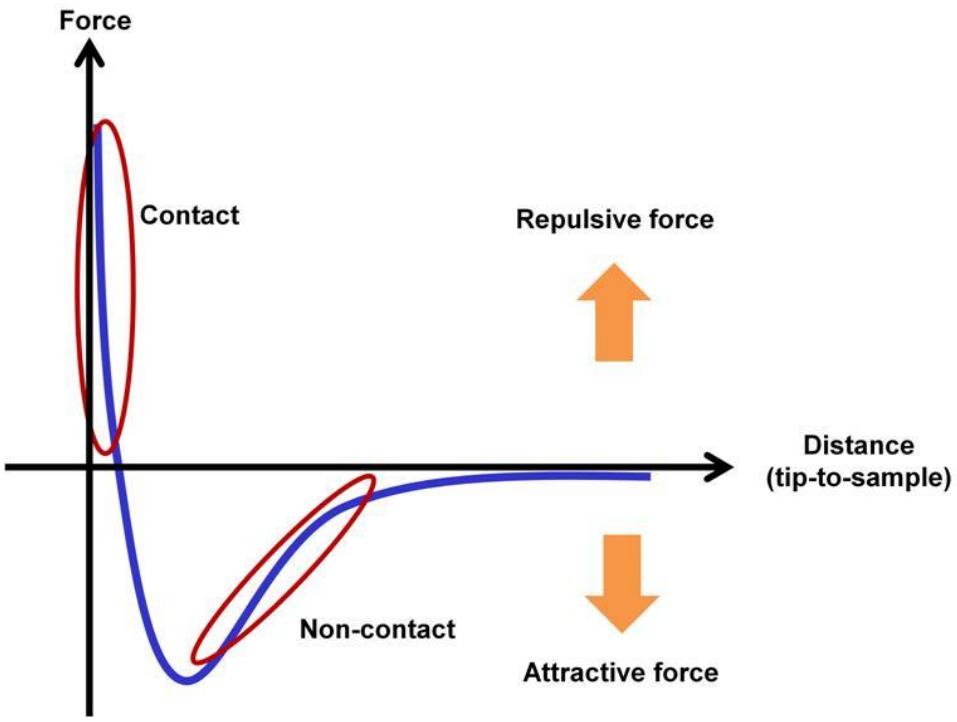

Figure 2.7. Different regions for AFM modes.

2.5.2 Magnetic force Microscopy (MFM)

In the last decade, several characterization techniques such as Lorentz transmission electron microscopy (LTEM), scanning electron microscopy with polarization analysis (SEMPA), spin-polarized low-energy electron microscopy (SPLEEM), magnetic resonance force microscopy (MRFM) and scanning transmission X-ray microscopy (STXM) have been developed extensively to understand underlying magnetic behaviors of magnetic materials [11-14]. These techniques require high vacuum and special sample preparation procedures. Magnetic force microscopy (MFM), on the other hand, has been considered as a common technique to resolve fine magnetic features in magnetic nanostructures without difficulties as mentioned above [15-20].

Magnetic force microscopy is an extension of atomic force microscopy (AFM) that images magnetization patterns with sub-micron resolution, employing a sharp magnetic tip attached

to a flexible cantilever. The tip is placed close to the sample surface (typically within 5-35 nm) and interacts with the stray field emanating from the sample. The image is formed by scanning the tip laterally with respect to the sample and measuring the force (or force gradient) as a function of position. The interaction strength is determined by monitoring the motion of the cantilever using a high-sensitivity sensor, such as an optical interferometer or tunnelling sensor. The ability to make images of the magnetic domain structure makes MFM complementary with the techniques of Kerr microscopy. In this part firstly, the principle of MFM measurement is discussed and in second part the MFM tip with perpendicular magnetic anisotropy (PMA) is introduced. It should be highlighted that all the MFM images in this dissertation are measured by PMA-MFM tip.

2.5.2.1 Basic principle for MFM measurement

There are currently two main approaches to MFM imaging: (1) force mode MFM and (2) force gradient mode MFM. In the force mode MFM, a magnetically active tip is scanned at a spacing of a few tens of nanometers above the sample of interest and the magneto-static interaction between the stray field from the sample and the magnetization of the tip produces a force that deflects the tip and its associated cantilever from its nominal position. The cantilever deflection is measured as in a standard AFM and an image of the magnetic structure of the sample is thus obtained. This mode of operation is also often referred to as static or DC mode MFM [21].

2.5.2.2 MFM tip trilemma

Recording media, where information is written closely at spacing of sub-30 nm, are commonly used to demonstrate the advantage of the proposed method. Interestingly, very

similar to the recording media trilemma, the desired factors for high resolution MFM are conflicting in nature too, and we call this MFM trilemma. The resolution of MFM has been considered as a main issue in characterizing magnetic nanostructures smaller than 30 nm; especially for high density recording media beyond 1 Tbit/in^2. Figure 2.8 describes the MFM trilemma - interaction between three factors - viz., signal, resolution and tip-sample interaction. The signal from the sample, from the imaging perspective, depends on the magnetic moment of the tip. Therefore, the signal can be enhanced by increasing the thickness or the saturation magnetization of the coating magnetic film, for example. However, a thicker coating will result in a loss of resolution, as the interaction volume with the sample will be increased. Increasing the saturation magnetization may also increase the tip – sample interaction, where, tip magnetic moment may disturb the domain structure of the sample itself [22-24]. A decrease in the spacing between the tip and the sample can enhance the signal and may increase the resolution. However, this will also lead to an enhancement of the tip - sample interaction. For the improvement of the lateral resolution (interaction volume), high aspect ratio tips -trimmed by focus ion beam (FIB)- have been proposed [25]. Antiferromagnetically coupled tips in longitudinal geometry, which act like pointed dipoles, have also been proposed for improving the lateral resolution. Tips with low magnetic moment have been proposed to reduce tip-sample interaction. However, because of the low magnetic moment of such thin magnetic films the sensitivity is affected [15-20, 24]. A suitable MFM technique should consider the three factors together, in addition to easier fabrication method.

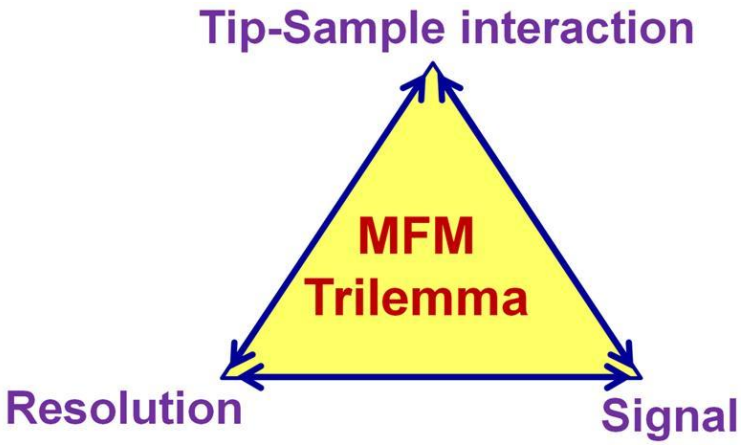

Figure 2.8. Magnetic force microscopy (MFM) Trilemma.

2.5.2.3 MFM tip with perpendicular magnetic anisotropy (PMA)

In our work, in order to measure the magnetic domains for thin films and switching mechanism of bit patterned media, we fabricated two different types of tips. The objective was to achieve higher resolution through easier fabrication methods instead of complex techniques such as FIB trimming or MFM under high vacuum.

The two kinds of MFM tips include those with a perpendicular magnetic anisotropy (PMA), tips with a reference tip with no perpendicular magnetic anisotropy (no PMA) [26, 27]. Comparison between the fabricated tips with commercial tips (which are similar to our reference tips) was made by studying their resolution on pre-recorded bits onto a perpendicular recording medium. The following MFM tip structures were deposited by dc magnetron sputtering using a BPS Circulus M12 sputtering system: Ta (10 nm)/Ru (10 nm, at 0.5 Pa)/Ru (10 nm, at 8 Pa)/ CoCrPt: SiO_2 (15 nm at 8 Pa)/ Ta (5 nm) as PMA tip, previous structure without Ta (10 nm) for tip with no PMA. The layers of Ta and Ru deposited help to induce PMA to CoCrPt: SiO_2 magnetic layers. The structure without Ta seedlayer is expected to have a random crystallographic texture and hence PMA cannot be developed.

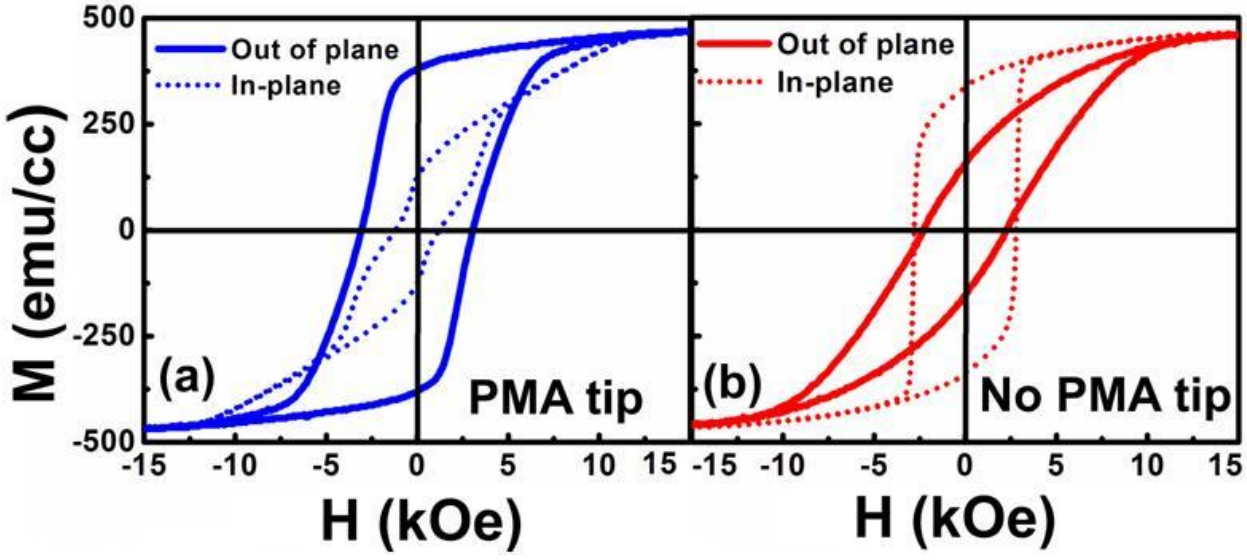

Figure 2.9. Out-of-plane and In-plane hysteresis loops of the (a) magnetic layers deposited on Ta/Ru seedlayers (similar to PMA-tip), (b) without Ta seedlayers (as no PMA tip similar to commercial tip).

Figures 2.9a and 2.9b show the out-of-plane and in-plane hysteresis loops for samples with PMA and no PMA, respectively. It can be noticed from the out-of-plane hysteresis loops that the films grown on Ta/Ru seedlayers (PMA tip) show a larger coercivity field of 3.1 kOe and a larger remanence magnetization of 470 emu/cc as compared to films without Ta seedlayer (no PMA tip), which have a coercivity field of 2.1 kOe and remanence magnetization of 200 emu/cc. The magnetic anisotropy constant (K_u) - as determined by measuring the in-plane and perpendicular hysteresis loops[28] – was found to be 2.8×10^6 erg/cm^3 for the film with Ta/Ru seedlayer, while it drops to -0.96×10^6 erg/cm^3 for the case of film with Ta seedlayer.

2.5.2.4 Hypothesis of PMA-MFM tip

Figure 2.10 shows scanning electron microscopy (SEM) images of (a) atomic force microscopy (AFM tip) before deposition of magnetic layers, (b) tip coated with PMA thin

film and (c) Commercial (random anisotropy) MFM tip along with an illustration of two bits of a recording medium.

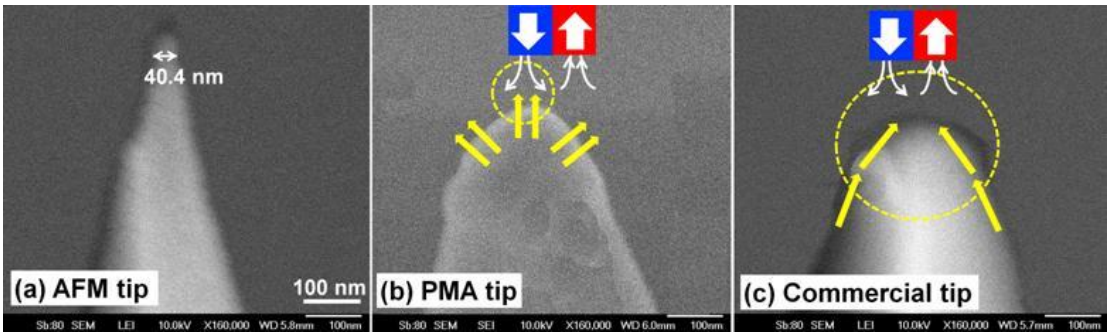

Figure 2.10. Scanning electron microscopy (SEM) images of (a) Tip before deposition of magnetic layers, (b) tip coated with perpendicular magnetic anisotropy (PMA) layers and (c) Commercial MFM (random anisotropy) tip, respectively.

It can be noticed that the radius of MFM tips after deposition of magnetic layers is the same as in commercial tip. In the case of later one, the magnetization of the whole of the tip region interacts with the flux from recording media as there is a perpendicular component around the tip curvature. Hence, the interaction volume of the tip with no PMA is larger and hence the resolution cannot be higher. In contrast, for tips with PMA configuration, only the apex of the tip has a perpendicular magnetization and hence it has a smaller interaction volume with the stray field from the media. As a consequence, the resolution of image response is expected to increase due to the perpendicular component of tip magnetization.

2.5.2.5 Resolving of magnetic domains in granular media

In order to compare commercial MFM tips and PMA-MFM tips, the MFM images have been taken from data tracks written onto a CoCrPt: SiO_2 perpendicular medium at linear recording densities ranging from 400 kilo-flux cycles per inch (kfci) to around 800 kfci,

which correspond to bit lengths of 63 nm and 31 nm, respectively. MFM scans were obtained with a Veeco Dimension 3100 scanning probe microscope in tapping lift mode.

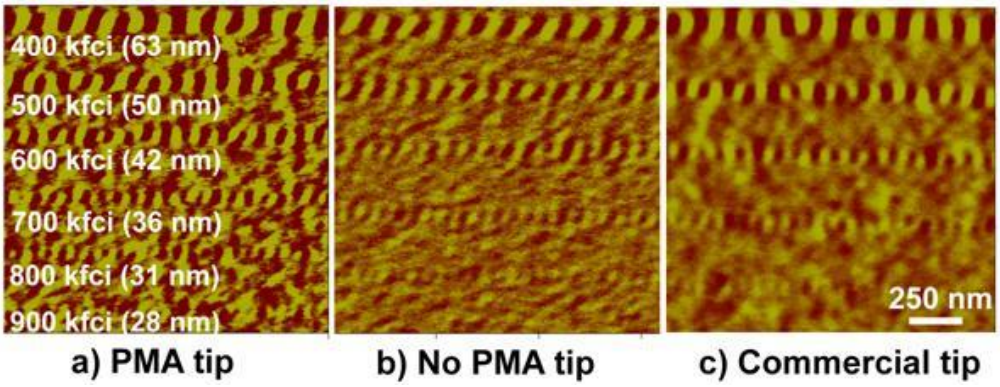

Figure 2.11. Magnetic force microscopy (MFM) images of recorded patterns measured using tips with PMA, without PMA and standard tips at 10 nm scan height.

Figure 2.11 shows MFM images of written bits in a perpendicular recording medium at a scan height of 10 nm, for tips with PMA, no PMA (20 nm thick magnetic layer coating), and commercial tips. It can be seen that the tip with PMA resolves the patterns clearly at 800 kilo-flux change per inch (kfci); the tips without PMA and commercial tips have a poorer signal. This is understandable; because the tip with PMA has a larger remanent moment compared to the tip without PMA, as discussed above, and hence can provide better signals with thinner coatings. It has to be mentioned that the medium used in this study has a surface roughness of 3 Å measured by AFM probe, showing that there is no topographic effect on MFM images.

2.5.2.6 Resolving of magnetic island for bit patterned media

In addition, in order to evaluate the improved performance of tips with PMA, MFM measurements were carried out on BPM. The patterned dots were achieved with high resolution electron beam lithography using hydrogen silsesquioxane (HSQ) as resist [29]. The dots were of 40 nm in diameter with 10 nm spacing between them. Figure 2.12 shows AFM and MFM images of bit patterned media over the area of 6 μm× 6 μm using (a, b) PMA tips

and (c, d) commercial tips, respectively. In addition, the enlarged AFM/MFM images of the patterned islands are shown in the inset of figure 2.12.

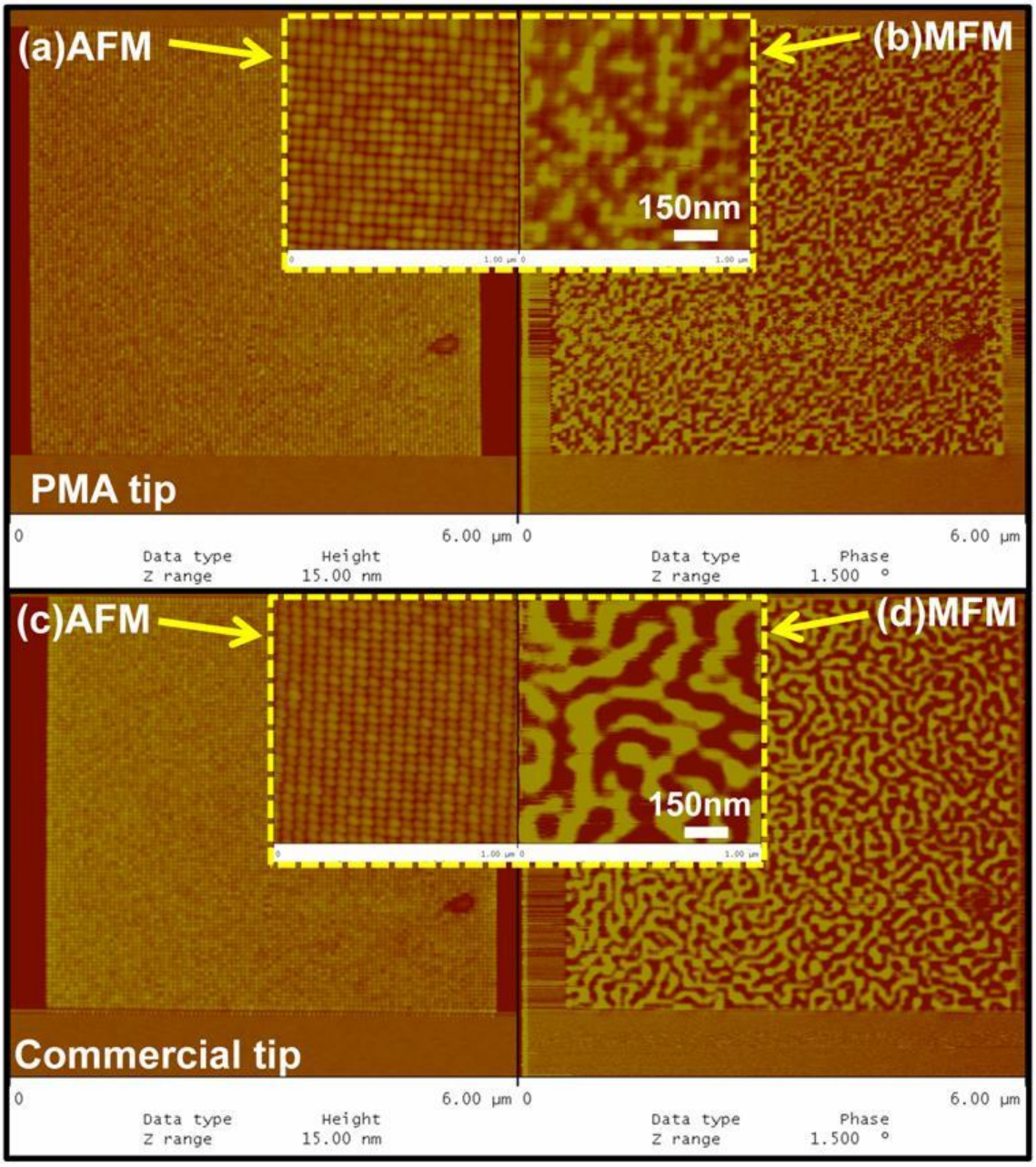

Figure 2.12. AFM and MFM scans of bit-patterned media samples with 10 nm spacing as measured by the PMA tips (top) and commercial tips (bottom).

It can be seen clearly that the MFM images are not topographic images and the individual switching of dots can be observed by PMA tip. Alternatively, the MFM images from the

PMA tips show a clear separation between the magnetic dots, highlighting that the magnetic flux can be resolved at spacing of 10 nm with PMA tips.

2.5.2.7 Response modeling for PMA tip

In order to provide further evidence on the effect of perpendicular magnetic anisotropy in enhancing the resolution of MFM tip, modeling was carried out to simulate the magnetic response of a tip with PMA and tip without PMA to written magnetic transitions. Stray fields from perpendicular magnetic recording media were considered by the two following equations [30, 31]:

$$H_z(x,z) = 4M_r \left[\tan^{-1}\left(\frac{x(\delta+z)}{x^2+a^2+a(\delta+z)}\right) - \tan^{-1}\left(\frac{xz}{x^2+a^2+a(\delta+z)}\right)\right] \quad (2.1)$$

$$H_x(x,z) = 2M_r \log\left(\frac{x^2+(\delta+z+a)^2}{x^2+(z+a)^2}\right) \quad (2.2)$$

Where δ =15 nm is media thickness, a =15 nm is bit length, M_r = 400 emu/cm^3 is remanent magnetization of media, and z_0 = 5 nm is height above the top surface. The remanence magnetization of PMA tip and no PMA tip are considered to be 500 emu/cm^3 and 200 emu/cm^3, respectively.

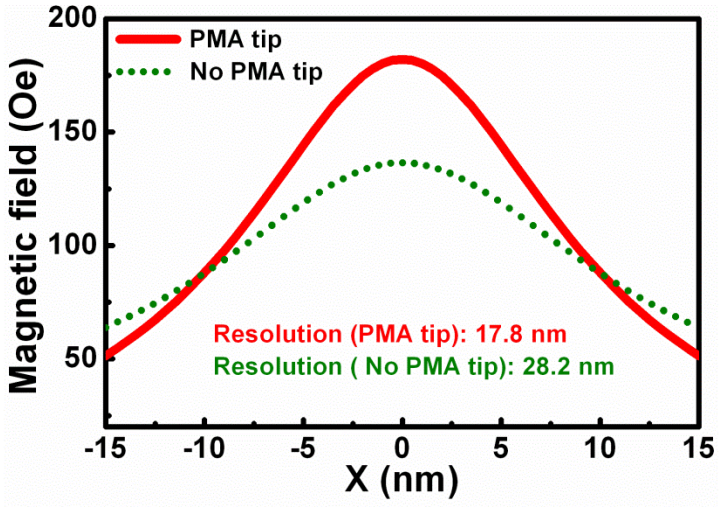

Figure 2.13. Model calculated image response of MFM tips with PMA and no PMA, respectively.

In this calculation we considered 5 magnetic elements for both tips at different height such as 5 nm, 7 nm, 9 nm, 11 nm and 13 nm from the media. The height, radius, and saturation magnetization of both tips are 40 μm, 30 nm and 800 emu/cc, respectively. The image resolution between magnetic moments of tip (μ) and stray fields from the media is calculated from equation 2.3:

$$\begin{bmatrix} F_x \\ F_y \\ F_z \end{bmatrix} = \begin{bmatrix} \partial H_x/\partial x & \partial H_y/\partial x & \partial H_z/\partial x \\ \partial H_x/\partial y & \partial H_y/\partial y & \partial H_z/\partial y \\ \partial H_x/\partial z & \partial H_y/\partial z & \partial H_z/\partial z \end{bmatrix} \begin{bmatrix} \mu_x \\ \mu_y \\ \mu_z \end{bmatrix} \quad (2.3)$$

Figure 2.13 shows the calculated image response of MFM tips. PMA tip response shows a full-width at half maximum (FWHM) of about 18 nm, as compared to a FWHM of only 28 nm in tips with no PMA. The model calculations confirm the potential improvement of resolution when MFM tip with PMA is used.

2.6 Anomalous Hall Effect (AHE) measurement

The Anomalous Hall effect (AHE) has been used for a very long time [32-34], and a lot of works have been done by researchers to understand the physics of this phenomenon. At the first glance, the AHE is the same as ordinary Hall effect in semiconductors or metals: if we put a sample with an electric current into an external magnetic field H in which perpendicular to the current, then there happens a voltage in the direction of perpendicular to current and the magnetic field. This phenomenon is named ordinary Hall effect which is related to the Lorentz force acting on electrons moving in the field H. However, if the electrical current is passed through ferromagnetic materials and simultaneously a magnetic field is applied, because spin orbit interaction between magnetization and electric charge the hysteresis loop of magnetic sample can be obtained.

The conventional magnetic characterization techniques such as: Alternating gradient magnetometer, Magnetic Force Microscopy can only measure one magnetization direction at a time. Moreover, the out-of-plane and in-plane hysteresis loops cannot be obtained using those techniques. Anomalous Hall Effect can, however, distinguish in plane and out of plane magnetization. In addition, this method is useful to measure full hysteresis loop of patterned media even over small area. Thus, in the chapter 6 of this thesis AHE is used to investigate magnetic properties of Capped bit patented media.

2.6.1 Hall bar fabrication and AHE measurements

In our work, Hall effect (HE) measurements were carried out to observe the anomalous and planar hall voltages and to quantify the perpendicular and in-plane components of magnetization and also to measure the full M-H loop of patterned structures. For the AHE measurements, the Hall cross-bar was first lithographically patterned onto thermally oxidized Si substrates using the Karl-Suss mask aligner and a positive-tone photoresist. Materials consisting of the film stack were then deposited into the exposed region followed by a lift-off process. Contact pads were then fabricated in the same manner onto each arm of the Hall bar and finally wire-bonded to a chip carrier for measurement.

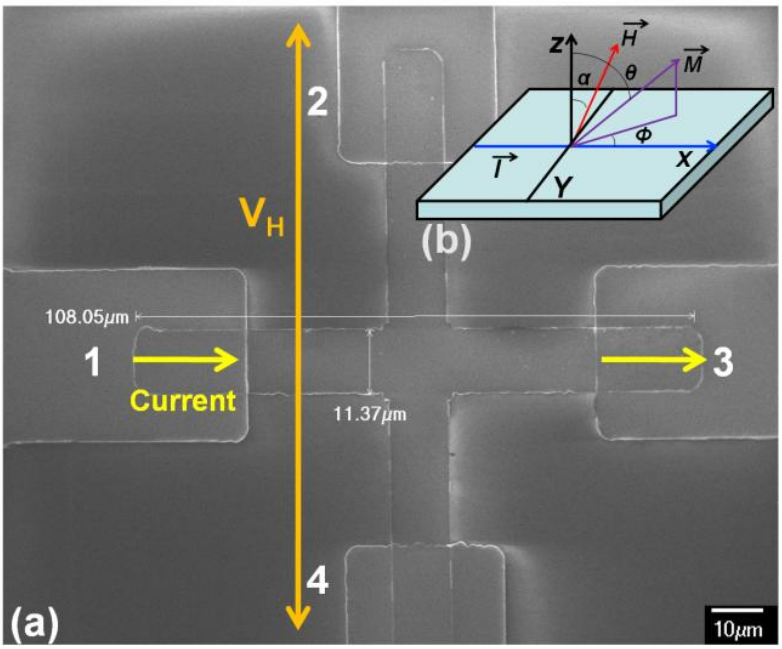

Figure 2.14. (a) SEM image from Hall bar, (b) schematic diagram showing the relative angles between the external magnetic field *H*, Magnetization *M* and the current *I*.

Figure 2.14 shows a typical scanning electron microscopy (SEM) image of a fabricated device ready for AHE measurements. A vibrating-sample magnetometer (VSM) with magnetoresistance (MR) controller was used to perform the AHE measurements. The magnet in the VSM provides a field up to 20 kOe at various angles with respect to the film normal. The MR controller provides a constant current of 2 mA through the Hall bar and measures the resistance in a direction perpendicular to the current flow.

2.6.2 Extracting the Anomalous and Planar Hall voltages

The Hall voltage is obtained by multiplying the measured resistance with the applied current as shown in following equation [35-37]:

$$V_H = \left(\frac{R_H I}{t}\right) H\cos(\alpha) + \left(\frac{\mu_0 R_{SH} I}{t}\right) M\cos(\theta) + \left(\frac{kI}{t}\right) M^2 (\sin\theta)^2 \sin(2\varphi) + V_{offset} \quad (2.4)$$

Where t is the layer thickness, R_H the ordinary Hall coefficient, R_S is the anomalous Hall coefficient and *K* is the planar-Hall coefficient. The in-plane and out of plane magnetization signals extract from following formulas [37-39].

$$V_{out-of-plane} = V_{anomalous} = \frac{1}{2}\left[V_{13,24d}(H) - V_{13,24u}(-H)\right] - \left(\frac{R_H I}{t}\right) Hcos(\alpha) \quad (2.5)$$

$$V_{in-plane} = V_{planar} = \frac{1}{2}\left[V_{13,24d}(H) + V_{13,24u}(-H)\right] - V_{offset} \quad (2.6)$$

The offset voltage arises from misalignment error between the Hall bar and the contact pads, and non-uniformity of magnetic field and temperature. In order to eliminate the offset voltage, a total of eight sets of data were taken: *V*13, 24d, *V*13, 24u. The subscript *u* shows increasing the field [40, 41]. Because the planar-Hall voltage is an even function of magnetization M, when the Anomalous Hall voltage is an odd function of *M*, both can be separated by taking the difference or the sum of the down and up curves.

Summary

In this chapter, we explained the fabrication and characterization methods with their principles as employed to study the different properties of our structures. Since the main objective of our work is trying to understand and minimize the switching filed distribution in patterned media, it is necessary to measure the dipolar interaction between patterned dots. In the next chapter, this effect is discussed based on modeling, simulation and experimental works. Moreover in last part of next chapter, the antiferromagnetically coupled bit patterned media is introduced as one method to reduce the dipolar interaction and hence decrease the SFD.

References

1. N. Broers, J. M. E. Harper and W.W. Molzen, Appl. Phys. Lett. **33**, 392 (1978)
2. S.P. Beaumont, P.G. Bower, T. Tamamura and C.D.W. Wilkinson, Appl. Phys. Lett. **38** (1981), 436.
3. A. Tavakkoli K. G, S. N. Piramanayagam, M. Ranjbar, R. Sbiaa and T. C. Chong, J. Vac. Sci. Technol. B., **29,** 011035 (2011).
4. L. F. Zhang, C. Xu and Y. Q. Ma, Phys. Lett. A, **338,** 373 (2005).
5. Stephen Y. Chou, Peter R. Krauss, and Preston J. Renstrom, Appl. Phys. Lett. **67**, 3114 (1995).
6. B. Heidari, A. Lofstrand, E. Bolmsjo, E. Theander, M. Beck, US Patent App. 20,060/279,025 (2005).
7. E. L. Tan, K. O. Aung, R. Sbiaa, S. K. Wong, H.K. Tan, W. C. Poh, S.N. Piramanayagam, and C. C. Chum, J. Vac. Sci. Technol. B, **27**, 2259 (2009).
8. G. Binning; C.F. Quate and Ch. Gerber, Phys. Rev. Lett., **56**, 930 (1986).
9. L.T. Hansen; A. Kuhle; A.H. Sorensen; J. Bohr and P.E. Lindelof, Nanotechnology, **9**, 337 (1998).
10. M. Sitti, IEEE/ASME Trans. Mech., **9**, 343 (2004).
11. Kovács, A. Kohn, J. Dean, T. Schref, A. Zeltser, and M. J. Carey, IEEE Trans. Magn. **45**, 3873 (2009).
12. J. McMorran, A. C. Cochran, R. K. Dumas, Kai Liu, P. Morrow, D. T. Pierce, and J. Unguris, J. Appl. Phys. **107**, 09D305 (2010).
13. N. Rougemaille, and A.K. Schmid, Eur. Phys. J. Appl. Phys. **50**, 20101 (2010).
14. H. J. Mamin, M. Poggio, C. L. Degen and D. Rugar, Nature Nanotechnol, **2**, 301 (2007).

15. R. B. Proksch, T. E. Schaffer, B. M. Moskowitz, E. D. Dahlberg, D. A. Bazylinski, and R. B. Frankel, Appl. Phys. Lett. **66**, 2582 (1995).
16. A. Wadas and P. Grutter, Phys. Rev. B. **39**, 12013 (1989).
17. R. Sbiaa, K. O. Aung, S. N. Piramanayagam, E. L. Tan, and R. Law, J. Appl. Phys. **105**, 73904 (2009).
18. K. Babcock, V. Elings, M. Dugas, and S. Loper, IEEE Trans. Magn. **30**, 4503 (1994).
19. C. D. Wright and E. W. Hill, Appl. Phys. Lett. **67**, 433 (1995).
20. R. Sbiaa, C. Z. Hua, S. N. Piramanayagam, R. Law, K. O. Aung and N.Thiyagarajah, J. Appl. Phys. **106**, 23906 (2009).
21. H. Saito, J. Chen and S. Ishio, , IEEE Trans. Mag., **35**, 3992 (1999).
22. N. Amos, R. Ikkawi, R. Haddon, D. Litvinov, and S. Khizroev, Appl. Phys. Lett. **93**, 203116 (2008).
23. C. B. Catherine and S. G. C. Adam, J. Phys. D: Appl. Phys. **36,** R198 (2003).
24. Y. Wu, Y. Shen, Z. Liu, K. Li, and J. Qiu, Appl. Phys. Lett. **82**, 1748 (2003).
25. L. Gao, L. P. Yue, T. Yokota, R. Skomski, S. H. Liou, H. Takahoshi, H. Saito, and S. Ishio, IEEE Trans. Magn. **40**, 2194 (2004).
26. S. N. Piramanayagam, M. Ranjbar, R. Sbiaa, A. Tavakkoli KG, and T. C. Chong, Journal of Physica status solidi (RRL) - Rapid Research Letters, **6**, 141(2012).
27. S. N. Piramanayagam, M. Ranjbar, E. L. Tan, R. Sbiaa, and T. C. Chong, J. Appl. Phys. **109**, 07E326 (2011).
28. H. Meng, W. H. Lum, R. Sbiaa, S. Y. H. Lua, and H. K. Tan, J. Appl. Phys. **110,** 33904 (2011).
29. X. M. Yang, S. Xiao, W. Wu, Y. Xu, K. Mountfield, R. Rottmayer, K. Lee, D. Kuo, and D. Weller, J. Vac. Sci. Technol. B **25**, 2202 (2007).
30. M. Mansuripur, IEEE Trans. Magn. **25**, 3467 (1989).

31. D. Rugar, H. J. Mamin, P. Guethner, S. E. Lambert, J. E. Stern, I. Mc-Fadyen, and T. Yogi, J. Appl. Phys. **68**, 1169 (1990).
32. E. H. Hall, Amer. J. Math. **2**, 287 (1879).
33. C. M. Hurd, *The Hall Effect in Metals and Alloys* (Plenum Press, New York, 1972);
34. *The Hall Effect and Its Applications*, edited by C. L. Chien and C. R. Westgate (Plenum, New York, (1979).
35. 1S. Nakagawa, I. Sasaki, and M. Naoe, J. Appl. Phys. **91**, 8354 (2002).
36. S. Das, S. Kong, and S. Nakagawa, J. Appl. Phys. **93**, 6772 (2003).
37. S. Nakagawa, K. Takayama, A. Sato, and M. Naoe, J. Appl. Phys**. 85**,4592 (1999).
38. S. Kumar and D. E. Laughlin, IEEE Trans. Magn. **41**, 1200 (2005).
39. C. Hurd, The Hall Coefficient of Metals and Alloys (Plenum, New York, 1972).
40. *Annual Book of ASTM Standards*, edited by P. C. Fazio *et al. (*ASTM, Philadelphia), Vol. 10.05, p. 116. (1992).
41. S .K. Wong, B. H. Chia, K. Srinivasan, R. Law, E. L. Tan, H. K. Tan, R. Sbiaa, and S. N. Piramanayagam, J. Appl. Phys. **106**, 093904 (2009).

Chapter 3. Investigation of dipolar interactions on switching field distribution bit patterned media

3.1 Introduction

As mentioned in previous chapter, dipolar interactions have an important role to induce wide switching field distributions in bit patterned media. In this chapter, dipolar interactions on square and staggered bit patterned media with 50 nm pitch size and 30 nm dot diameter were investigated from fundamental point view. In addition, we have also extended this study to layers with antiferromagnetically coupled (AFC) structures to see the effect of AFC structures on the SFD in the two geometries [1, 2]. Furthermore, a systematic simulation was carried out to understand the effect of various parameters such as magnetic anisotropy field, saturation magnetization and their distribution, on the SFD of the two lateral configurations.

3.2 Conventional vs staggered BPM configurations

Bit patterned media (BPM) technology has been considered as a promising candidate to overcome the superparamagnetic limit faced by the current granular medium based perpendicular recording technology [3-6]. In BPM, the element to element variation in intrinsic magnetic properties will result in the widening of switching field distribution [7, 8], and will cause an increase in write-in-error. Different magnetic properties were observed to cause the spread in switching field distribution for patterned arrays [1], [7]. Many factors of switching field distribution have been studied such as: materials of continuous film [8], difference in dot size, dot shape [2], and effect of different seedlayers [9]. In addition to the intrinsic properties, the magnetostatic interaction will also contribute to further widening of SFD, especially at high densities. Therefore, SFD is one important issue to be understood and controlled before implementation of BPM technology.

Another problem in implementing BPM is the technological challenge of achieving a high track pitch. Conventionally, bit-patterned media at 1 Terabits per square inch (Tbpsi) will require dots at a pitch of 25 nm, when arranged in a square lattice. This arrangement indicates a track pitch of about 1000 kilo-tracks per inch (ktpi) which is about 3 times the value of track density in products to date. In addition, such narrow track width also requires a reduction in the width of the reader and writer, resulting in sensor noise and writing field limitation issues. A staggered lattice, which is basically a rearrangement of the conventional BPM by causing an offset in the neighbouring tracks, has been proposed in order to overcome such problems [10, 11].

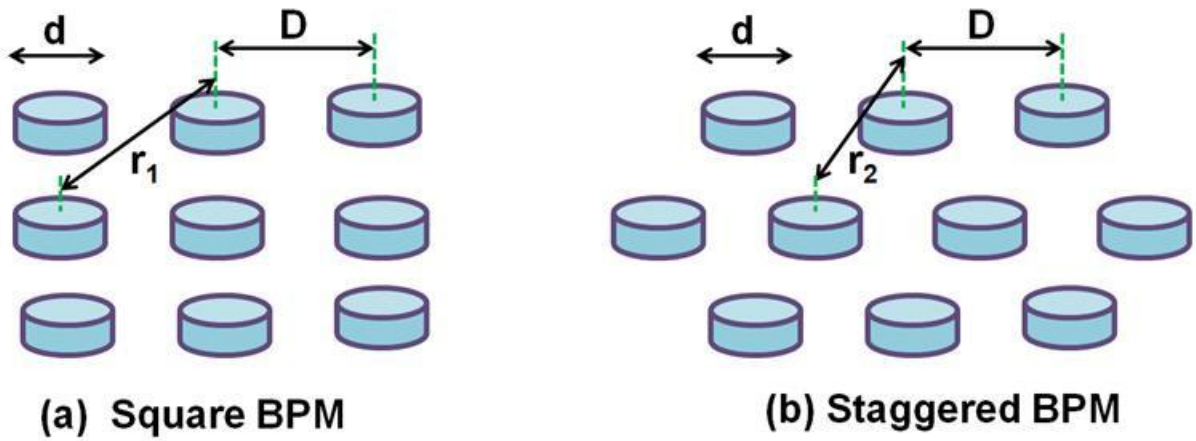

Figure 3.1. Schematics of (a) square and (b) staggered bit patterned media (BPM).

Figure 3.1 shows schematics of (a) square and (b) staggered bit patterned media (BPM), respectively. We consider the same pitch size (D) and dot size (d) to keep constant the areal density for both geometries. However, the number of nearest neighbors and distance between dots is different in the two cases and as a result; the dipolar interaction is also expected to be different.

In staggered scheme, the writer and the reader can cover two tracks and this relaxes the head design requirements. It is interesting to study the SFD of magnetic dots in square and staggered geometries. Figure 3.1 shows that the concerned bit in a staggered lattice has a

different number of nearest neighbours as compared with that in a square lattice BPM. In case of staggered configuration each bit is surrounded with six dots in which they have the same distance from central bit. However, in conventional patterned structure there are 8 bits around the central dot. The four dots which are allocated in cross shape have the same distance from centre, and other four dots in diagonal direction have longer distance from centre. Since dipolar interaction has an inverse proportional ratio to distance, the switching field distributions are different in both cases.

In this chapter, we have investigated the SFD of dots in square and staggered geometries to understand the influence of magnetostatic interaction arising from the differences in the nearest neighbours.

3.3 Magnetic properties of single layer and AFC continuous media

The starting magnetic materials used for patterned media are highly exchanged coupled films obtained by sputtering. Material with high perpendicular magnetic anisotropy such as Co/Pd or CoPt multilayers were considered to obtain media with higher coercivity after patterning. In this chapter two types of magnetic layers such as single layer and antiferromagnetically coupled media were prepared by dc magnetron sputtering. In order to study the effect of dipolar interaction on SFD, patterned islands were fabricated for both media.

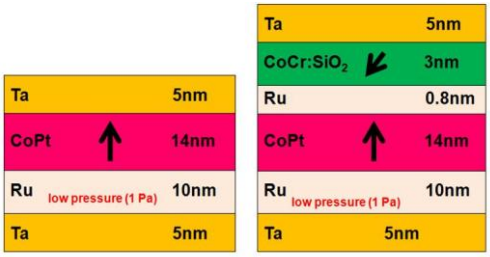

Figure 3.2. Schematics of single layer (left) and AFC structure (right).

The sputtered samples for our study were as following: (A) single layer Si substrate/Ta(5 nm)/Ru(15 nm)/$Co_{80}Pt_{20}$(14 nm) and (B) antiferromagnetically coupled media (AFC): Si substrate/Ta(5 nm)/Ru(15 nm)/$Co_{80}Pt_{20}$(14 nm)/Ru(0.8 nm)/CoCr:SiO_2(3 nm). The Ta and Ru seedlayers help us to achieve a good perpendicular anisotropy [4]. The schematics of both structures are shown in figure 3.2. In addition, the Ru below CoPt layer is deposited at low sputtering gas pressure (1 Pa) to induce high exchange coupled magnetic domains in recording layer.

Therefore, after pattering the patterned islands have high thermal activation volume and can act as single magnetic islands. The Ru layer was deposited between the two recording layers provided the highest antiferromagnetic coupling constant at 0.8 nm. The Ta layer on top of recording layer is used as capping layer to protect from oxidization and corrosion of magnetic layers.

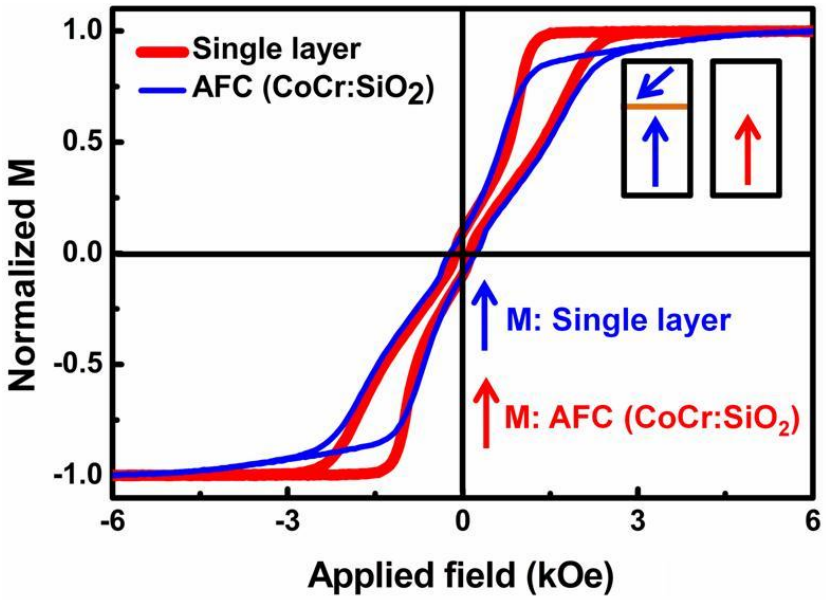

Figure 3.3. Perpendicular hysteresis loop of single layer and AFC media.

Figure 3.3 shows the hysteresis loops of unpatterned samples. In order to achieve a single domain state in the dots after patterning, the films were deposited at low pressure and at room

temperature to induce a highly exchange coupled thin film system. As a result, the coercivity of the samples is not high (about 200 Oe) and all the samples have tilted magnetizations as can be seen from hysteresis loop with a nucleation field in the first quarter because of the demagnetizing field. The sample with CoCr:SiO_2 layer does not show a clear kink as this sample does not have a large anisotropy constant to keep the moment out of plane against the demagnetizing field. While this may appear to be a problem based on the thin films, it will be shown later that this problem vanishes when the samples were patterned as the demagnetizing fields are negligible for patterned dots.

3.4 SFD of conventional and staggered BPM

In order to study the effect of magnetostatic interaction on the switching field distribution (SFD) of nanodots, square (conventional) and hexagonal (staggered) lattice islands were fabricated with a 50 nm pitch size and diameter of 30 nm by using electron beam lithography (EBL) method.

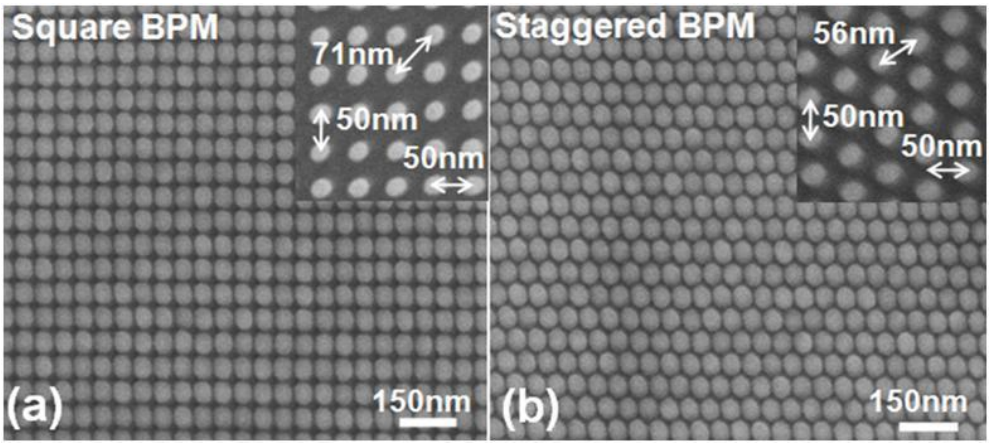

Figure 3.4. SEM images of patterned media in (a) square lattice and (b) staggered lattice configuration for the dots size of 30 nm and a pitch of 50 nm. The insets show schematic of the nearest neighbor distances in the two geometries.

Figure 3.4 shows the scanning electron microscope (SEM) images of (a) square and (b) staggered lattice configurations, respectively which were obtained using a JEOL JSM-7401F

SEM. It can be seen that the pitch size and dot size for both configurations are 50 nm and 30 nm, respectively. However, the distance between the patterned neighbours is different. In case of square lattice configuration the distance between two dots in different rows is 71 nm. On the other hand, the patterned distance in staggered lattice is 56 nm. Therefore, different kinds of magnetostatic interactions exist in samples and it is important to understand their influence on SFD.

Measurement of direct current demagnetization (DCD) or remanent hysteresis curves is one of the methods to calculate the SFD of patterned dots. For this measurement, the square and staggered patterned samples were saturated in large negative field (-19 kOe) direction. Then after, a reversal field was applied perpendicular to the sample. Magnetic force microscopy (MFM) images using high resolution perpendicular magnetic anisotropy MFM tips as mentioned in chapter 2, were carried out to measure the remanent state [1, 8]. As the applied field increased, the magnetizations of patterned dots start to switch. Figure 3.5 shows typical MFM images of the square and staggered BPM for single layer CoPt samples at 6 kOe and 9.5 kOe over an area of 1 μm × 1 μm. These values of field roughly correspond to the beginning of dot reversals (represented by brown dots) and yellow (brighter) dots indicate the regions that were not reversed. A series of MFM images, measured at remanence after applying different reversal fields, were used to measure SFD of the dots in square and staggered geometries.

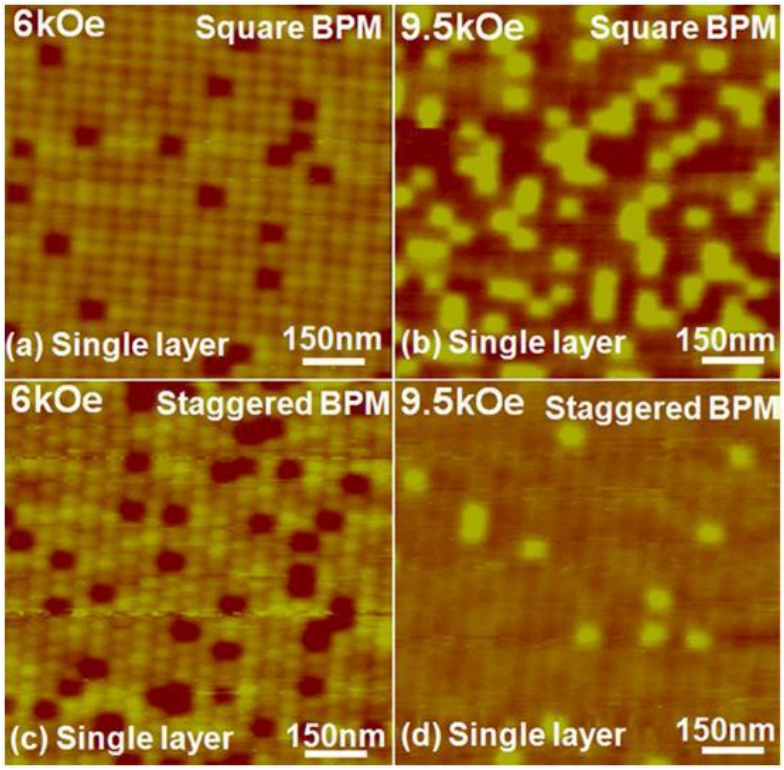

Figure 3.5. MFM images in square-lattice BPM at (a) 6 kOe, (b) 9.5 kOe and staggered BPM at (c) 6 kOe, (d) 9.5 kOe reversal field for the single layer patterned media, respectively.

The DCD curves were obtained by counting the number of reversed dots from the magnetic force microscopy (MFM) images. The curve, thus obtained, was differentiated to obtain a bell-shaped curve. The full-width at half-maximum (FWHM) of this curve is denoted in the subsequent discussions by the symbol ΔH^e (experimental SFD). Figure 3.6 shows the percentage of dots that reversed their magnetization at different reversal fields. It can be noted that the reversal starts happening at lower reversal fields for the dots in the staggered lattice than in the square lattice. Moreover, saturation fields for staggered and square lattices occur nearly from 9.5 kOe and 11 kOe, respectively. It has to be highlighted that the SFD of the two structures has been investigated in the same samples but at two different locations.

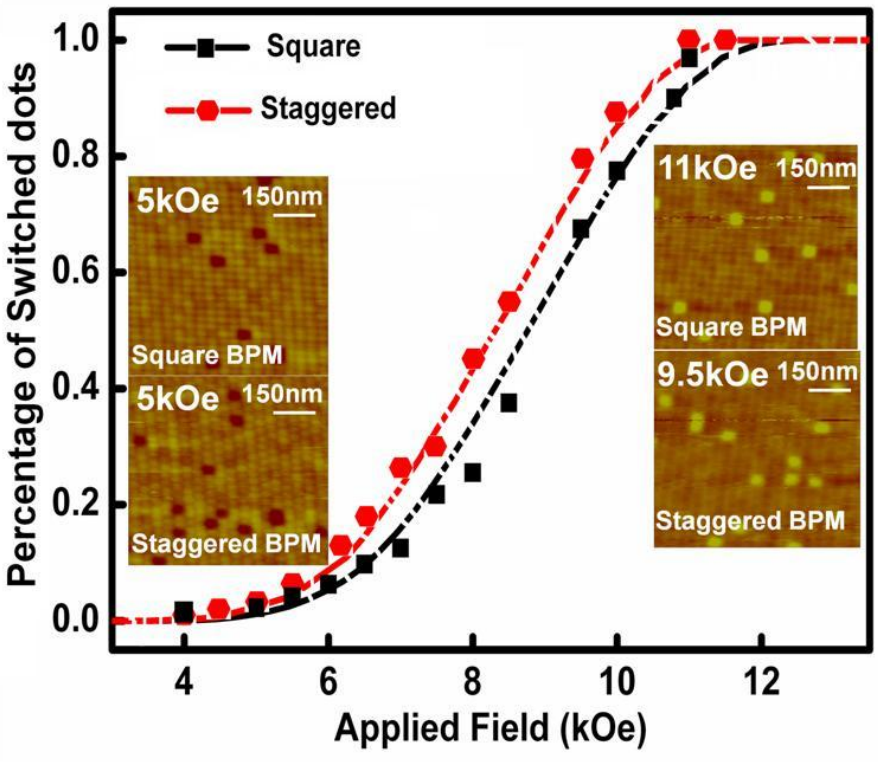

Figure 3.6. Demagnetization curves (experiment and simulation) of single layer patterned media with 50 nm pitch for square and staggered lattices. (The inset shows schematic of the simulated patterns.)

Considering that the samples have been sputtered using a production sputtering machine with a good spatial homogeneity, the observed differences are affirmatively arising from the difference in the lateral configurations. The reason for the observed difference in SFD between square and staggered lattices can be understood to arise from the different magnetostatic interactions in the two configurations having different number of nearest neighbours. For the staggered structure, there are two neighbours within 50 nm distance and four neighbours at a distance of 56 nm. That means, within a distance of 56 nm, there are six nearest neighbours. Whereas, for a square lattice, there are four neighbours at 50 nm distances and the four next nearest neighbours are at a distance of 71 nm. Therefore, it is believed that the resulting dipolar interactions are different in the two configurations, resulting in different SFDs. In section 3.6 similar measurements were also extended to the media with AFC layers and their effects on SFD of both configurations.

3.5 Effect of AFC configuration on SFD

In order to further understand the effect of magnetostatic interactions, we investigated the effect of synthetic antiferromagnetically coupled (AFC) magnetic recording layers [1] as a method to reduce the switching field distribution of square and staggered patterned media. This section describes such an investigation.

It is well known that the superparamagnetism limits the magnetic data storage density. In 2000, a new media structure namely an antiferromagnetically coupled recording medium, has been proposed as a way to mitigate the effects of thermal decay and to extend longitudinal recording technology at higher areal density [12, 13]. A schematic of synthetic perpendicular AFC layers is shown in figure 3.7. The AFC recording medium consists of two ferromagnetic layers separated by very thin non-magnetic layer such as Ru. The thicker layer and thinner layers are called recording layer (RL) and stabilizing layer (SL), respectively. The magnetization (**M**) of ferromagnetic layers are aligned antiferromagnetically coupled via *Ruderman-Kittel-Kasuya-Yosida (RKKY)* like exchange interaction [15] across the Ru layer. In synthetic AFC media, due to the interlayer antiferromagnetic exchange coupling, the effective magnetic switching volume $K_U V_{\text{eff}}$ will be in the range of $K_U V_1 \leq K_U V_{\text{eff}} \leq K_U V_1 + K_U V_2$, where $K_U V_1$ and $K_U V_2$ are the anisotropy energies of the grains in recording layer and stabilizing layer, respectively. The effective magnetic areal moment of the AFC medium is $M_r t = M_r t_1 - M_r t_2$, therefore by reduction of effective remanent moment, the dipolar interactions will be reduced and consequently the SFD can be minimized.

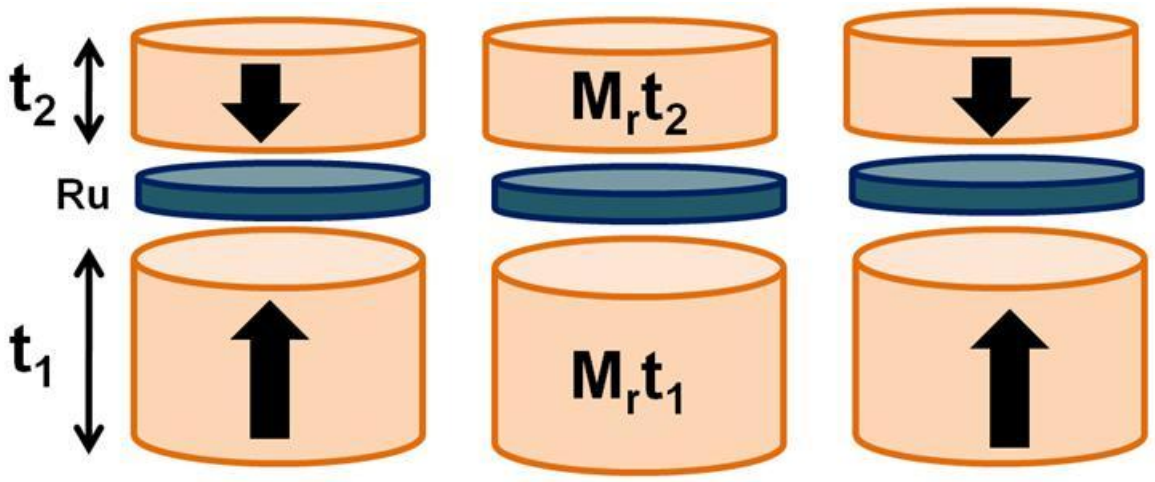

Figure 3.7. A schematic of synthetic perpendicular AFC layers. t_1 and M_rt_1 are thickness and areal remanent magnetic moment of recording layer. Additionally, t_2 and M_rt_2 are thickness and areal magnetic moment of stabilizing layer, respectively.

In AFC structure, the exchange coupling constant between two layers is an important parameter. The antiferromagnetic exchange coupling constant *J* can be estimated using the following formula 1: [14]

$H_{ex} = J/M_s t$ (3. 1)

Where, in formula 3.1, H_{ex} (Oe) is the effective surface exchange energy density, M_s is the saturation magnetization (emu/cm^3), *J* (erg/cm^2) is the antiferromagnetic interlayer exchange energy between two ferromagnetic layers and *t* is the thickness (nm) of magnetic stabilizing layer.

In order to measure exchange coupling field for AFC structure in this work, a differentiation from minor loop carry out. The exchange field was found 2.5 kOe and J was obtained 0.13 (erg/cm^2) for CoCr:SiO_2 layer thickness 3 nm.

In order to investigate the effect of AFC layer on SFD, the AFC patterned medium was fabricated using the same method as the one to make single layer (CoPt) BPM. For this purpose, series of MFM images were taken to count the reversal dots and calculation of DCD

curves. Typical MFM images of the square and staggered lattice samples at 6 and 9.5 kOe over an area of 1 μm × 1 μm are shown in figure 3.8. Although the dots were fabricated at a pitch of 50 nm and the dot diameter is smaller than 50 nm, the reversed dots appear to be much bigger. This is because of the reduced field from the spacing between the dots as well as the regions where the magnetic field flows sideways to the reversed bit.

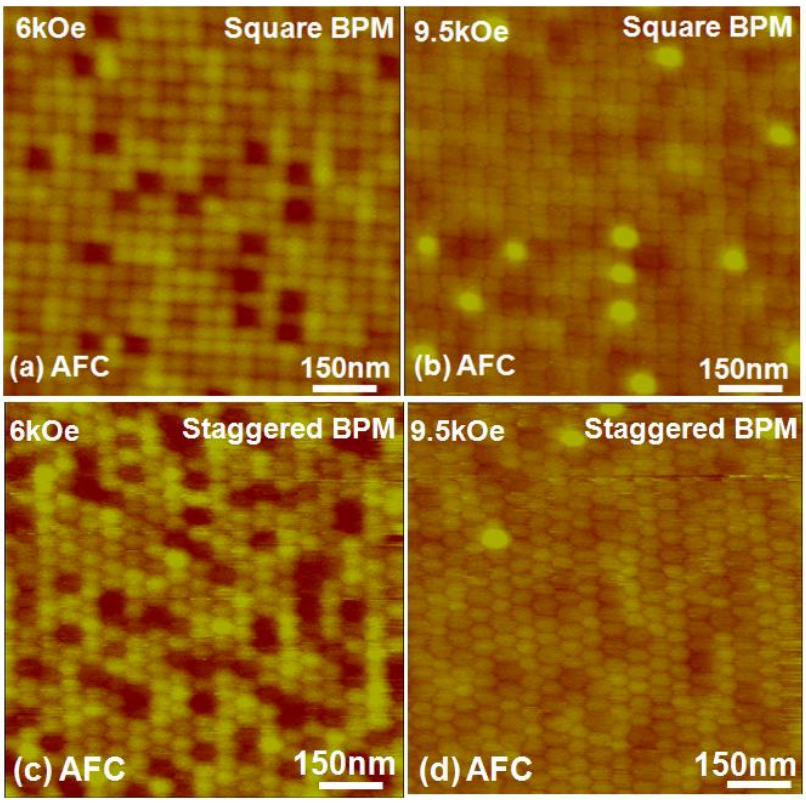

Figure 3.8.MFM images in square BPM at (a) 6 kOe, (b) 9.5 kOe and staggered BPM (c) 6 kOe, (d) 9.5 kOe reversal field for the AFC patterned media, respectively.

Figure 3.9 (*a*) shows the normalized magnetization taken from the number of reverse dots divided by the total number for the media with single layers and AFC media. It can be noted that the reversal starts at lower reversal fields for the dots in the staggered BPM compared with the case of square lattice. The width of the switching curve (SFD) obtained by differentiating this curve and measuring the FWHM (ΔH^e) of this curve, is shown in figure 3.9(*b*). For square lattice, the SFD is narrower and appears to be symmetric around the

coercive field. However, for the staggered lattice, the SFD shows broadening at smaller applied fields. From the fit of the derivative of the plots in figure 3.9(*a*) to a Gaussian distribution, the (SFD/H_c) were found to be 0.36 and 0.48 for the square and staggered lattice, respectively.

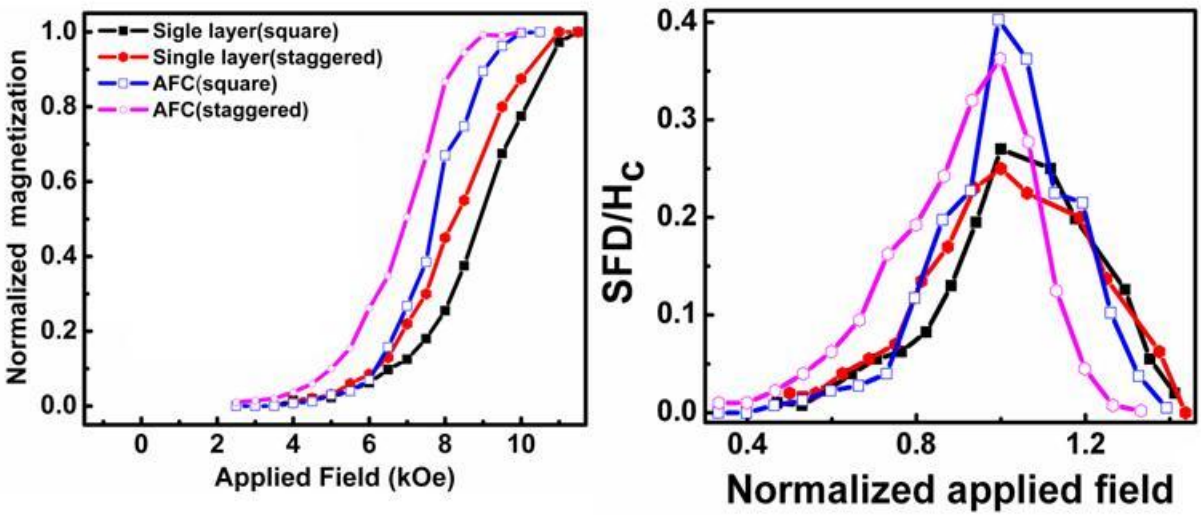

Figure 3.9.SFD of patterned media with single layer and AFC structures. (a) Percentage of switched dots and (b) normalized SFD with 50 nm pitch for square and staggered lattices.

As mentioned earlier, the SFDs of the two structures have been investigated in the same samples but at two different locations. Therefore, the observed differences are mainly arising from the different lateral configurations which lead to different magnetostatic interactions in the two configurations. In order to have a better understanding about the effect of dipolar interactions on SFD of both configurations, we calculate the exact value of dipolar fields in square and staggered bit patterned media based on modeling computations as will be discussed in next section.

3.6 Modeling computations of dipolar interactions

To understand the basic physics behind the experimental data on switching field distribution of square and staggered BPM, we have conducted a systematic modeling

computation. Therefore, to get the magnetization configurations for magnetic islands when they face an external applied magnetic field, the effective field experienced by the system needs to be calculated based on the following energy terms: the magneto-crystalline anisotropy energy, the exchange coupling energy, the Zeeman energy and dipolar energies.

3.6.1 Magneto-Crystalline Anisotropy Energy

Due to the lattice arrangement of the ferromagnetic materials, the internal magnetization possesses energy minima along some directions and unstable energy maxima along other directions. The minimum energy axis is called 'easy' axis. Magnetocrystalline anisotropy is the energy necessary to rotate the magnetic moment from the easy axis to the hard axis. The phenomenon of hard and easy axis arises from the interaction of the spin magnetic moment with the lattice (Spin-orbit coupling) under zero applied field, atomic dipole moments will tend to align along the direction which minimize the free energy of the spin. Different materials have different direction of easy axis. For cubic crystals, the magneto-crystalline energy density is given by following formula:

$$E_a = K_1(\alpha_1^2\alpha_2^2 + \alpha_2^2\alpha_3^2 + \alpha_3^2\alpha_1^2) + K_2\alpha_1^2\alpha_2^2\alpha_3^2 \qquad (3.2)$$

Where a_i is the different cosines of **M** with respect to crystal axes, K_1 is constant and much bigger than K_0 and K_2. From the equation, we can see in figure 3.10 that the cube edges are the easy axis of direction of magnetic moment while the body diagonals being the hard directions of magnetic moments. The highest energy bulges are in directions perpendicular to the cubic faces ([001, 010, 100]). The lowest energy dimples are along the body diagonals ([111]). In the absence of the applied magnetic field, the magnetic moments of the particles tend to align themselves to the direction which makes the magnetostatic energy minimum, this direction is called the easy direction, briefly, and magnetic anisotropy shows how the

magnetic properties depend on the direction of measuring the magnetization. There are several types of anisotropy and the most common one is the magnetocrystalline anisotropy.

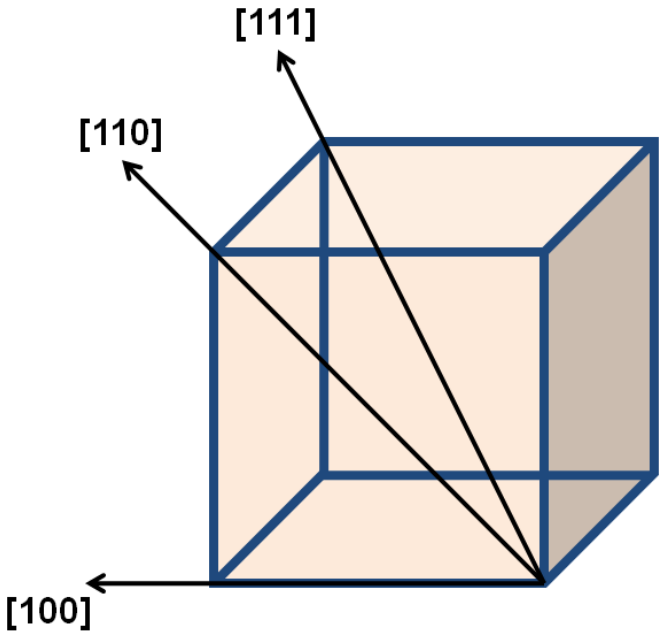

Figure 3.10. Magnetocrystalline anisotropy direction in a cube lattice.

When single domain particles are magnetized to saturation state, the magnetization has an easy axis along which it prefers to stay. In this case, the total internal energy is minimum. Rotation of the magnetization vector away from an easy axis is possible only by applying an external magnetic field. Thus, the magnetic energy is direction-dependent, and this kind of energy is called magnetic anisotropy energy.

3.6.2 Exchange Energy

The exchange energy tries to align the magnetic moments parallel to each other. Basically, this energy is originating from the quantum mechanical exchange coupling effect between adjacent spins. In the case of a continuous magnetization distribution, the exchange energy density can be written as following:

$$E_{ex} = -2JS_1.S_2 \qquad (3.3)$$

Where J is the exchange coupling constant and S_1 and S_2 are the spin vectors. It can be noticed that the exchange energy is at a minimum while electronic spins are aligned parallel or anti-parallel and it depends on the details of the crystal structure (that determines the size and sign of the exchange integral).

3.6.3 Zeeman Energy

Zeeman energy is the energy which refers to the energy of a magnetic moment under the presence of an externally applied magnetic field. The related energy equation is as following:

$E_{ze} = -M.H$ (3. 4)

Where *H* is the applied magnetic field and *M* is magnetic moment of structure.

3.6.4 Demagnetization Energy

Normally, when a ferromagnetic material magnetized by external applied magnetic field, other internal field will be generating inside of magnetic volume. This field is opposite of external field which resists further increases in the magnetization. This opposing field is named the demagnetization field (H_d). H_d is proportional to the magnetization of the structure and is sensitive to the shape. For example, for a simple sphere, the demagnetizing field is given by:

$H_d = -N.M$ (3. 5)

Where *N* is a demagnetizing factor determined by the shape. In fact, the demagnetizing factor depends on the orientation of **M** within the crystal and therefore is a tensor for review of tensors.

Now we can write the total energy density of each magnetic structure which is the summation of all the above energy terms:

$E_{tot} = E_{an} + E_{ex} + E_{ze} + E_d$ (3. 6)

3.6.5 Calculation of dipolar interactions for square and staggered BPM

During the discussion about switching field distribution of square and staggered media, it was emphasized that the dipolar interaction has an important role in the SFD. Therefore, it is crucial to calculate real value of dipolar interactions and compare its effect on SFD of both configurations. Hence, we consider dipolar field as the most important energy term from formula 6 for patterned islands.

In order to better understand the effect of different configurations and saturation magnetization on dipolar interaction between the bits and consequently on SFD, dipolar field for different configurations was calculated for different values of M_S using the following equation [12]

$$H_{dip} = M_s h_d \sum_{i \neq j} \frac{3(\hat{r}_{ij}.\hat{m}_{ij})\hat{r}_{ij} - \hat{m}_j}{\hat{r}_{ij}^{\,3}} \qquad (3.7)$$

Where H_{dip} is the dipolar field, M_s is the saturation magnetization, $\hat{r}_{ij}$ is the unit vector pointing from dipole moment m_i to m_j, $\hat{m}_j$ is the unit vector of moment m_j and $\hat{r}_{ij} = \frac{r_{ij}}{a}$. h_d is a ratio factor which depends on the geometry of the dots and it is a constant. The dipolar interaction between the bits can be calculated in two different manners. First, when all the magnetic bits are saturated and we have maximum dipolar interaction. Second, when magnetization of bits are half up and down in a symmetric system in which we have minimum dipolar interaction. Then by calculating the difference (simulated SFD: ΔH^s /2) between in these two cases, we can correlate it to the experimental SFD (=ΔH^s).

Figure 3.11 shows H_{dip} and ΔH^s as a function of M_s. ΔH^s is equivalent to the SFD arising from dipolar fields alone. It was observed that dipolar interaction in staggered BPM is stronger than square BPM (for larger values of saturation magnetization). It can also be seen that the rate of change of SFD with saturation magnetization for staggered lattice is higher.

It has to be highlighted that the calculation only considers the interaction of the concerned dot with the neighbouring dots but ignores the interaction between the neighbouring dots themselves. In addition, it must also be mentioned that the difference in the non-zero dipolar field when half of the dots are magnetized in opposite directions could explain the slight difference in the coercivity between the two samples. The additional factors for the difference in the coercivity could also arise from the ion-milling induced effects on switching field.

A point that needs to be mentioned from the applied perspective is the following: although staggered lattice structure may help us to improve the track density in bit patterned media recording, it results in a wider SFD, especially producing dots with a lower writing field than is possible in square lattice configuration. Therefore, adjacent bit erasure may be taken into consideration when choosing a staggered structure. This is a significant issue compared with a square lattice configuration, as the linear density of staggered patterned media will be double the linear density of square lattice patterned media and write-synchronization would be more stringent.

Therefore, implementation of staggered patterned media needs consideration of these challenges. Checker-board type patterned media, where the track direction lies on the diagonal of the square lattice media, may be a better alternative to overcome this problem [11, 17–19].

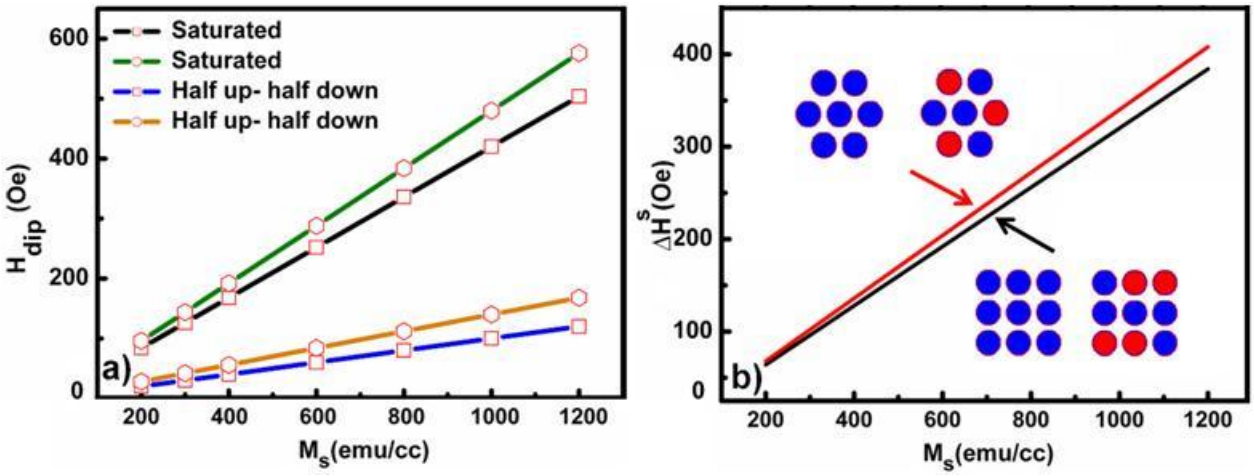

Figure 3. 11. The values of dipolar field H_{dip} and ΔH^s versus saturation magnetization obtained from modeling of the staggered and square BPM in various magnetization states (as shown in the inset—all saturated or half-up, half-down). ΔH^s is the difference in H_{dip} between the two configurations.

3.7 Micromagnetic simulation of SFD for staggered and square bit patterned media

In order to further understand the effect of dipolar coupling on SFD, we also carried out micromagnetic simulation using a commercial software Advanced Recording Model (ARM). Bit patterned media for both the staggered and square configurations were simulated with a dot size of 30 nm, pitch of 50 nm, 14 nm in thickness and schematics of square and staggered bit-patterned media.

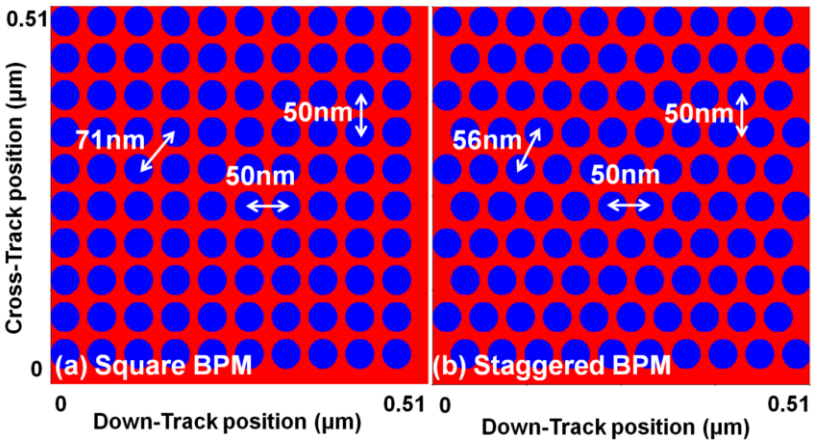

Figure 3.12. Simulated square and staggered geometries with 50 nm pitch size and 30 nm dot size using ARM micromagnetic simulation software.

Figure 3.12 shows a simulated geometry for (a) square and (b) staggered configurations, respectively. After several times running simulation to achieve closer results with experiments, the easy axis dispersion, anisotropy field H_K, saturation magnetization M_S and exchange constant A were fixed at 4°, 12 kOe, 650 emu cm^{-3} and 6×10^{-7} erg cm^{-1}, respectively. The standard deviations in σ_{Ms} and σ_{Hk} were varied in order to fit the SFD for the two configurations. Best fitting as shown in figure 3.13, was obtained for σ_{Hk} = 15% in both the samples. The simulation results as shown in figure 3. 13 also indicate that the difference arises from the magnetostatic interaction.

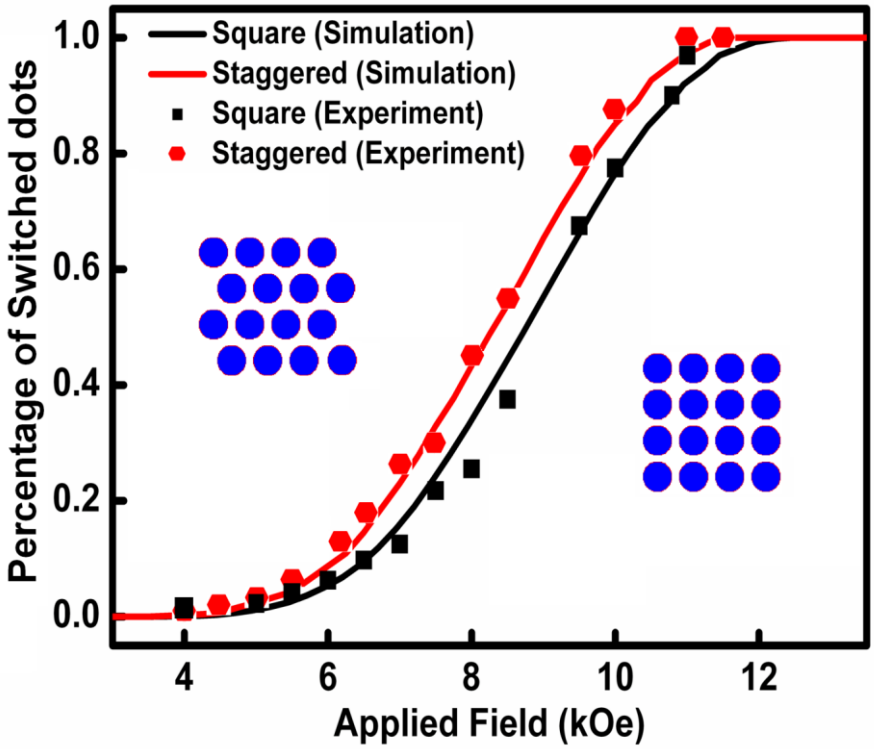

Figure 3. 13. Percentage switching dots for both square and staggered lattices based on simulation and experimental results.

From the simulation and experimental results, it can be highlighted that the coercivity of media in the two configurations is different by about 500 Oe. There are a few reasons for this observation: (a) The MFM measurement by magnetizing the sample in a magnetometer

externally is an exhaustive exercise and hence the measurements were made in steps of 500 Oe. So, one might say that the difference is not more than a data point on the x-axis. (b) Our modeling shows that the dipolar field (when the neighbors are with magnetization in half-up and half-down directions) is about 100 Oe. (c) There might still be some differences in the ion-milling induced damages to the boundary of the bit-elements in the two configurations, affecting slightly the coercivity.

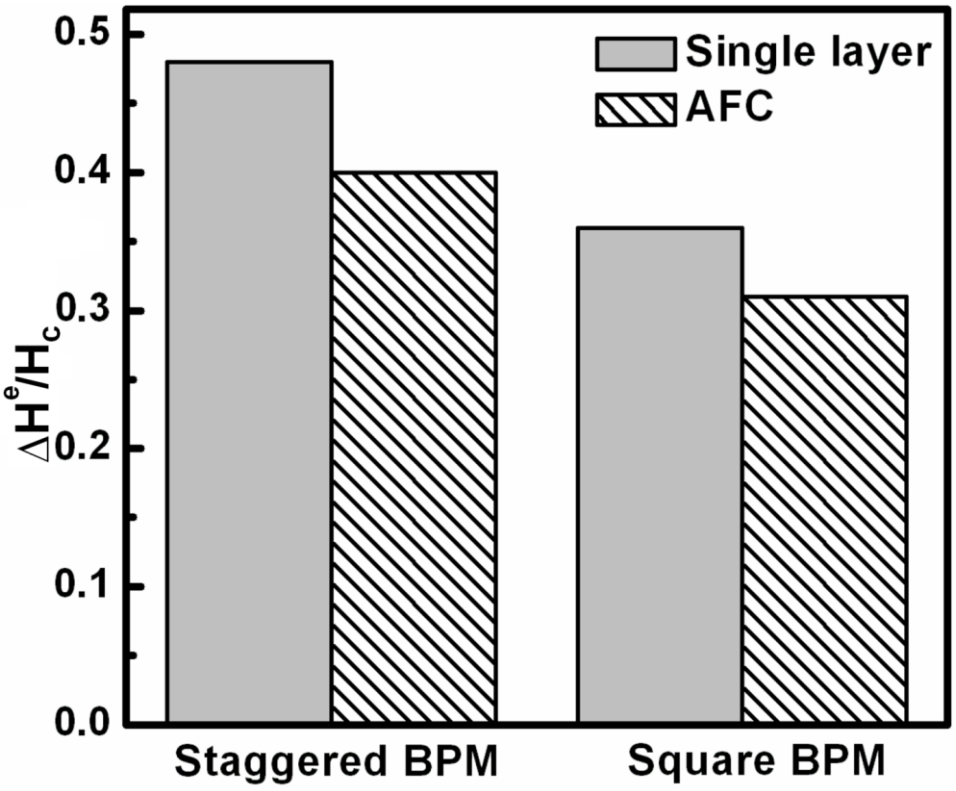

Figure 3. 14. Comparison of experimental $\Delta H^e/H_c$ for patterned media with single layer and AFC structures with 50 nm pitch for square and staggered lattices.

Figure 3.14 shows a comparison of switching field distribution (ΔH^e) in single-layered and AFC sample cases. The ΔH^e is experimental switching field measured from DCD curve. It means that a series of MFM images measured at remanence after applying different reversal fields to measure SFD. After derivation from the DCD curve, full width of half maximum is

as ΔH^e. As we mentioned the method of calculating of ΔH^s in question 4.7, we can find that the ΔH^s and ΔH^e are the same.

It can be noted the normalized SFD ($\Delta H^e/H_c$) obtained from the experimental data for both square (0.32) and staggered (0.4) lattices in the case of AFC bit patterned media are smaller than the single layer. Although normalized SFD of staggered BPM is still wider than squarelattice for both magnetic structures, AFC shows a reduced SFD [20-23]. This is due to the reduction in effective remanent magnetic moment in AFC structures and can help to minimize the dipolar interactions and SFD.

Summary

In this chapter, the effect of magnetostatic interactions on the SFD of nanodots was investigated experimentally using patterned media fabricated in two geometries: square and hexagonal lattice configurations. Micromagnetic simulation was described and a fit of experimental results to the simulation was made to understand the observed trends. In addition, magnetic layers with an antiferromagnetic coupling configuration were also studied in the two geometries.

It was observed that the SFD was wider in the staggered (hexagonal) lattice in comparison with that of the square lattice, explained to be arising from the difference in magnetostatic interaction. SFD of AFC dots was also studied as the AFC configuration can minimize the magnetostatic interaction. It was found that SFD is smaller in AFC patterned media in both the configurations due to reduced magnetostatic interactions. Based on these results, the focus in chapters 4 and 5 will be on our first approach to reduce the SFD by tailoring the design of stabilizing layer in AFC media to achieve anti parallel magnetization after pattering.

References

1. S. N. Piramanayagam, K. O. Aung, S. Deng and R. Sbiaa, J. Appl. Phys. **105,** 07C118 (2009).
2. E. E. Fullerton, D. T. Margulies, M. E. Schabes, M. Carey, B. Gurney, A. Moser, M. Best, G. Zeltzer, K. Rubin, H. Rosen and M, Doerner, Appl. Phys. Lett. **77,** 3806 (2000).
3. B. D. Terris and T. Thomson, J. Phys. D: Appl. Phys.**38,** R199 (2005).
4. S. N. Piramanayagam, J. Appl. Phys. **102,** 011301(2007)
5. R. Sbiaa and S. N. Piramanayagam, Recent Patents on Nanotechnology. **1,** 29 (2007).
6. D. Weller, L. Folks, M. Best, E. E. Fullerton, B. D. Terris, G. J. Kusinski, K. M. Krishnan and G. Thomas, J. Appl. Phys. **89,** 7525 (2001).
7. Y. Kitade, H. Komoriya and T. Maruyama, IEEE Trans. Magn. **40,** 2516 (2004).
8. M. Ranjbar, S. N. Piramanayagam, D. Suzi, K. O. Aung, R. Sbiaa, Y. S. Key, S. K. Wong and T. C. Chong, IEEE Trans. Magn. **46,** 1787 (2010).
9. J. M. Shaw, W. H. Rippard, S. E. Russek, T. Reith and C. M. Falco, J. Appl. Phy. **101,** 023909 (2007).
10. H. J. Richter, A. Y. Dobin and D. K. Weller, US Patent US2007/0258161/A1 (2007).
11. M. Ranjbar, A. Tavakkoli K. G, S. N. Piramanayagam, K. P. Tan, R. Sbiaa, S. K. Wong and T. C. Chong, J. Phys. D: Appl. Phys. **44** 265005 (2011).
12. E. N. Abarra, A. Inomata, H. Sato, and Y. Mizoshita, Appl. Phys. Lett., **77**, 2581 (2000).
13. E. E. Fullerton, D. T. Marguiles, M. E. Schabes, and Doerner, Appl. Phys. Lett., **77**, 3806 (2000).
14. S. S. Parkin, N. More, and K. P. Roch, Phys. Rev. Lett. **64**, 2304 (1990).
15. Y. J. Chen, T. L. Huang, S. H. Leong, S. B. Hu, K. W. Ng, Z. M. Yuan, B. Y. Zong, J. Z. Shi, S. K. Hendra , B. Liu and V. Ng, J. Appl. Phys. **105,** 07C105 (2009).

16. R. Sbiaa, K. O. Aung, S. N. Piramanayagam, E. L. Tan and R. Law, J. Appl. Phys. **105,** 073904 (2009).
17. V. Parekh, E. Chunsheng, D. Smith, A. Ruiz, J. C. Wolfe, P. R. Hoeft, E. Svedberg, S. Khizroev and D. Litvinov, Nanotechnology. **17,** 2079 (2006).
18. P. Krone, D. Makarov, T. Schrefl and M. Albrecht, J. Appl. Phys. **106,** 103913 (2009).
19. O. Hellwig, T. Hauet, T. Thomson, E. Dobisz, J. D. Risner-Jamtgaard, D. Yaney, B. D. Terris and E. E. Fullerton, Appl. Phys. Lett. **95,** 232505 (2009).
20. O. Hellwig, J. K. Bosworth, E. Dobisz, D. Kercher, T. Hauet, G. Zeltzer, J. D. Risner-Jamtgaard, D. Yaney and R. Ruiz, Appl. Phys. Lett. **96,** 052511 (2010).

Chapter 4. Control of switching field distribution with antiferromagnetically coupled patterned media

4.1 Introduction

In chapter 3, the effect of magnetostatic interaction, which is one of the several factors that contribute to a wider switching field distribution (SFD) in bit patterned media, was investigated from a fundamental point of view. Moreover, antiferromagnetically coupled (AFC) bit patterned media was introduced as a first approach to reduce the SFD. However, the details of using AFC configurations were not discussed in detail in the previous chapter.

As the observation of AFC state at remanence is crucial to reduce the SFD, it is necessary to study the conditions at which the AFC state will be observed. Therefore, in this chapter AFC patterned media is studied in two aspects with emphasis placed on the effect of the top layer coercivity, which will determine the remanent moment (M_r) and hence the dipolar interaction. In the first aspect, the effect of pattering is discussed on stabilizing layer with different granularities. On the contrary, in the second aspect the effect of patterning on the stabilizing layers with different magnetic anisotropy constant such as CoPt and CoCr:SiO_2 layers have been studied to achieve AFC state at remanent magnetization.

4.2 Antiferromagnetically coupled patterned media at remanent state

As mentioned earlier, switching field distribution is one of the critical issues for writing in bit patterned media for high areal densities. It is well known that the SFD arises from extrinsic parameters such as, variations in size, shape, position of bits which are coming from fabrication process, and also intrinsic parameters such as, anisotropy constant (K_u), easy axis dispersion, exchange, and magnetostatic interaction. With the antiferromagnetically coupled structure, the magnetostatic interaction can be tailored to understand and reduce SFD. In AFC

structure, two ferromagnetic layers are separated with nonmagnetic thin film as a spacer layer. In this configuration magnetization direction of thicker ferromagnetic layer (recording layer) is opposite to that of thinner ferromagnetic layer (stabilizing layer) [11, 12]. Figures 4.1a and 4.1b show that schematic typical hysteresis loop of antiferromagnetically coupled and ferreomagnetically coupled bit patterned media at remanent state, respectively.

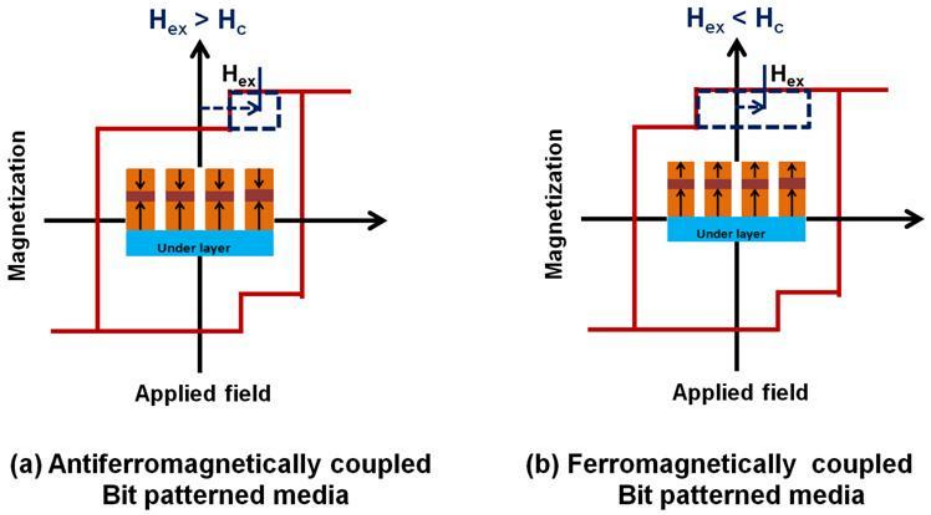

Figure 4. 1. (a) Typical hysteresis loop of antiferromagnetically coupled bit media, (b) schematic of ferromagnetically coupled bit patterned media at remanent state.

It can be noticed that, if the exchange coupling field becomes smaller than coercivity of stabilizing layer after patterning, the AFC configuration may not be achieved at remanent state. Therefore, In order to achieve AFC at remanence, it is necessary that the exchange coupling field (H_{ex}) acting on the thinner layer be greater than its coercivity [13].

With this objective in our mind, antiferromagnetically coupled (AFC) patterned media were studied with emphasis placed on the effect of granularity on the top layer coercivity , which will determine the M_r and hence the magnetostatic interaction on the SFD which might lead to several configurations for the top and bottom layer magnetization and hence a variation in the SFD.

4.2.1 Stabilizing layer with different granularities

Since the magnetostatic interaction is proportional to the remanent moment and writability is inversely proportional to the saturation magnetization, the concept of antiferromagnetically coupled patterned media have been proposed to minimize the SFD arising from magnetostatic interactions without sacrificing writability/thermal stability. In order to achieve AFC at remanence, it is a prerequisite that the exchange coupling field (H_{ex}) acting on the thinner layer be greater than its coercively. Whereas such criterion is achieved in well-designed AFC media, it is also likely that this condition may not be met at certain circumstances. This is especially so, as it has been observed by several researchers that the coercivity of a patterned structure is much greater than that in the continuous film [14-17]. Therefore AFC at remanence may not be achieved if proper understanding is not developed.

In order to provide the criteria $H_c<H_{ex}$ and reduction in coercivity of thinner layer after patterning, one way is to reduce the coercivity of the stabilizing layer. The coercivity of the stabilizing layer can be reduced if the layer is made granular and if the grains are superparamagnetic. The granularity of the film in the stabilizing layer can be varied by varying the sputter gas pressure during the deposition. For lower pressures (less than 1 Pa), the film will be continuous and for pressures above 5 Pa, granularity is expected. With this objective, samples of the types; Si substrate/Ta(5nm)/Ru(15nm)/ CoCrPt:SiO_2 (15 nm) /Ru(0.8 nm)/CoCrPt:SiO_2 (3nm) were prepared by dc magnetron sputtering using a BPS Circulus M12 sputtering system as shown in figure 4.2. The Ta and Ru layers below the recording layers (CoCrPt:SiO_2) help to induce good perpendicular anisotropy in the CoCrPt:SiO_2 layers. The Ru layer in between the two recording layers provides the highest antiferromagnetic coupling constant at 0.8 nm. Unlike the conventional AFC media, where the thinner layer is usually at the bottom, the design investigated in this study had an inverted

AFC structure [13, 17]. In the inverted AFC structure, the thinner layer is at the top, which eliminates the growth related effects and results in a better anti-ferromagnetic coupling. The thickness of the CoCrPt:SiO_2 bottom layer is 15 nm, and that of the top layer is 3 nm. The CoCrPt:SiO_2 bottom layer was sputtered at a lower pressure (0.5 Pa) without additional oxygen, in order to obtain an exchange coupling as high as possible. But the pressure during the deposition of the CoCrPt:SiO_2 layers at the top was varied from 0.5 Pa to 10 Pa as a way to control the magnetization reversal behavior of top layer grains and their coercivity.

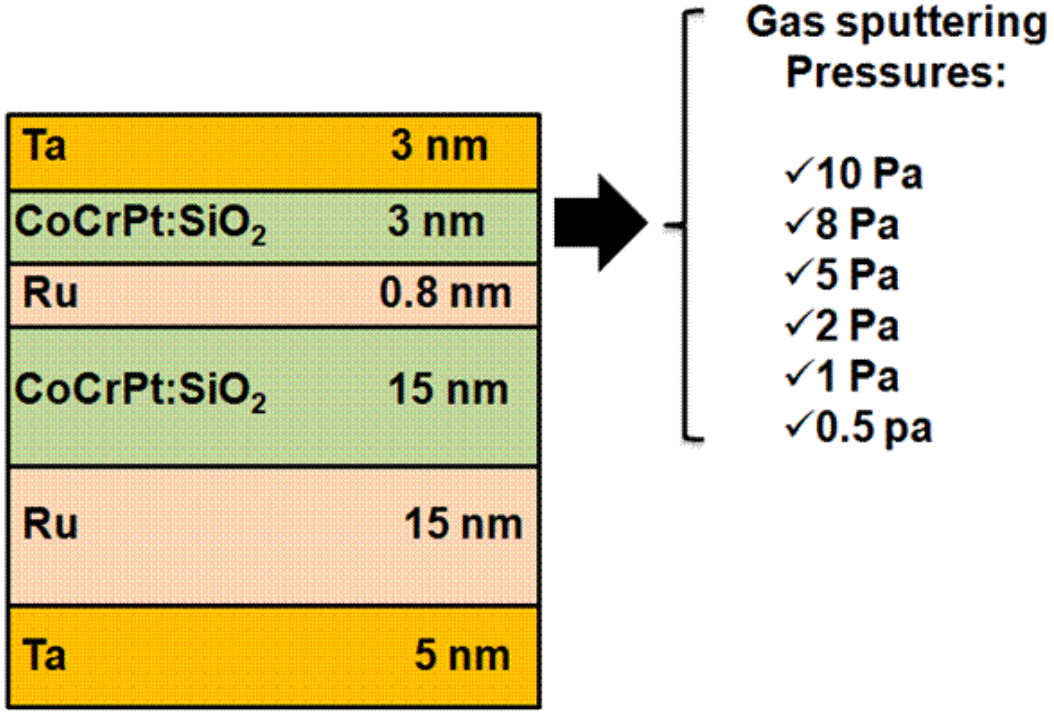

Figure 4.2. Schematic of AFC media at different top layer pressures sputtering deposition.

4.2.2 Magnetic and crystallographic properties of thin films

Magnetic properties of top and bottom layers were measured with alternating gradient magnetometer (AGM). Figures 4.3 show hysteresis curves for AFC structures with different deposition pressures of the top magnetic layer.

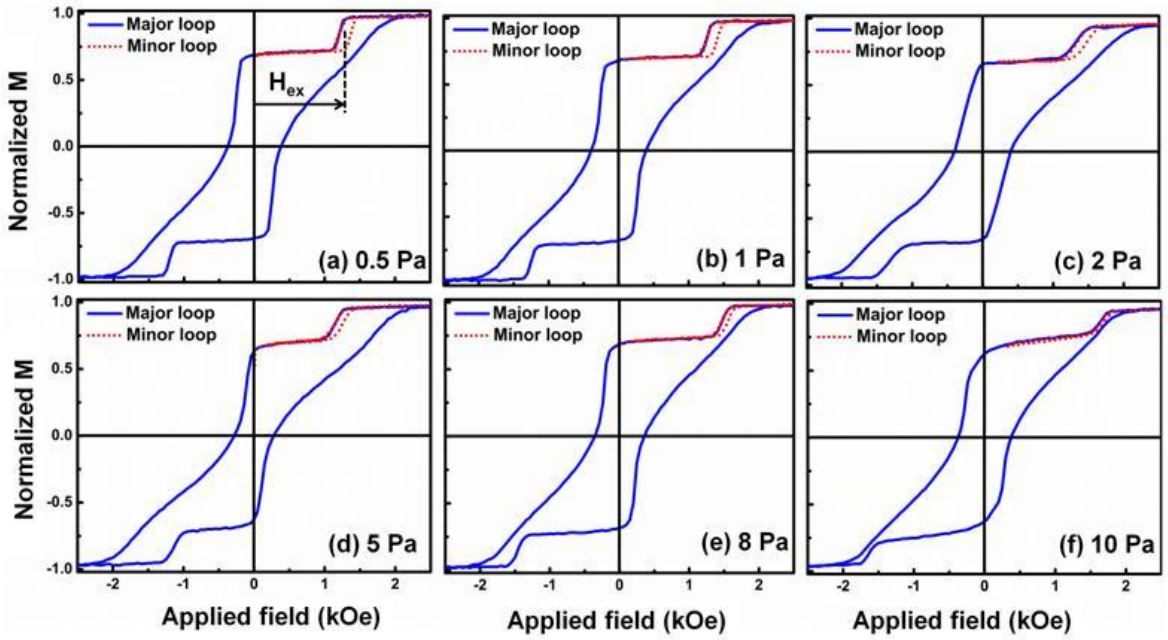

Figure 4.3. Hysteresis loop for AFC media with different pressures of top layer.

Antiferromagnetic coupling induced by the Ru layer and the reduction in remanent moment was observed in the continuous films at all pressures and the coercivity of top layer (stabilizing layer) for all samples at different pressures was smaller than exchange coupling field (H_{ex}). This helps to keep the magnetization of the stabilizing layer in an anti-parallel state with respect to the bottom recording layer and thereby making the kink lie in first quadrant.

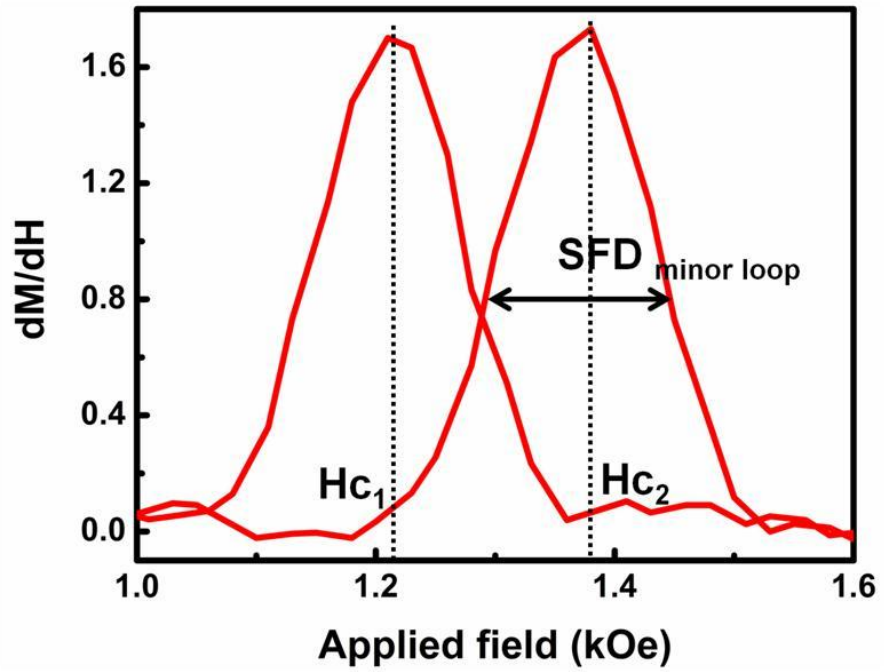

Figure 4. 4. Differentiation curves from minor hysteresis loop.

A differentiation from minor hysteresis was taken as shown in figure 4.4. There are two peaks corresponding to H_{c1} and H_{c2}. By using formulas 4.1 and 4.2, the exchange coupling field and coercivity of stabilizing layer were measured:

$$H_{ex} = \frac{H_{c1} + H_{c2}}{2} \qquad 4.1$$

$$H_c = \frac{H_{c1} - H_{c2}}{2} \qquad 4.2$$

The exchange coupling constant **J** was estimated using the following formula 4.3:

$$H_{ex} = \frac{J}{M_s t} \qquad 4.3$$

In formula 4.1, H_{ex} (Oe) is the exchange coupling field, M_s is saturation magnetization (emu/cm^3), J (erg/cm^2) is the AF interlayer exchange energy between two ferromagnetic layers and t is thickness (nm) of stabilizing layer. Coercivity of stabilizing layer, exchange coupling field and SFD of minor loops at different pressures are summarized in table 4.1.

The coercivity of the top layer determined from minor hysteresis loop shown in table 4.1, was found to be 70 Oe and 35 Oe at deposition pressures of 0.5 Pa and 10 Pa respectively. However the SFD of minor loops are increased at higher pressures. This reduction of the coercivity and increment in SFD of top layer at high deposition pressure are mainly due to grain segregation leading to almost superparamagnetic state.

Table 4. 1. Magnetic property of AFC media with stabilizing layer deposited at different pressures.

Top layer sputtering pressure (Pa)	**H_c of stabilizing layer (Oe)**	**AFC exchange field H_{ex} (Oe)**	**SFD of minor loop (stabilizing layer) (Oe)**
0.5	70	1210	150
1	65	1240	160
2	60	1330	190
5	50	1390	200
8	45	1500	230
10	35	1650	310

Nevertheless, while the stabilizing layer is sputtered at high pressure (10 Pa) the magnetic grains sizes are reduced. Since the thickness of stabilizing layer is 3 nm, magnetic grains will be thermally unstable. So, in this condition it is expected the coercivity of stabilizing layer after patterning will be smaller than AFC exchange field and the AFC can be achieved at the first quarter of hysteresis loop. Therefore, reduction in SFD can be obtained with using AFC structures.

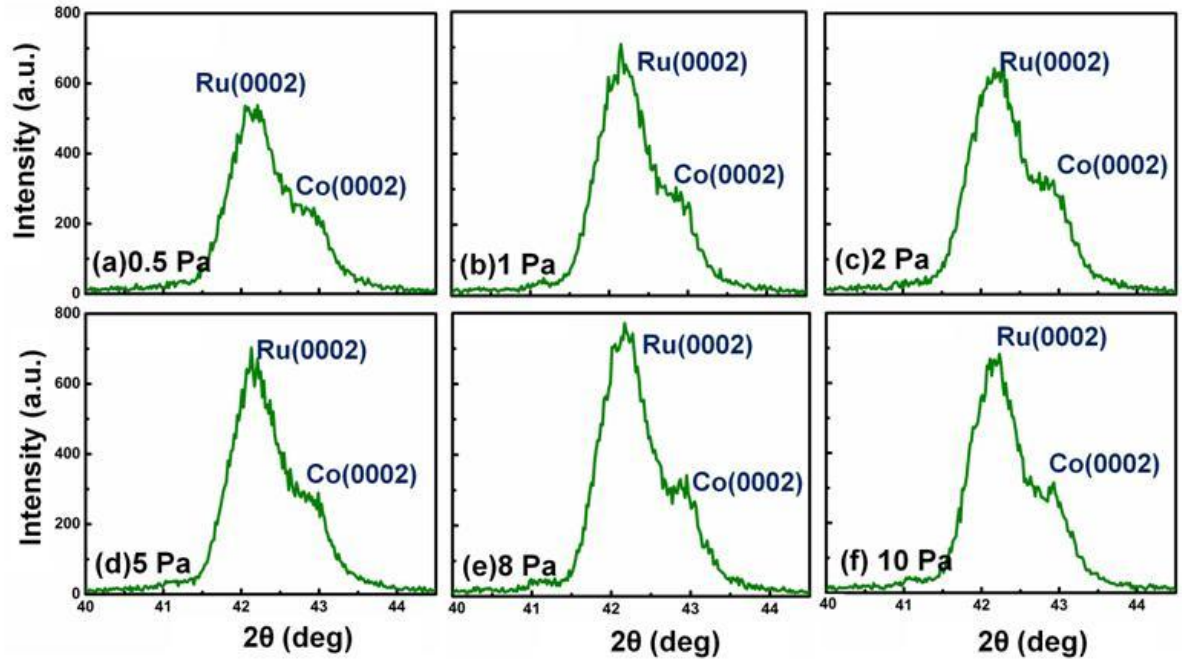

Figure 4.5. XRD patterns for AFC media with different pressures of top layer.

Structural properties of AFC thin films were measured with x-ray diffractometer (XRD) as shown in figure 4.5. Two peaks with hexagonal-closed-pack (hcp. 0002) orientations were observed for Ru and Co layers. The schematic of hcp is shown in figure 4.6. In hcp lattice cell top and bottom planes have 7 atoms, forming a regular hexagon around a central atom. In between these planes is a half-hexagon of 3 atoms.

Usually, almost magnetic perpendicular media [3-5], using intermediate layers such as Ru and the media layer are mixed layers of an oxide (e.g. SiO2, TiO2) and a Co based hcp magnetic alloy [6, 7]. This is because, the Ru obtains a strong (0002) texture and enables the Co alloy to have its c-axis strongly oriented perpendicular to the film. Moreover, all of the prepared samples showed a narrow full-width at half-maximum of the rocking curve measured using XRD. The (00.4) peak of the recording layer (RL), had a $\Delta\theta_{50}$ in the range of 4.09°–5.1°, the smallest $\Delta\theta_{50}$ observed at 1 Pa deposition pressure for top layer.

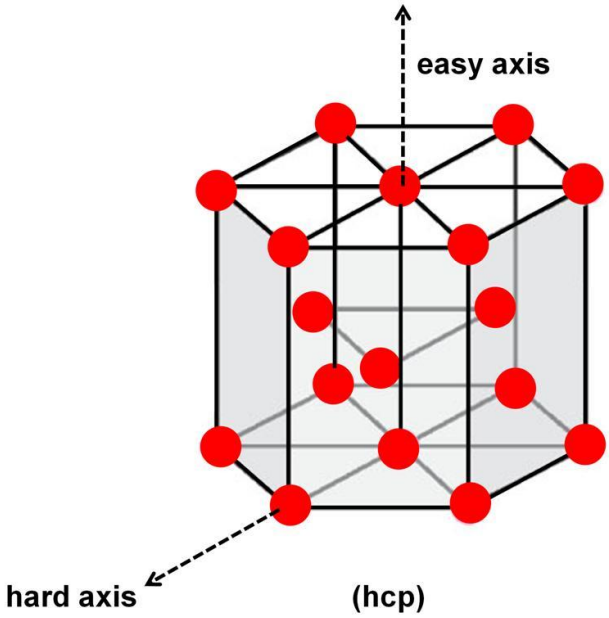

Figure 4.6. Schematic of hexagonal-closed-packed (hcp).

It means that the Co grains are oriented with the *c*-axis perpendicular to the film plane, the component of magnetization (M) in the perpendicular direction will be higher, and the noise will be lower. If the easy axes of some small grains are not oriented in the perpendicular direction; their magnetization can be easily reversed due to demagnetizing fields and thermal effects. Such grains will be a source of noise. Therefore, achieving a low value of $\Delta\theta_{50}$ is crucial to minimize SFD and writing errors in BPM.

In addition, remanence magnetization M_r influences the magnetostatic interaction, and leads to a larger SFD. So if M_r is reduced, the bits will be more stable and SFD can be reduced. However, M_r should be chosen at a suitable value for a reasonable read signal. In the conventional patterned media, M_r will be reduced by reducing M_s resulting in a larger H_k, which will lead to writability issues. The advantage of AFC structure is providing a way to reduce M_r without reducing M_s. By this way, both improvement in thermal stability and reduction of SFD can be achieved. However, M_s of the layer will remain the same. Since H_k

will be reduced due to higher M_s, stability is improved without affecting the writability. Despite, the AFC effect may not be observed when the films are patterned, as there have been several observations of increase in coercivity by a huge amount (10~ 15 times) after patterning [18]. Therefore, it is essential to study the SFD of the patterned samples.

4.2.3 Patterned dots fabrication and SFDs curves of switched dots

Electron Beam Lithography was carried out with an acceleration voltage of 75 kV on polymethylmethacrylate (PMMA) positive resist to obtain nanodots with a diameter and spacing of 60 and 40 nm, respectively. Figure 4.7 shows the scanning electron microscopy image of bit patterned media with 100 nm pitch size.

In order to obtain remanent hysteresis curves for the nanodot arrays, magnetic force microscopy images were used to count the number of reversed dots at remanent state. For this measurement, the samples were saturated in one direction and then a reversal field was applied perpendicular to sample surface and the MFM was carried out in the remanent direction.

Figures 4.8, 4.9 and 4.10 show magnetic force microscopy images for the sample deposited at pressures of 1 Pa, 2 Pa and 10 Pa. It can be seen that the magnetizations of dots with different anisotropy fields switch at different applied fields. The occurrence of reversal at random places also suggests that the dots are in single domain state and well separated.

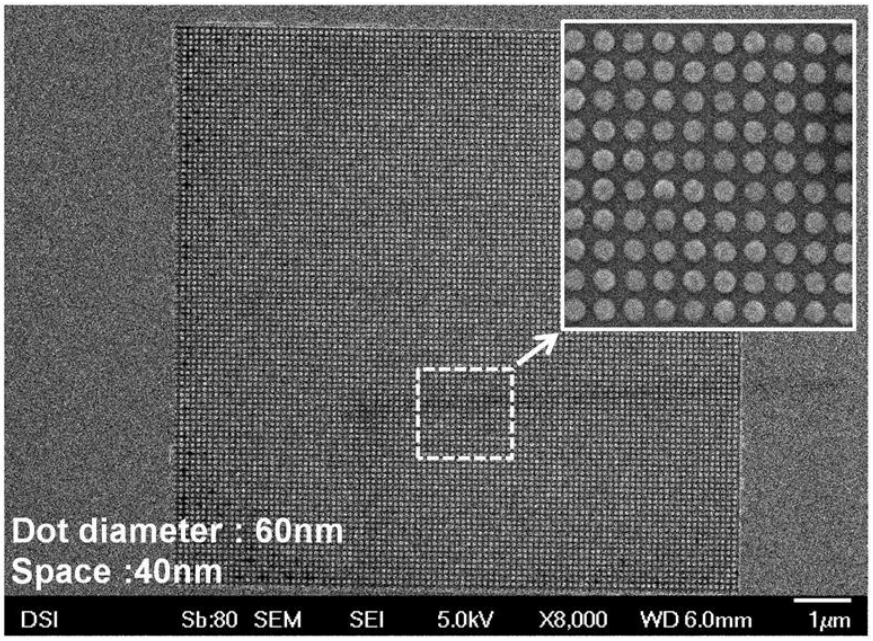

Figure 4.7. SEM image of the patterned magnetic medium with 60nm diameter and 100 nm pitch (distance from center to center of dots).

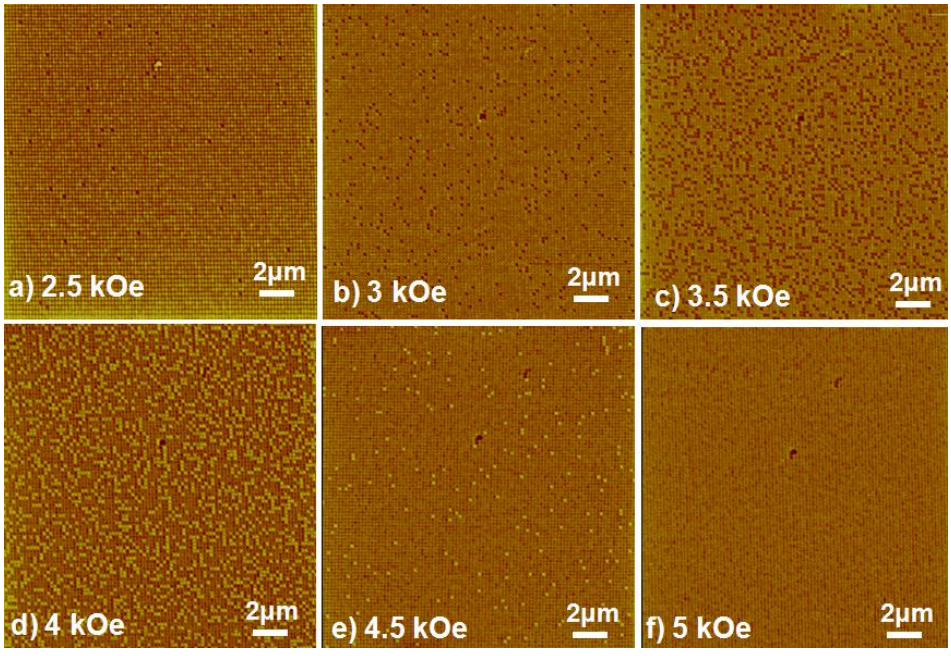

Figure 4.8. Selected MFM images at remanent states for the samples with top layer deposited at a pressure of 1 Pa.

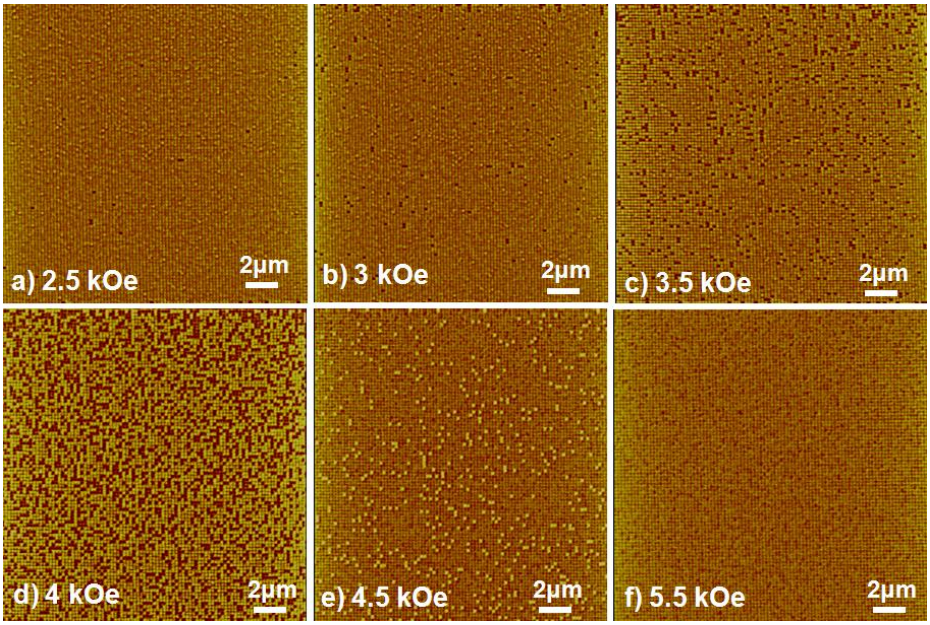

Figure 4. 9. Selected MFM images at remanent states for the samples with top layer deposited at a pressure of 2 Pa.

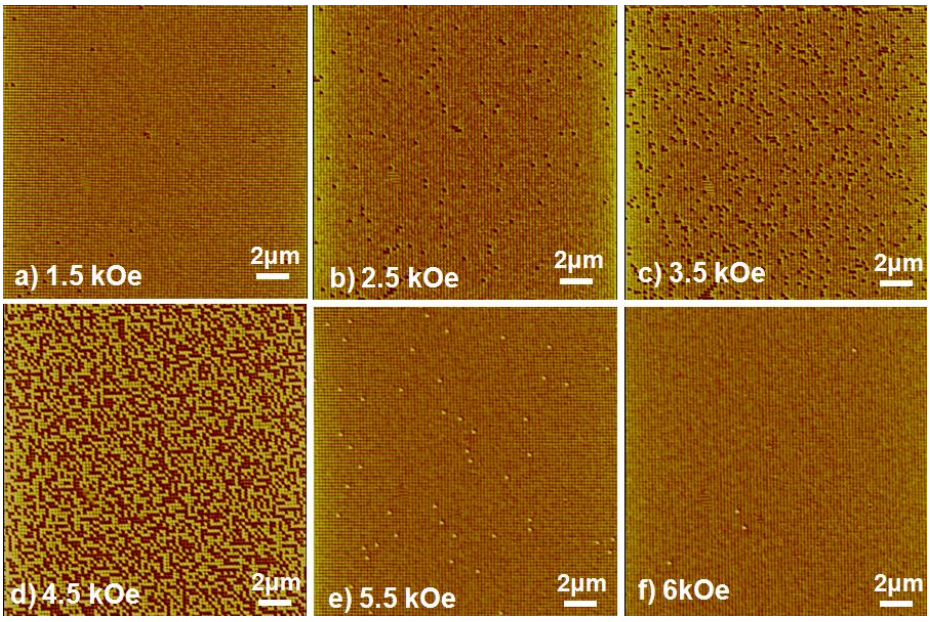

Figure 4.10. Selected MFM images at remanent states for the samples with top layer deposited at a pressure of 10 Pa.

In the case of the antiferromagnetic coupled patterned media at deposition pressure of 1 Pa for top layer, the first switched dots were observed at 2.5 kOe and the saturation of the dot

array in the 10 μm ×10 μm scanned area was completed at around 5 kOe. A similar switching mechanism was observed for all samples at different pressures from 0.5 Pa to 10 Pa of Ar gas for deposition of top recording layer with thickness of 3 nm.

Figure 4.11 shows the SFD curves for AFC samples in which the top layer was deposited at different Ar pressures. In the case of AFC patterned media with top layer deposition pressure at 1 Pa, the switching of the dots started at around 3.8 kOe. The normalized SFDs were measured 0.24, 0.33 and 0.4 for AFC patterned films with sputtered stabilizing layers at 1 Pa, 2 Pa and 10 Pa gas pressure, respectively. The SFD is the narrowest when the top layer was deposited at a pressure of 1 Pa.

The above result is contrary to what were expected based on patterned Co/Pd multilayers. It was believed that the coercivity of the thinner layer will increase after patterning and hence antiferromagnetic coupling may not be achieved for all the films. This is especially so for the film deposited at a lower pressure, because the film deposited at a lower pressure is expected to have highly coupled grains within a patterned island. Therefore, these islands could have a high coercivity after patterning, probably larger than the exchange field making it impossible to achieve AFC at remanence. Therefore, the SFD of sample with low pressure sputtered top layer (higher coercivity) was expected to be higher. Moreover, the film with top layer deposited at higher pressure was expected to show decoupled grains in the top layer. This will make them superparamagnetic and hence have a lower coercivity than the exchange field, making them antiferromagnetically coupled.

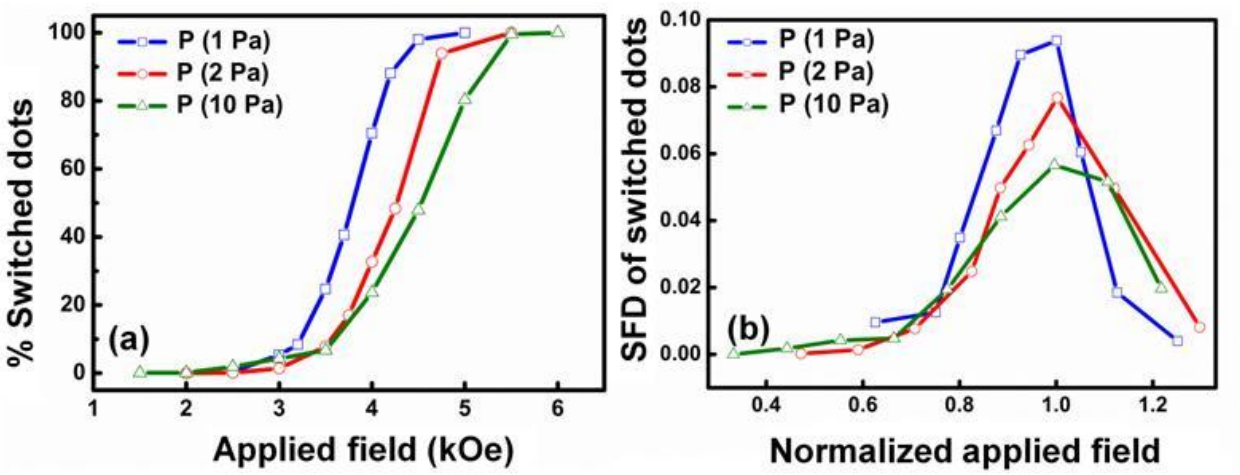

Figure 4.11. SFD of patterned media with AFC structures. Percentage of switched dots (a) and switching field distribution (b) for dots with 60 nm diameter and 40 nm spacing. The top layer with 3 nm thickness was deposited at different Ar-pressures.

Contrary to our expectations, the SFD in the case of CoCrPt-based samples seem to show a lower value at around 1 Pa, possibly because of two reasons: (i) If there is antiferromagnetic coupling for both low pressure and high pressure deposited thinner layer, the sample deposited at 1 Pa should have a lower M_rt, as the M_st of this particular layer will be larger than that of higher pressure samples. (ii) The increase of coercivity in patterned CoCrPt is different from that observed in patterned Co/Pd multilayers and hence AFC can be observed even for thinner layer deposited at lower pressure, resulting in a reduced M_r and lower SFD. This could possibly be because the CoCrPt:SiO_2 based layers would have lots of defects due to the presence of silicon and oxygen, leading to minor increase in coercivity after patterning. However, in the case of Co/Pd multilayers, the defects are fewer in the continuous films and hence the coercivity increases drastically after patterning.

It will be interesting to study the effect of different top layer materials such as CoCrPt:SiO_2 and Co/Pd with low and high magnetic anisotropy constant, respectively, on AFC patterned

media. Therefore, in the next section the studies on the effect of different magnetic anisotropy constant of stabilizing layers on SFD of AFC bit patterned media are reported.

4.3 AFC with various stabilizing layers (CoPt vs. CoCrPt)

Since the results to achieve AFC after patterning in the previous sections of this chapter were contrary to our prediction, we studied the effect of different material with different magnetic anisotropy and coercivity on stabilizing layer. As the observation of AFC at remanence depends on whether exchange coupling field (H_{ex}) is larger than the coercivity of stabilizing layer, it is necessary to study the conditions at which the AFC state will be observed. In this section, the effect of anisotropy constant of the stabilizing layer on the AFC state has been studied using different stabilizing layers such as CoPt and CoCr:SiO_2.

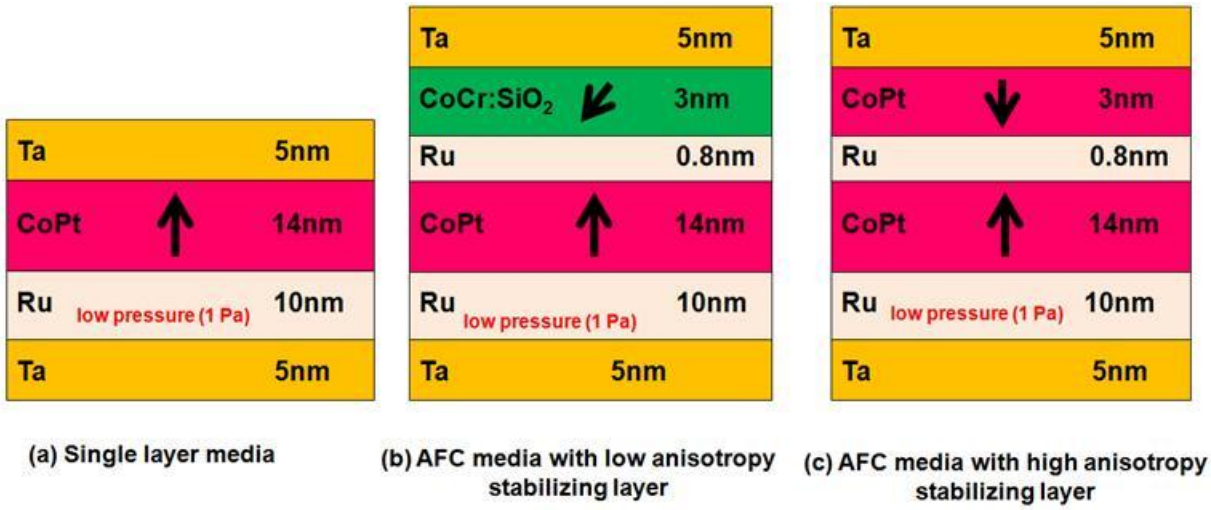

Figure 4.12. Layer structures of different configurations of media investigated in the study (a) Single-layered media (b) AFC with a lower anisotropy constant stabilizing layer (SL) and (c) AFC with a higher anisotropy constant stabilizing layer.

4.4 Magnetic properties of AFC structures with different stabilizing layers

Figure 4.12 shows the layer structure of the three different stabilizing layers. The following samples; SiO_2/Ta/ Ru/CoPt(14 nm)/Ru(0.8 nm)/stabilizing layer(3 nm)/Ta(5 nm) where stabilizing layer (SL) is CoPt and $CoCrSiO_2$ were prepared by dc magnetron sputtering

system. A sample with no stabilizing layer (single layer) was prepared as reference. $Co_{0.8}Pt_{0.2}$ alloy was used as the recording layer. Ta and Ru layers were deposited prior to the deposition of the recording layer in order to achieve a perpendicular magnetic anisotropy.

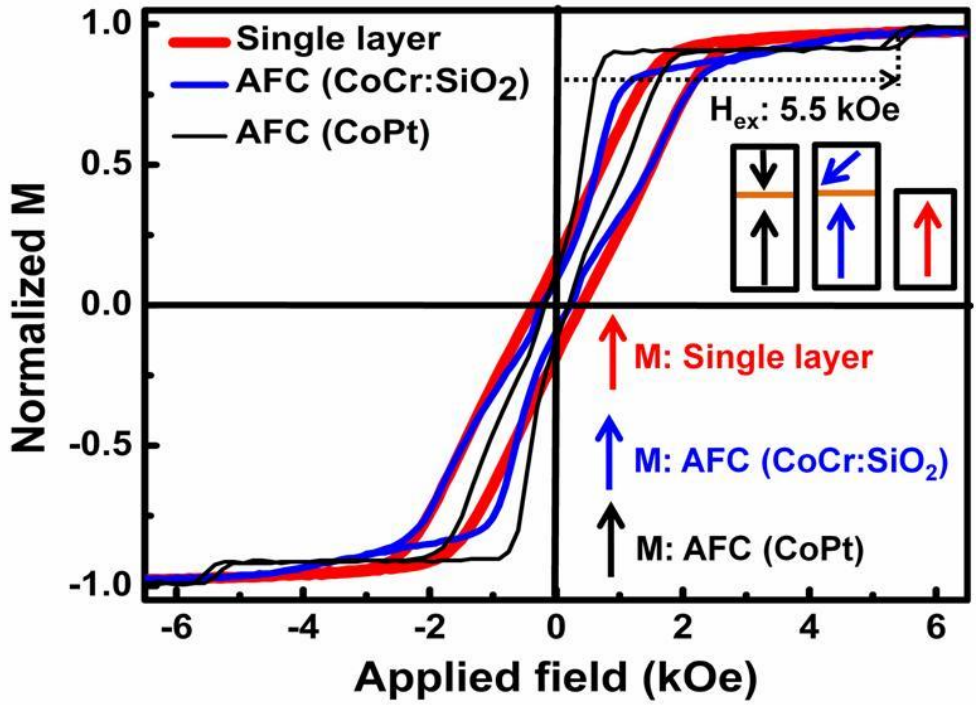

Figure 4.13. Hysteresis loops of unpatterned single layer AFC media with different top layers $CoCr:SiO_2$, and CoPt.

Two kind of stabilizing layers with low and high coercivity such as $CoCr:SiO_2$ and CoPt were used to study of effect of AFC configuration on bit patterned media. It believed that, because of lower coercivity for $CoCr:SiO_2$ than CoPt, AFC can be achieved after patterning.

Figure 4.13 shows the hysteresis loops of the three different types of unpatterned samples. In order to achieve a single domain state in the dots after patterning, the films were deposited at low pressure and at room temperature to induce a highly exchange coupled thin film system. As a result, the coercivity of the samples is not high and all the samples have tilted hysteresis loop with nucleation field in the first quarter because of the demagnetizing field.

Nevertheless, the important point to note is that the sample with CoPt stabilizing layer (SL) shows a clear kink at around 5.5 kOe. The sample with CoCr:SiO_2 layer does not show a clear kink as this sample does not have a large anisotropy constant to keep the moment out of plane against the demagnetizing field. While this may appear to be a problem based on the thin films, it will be shown later that this problem vanishes when the samples were patterned as the demagnetizing fields are negligible for patterned dots.

4.5 SFD curves of AFC patterned films with different stabilizing layers

The samples were patterned using electron beam lithography on hydrogen silsesquioxane (HSQ) as resist discussed in chapter 2. Figure 4.14 shows the SEM image of magnetic islands with 50 nm pitch size. MFM measurements were carried out as described before. Figures 4.15, 4.16 and 4.17 show typical MFM images of the AFC and single layer patterned media at remanence after the application of different reversal fields.

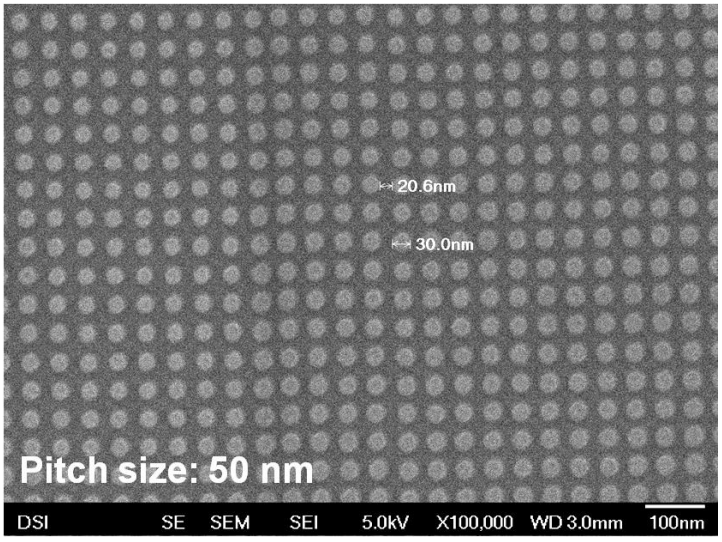

Figure 4.14. SEM image magnetic patterned samples with 50 nm pitch size.

The brown (darker) dots indicate the magnetic regions that have reversed and the yellow (brighter) dots indicate the regions that were not reversed. Although the dots were fabricated

at a pitch of 50 nm and the dot size is smaller than 50 nm, the reversed dots appear to be much bigger. This is because of the reduced field from the spacing between the dots as well as the regions where the magnetic field flows sideways to the reversed bit. It can also be noticed that the dots in the single magnetic layer start switching at 4.5 kOe and that several dots did not switch even at 10 kOe. The behavior is similar in the media with CoPt stabilizing layer. However, for the media with $CoCr:SiO_2$ the reversal start happening at 4 kOe and was completed before 10 kOe.

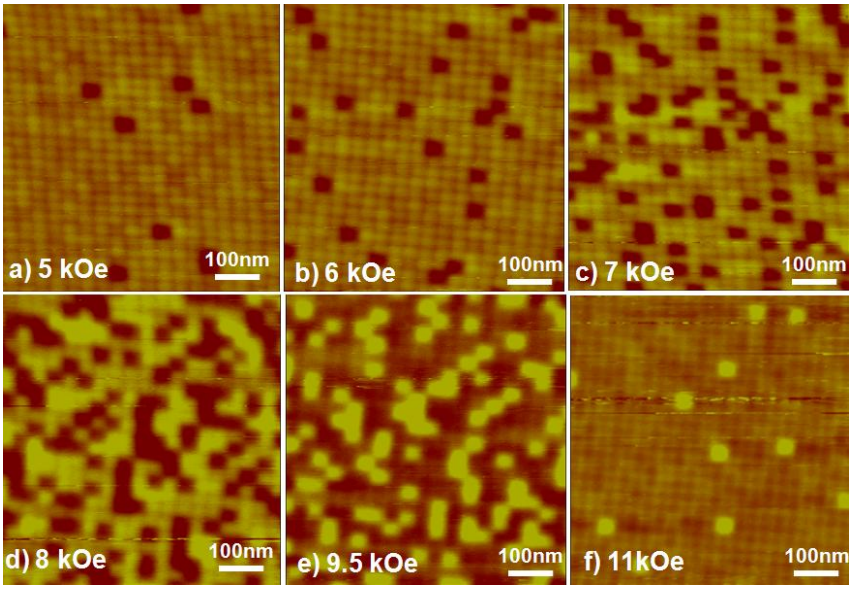

Figure 4.15. Selected MFM images for 50 nm pitch and 30 nm dot size at remanence states for single layer BPM.

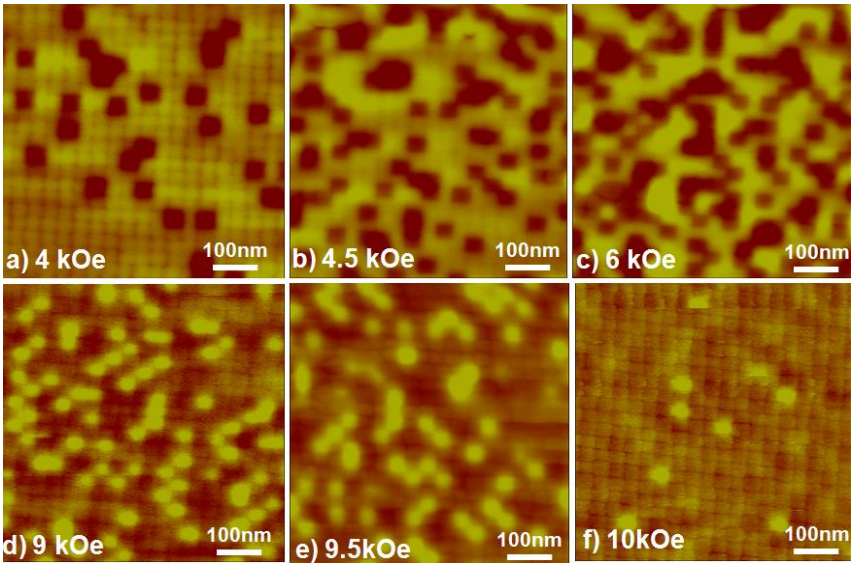

Figure 4.16. Selected MFM images of AFC with CoPt top layer for 50 nm pitch and 30 nm dot size at remanence states.

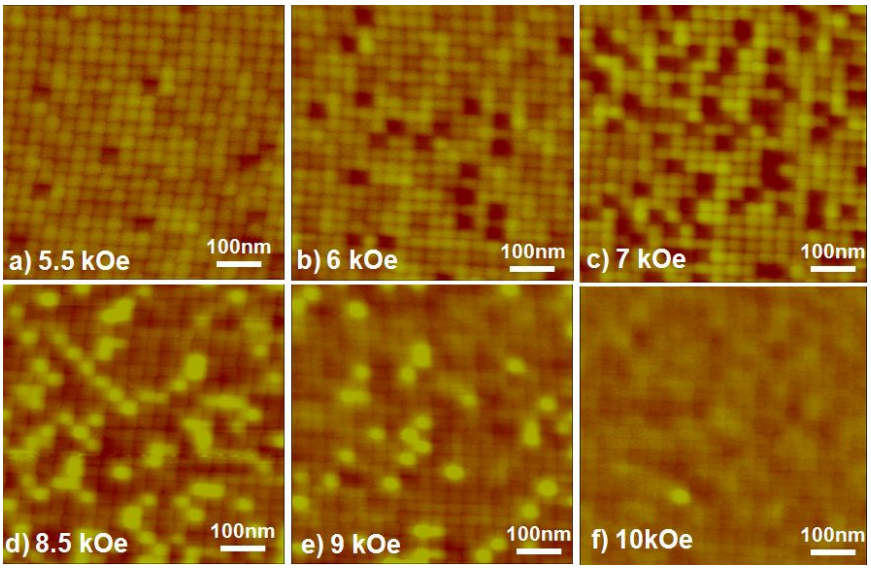

Figure 4.17. Selected MFM images of AFC with CoCr:SiO_2 top layer for 50 nm pitch and 30 nm dot size at remanence states.

Switching field distribution of their patterned samples is measured and it is shown in figure 4.18. It can be seen that the number of reversed dots is increased as a function of the reversed field. The SFD is obtained by differentiating from the reversal dot in figure 4.18a and it is shown in figure 4.18b. It can be noticed that the SFD is the largest for the sample with CoPt

stabilizing layer and the smallest for the sample with CoCr:SiO_2 stabilizing layer. The full width at half-maximum (FWHM) normalized by the switching field is 0.5 for the media with CoPt stabilizing layer and 0.32 for the media with CoCr:SiO_2 stabilizing layer. These results indicate that the media with a stabilizing layer of lower anisotropy constant provides the lowest SFD.

This result is closer to our prediction which laid the objective of this work. When the stabilizing layer has a larger anisotropy constant, the stabilizing layer part of the patterned dots may have a larger coercivity and hence they could not couple antiferromagnetically with the recording layer part. Therefore, this condition would have a larger remanent magnetic moment than the single layered configuration. Therefore, the media with a CoPt stabilizing layer will have a larger SFD. On the other hand, the media with a CoCr:SiO_2 stabilizing layer will possess an antiferromagnetically coupled configuration as the H_c of this CoCr:SiO_2 stabilizing layer will be smaller than the exchange coupling field.

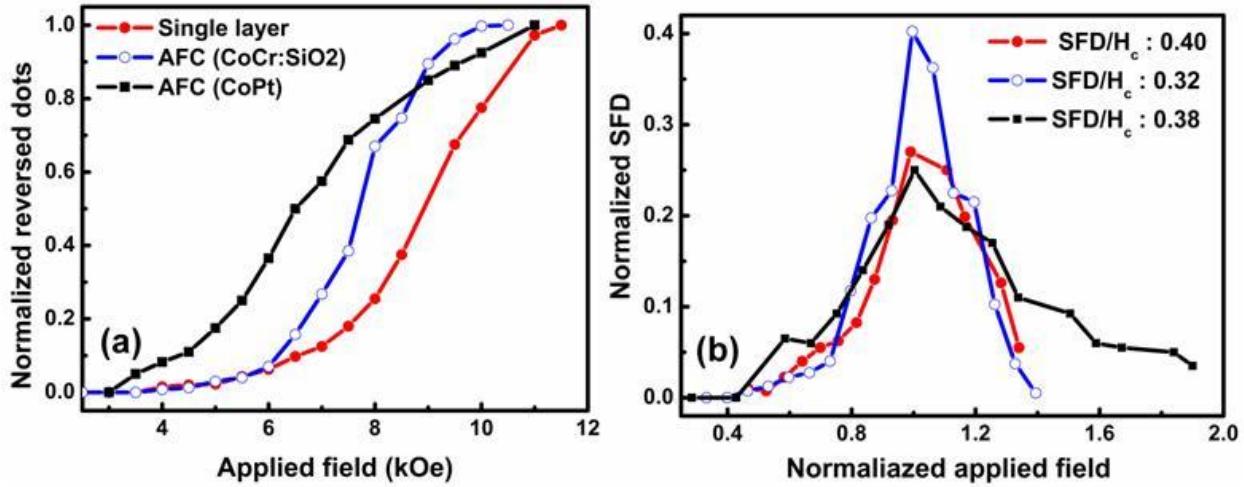

Figure 4.18. (a) The number of switched dots at different reversal fields for patterned single layered sample, AFC (CoPt) and AFC (CoCr:SiO_2). (b) SFD of patterned single layered sample, AFC (CoPt) and AFC (CoCr:SiO_2). The numbers indicate the full-width at half maximum normalized by the switching field.

Summary

In summary, in this chapter the effect of granularities of thinner layer in AFC structures and also AFC media with different stabilizing layers on SFD of patterned media and exchange coupling were investigated. With the AFC structure, the reduced remanence magnetization (M_r) leads to a reduced magnetostatic interaction. This is because the interactions between the magnetic dots in AFC patterned media can be minimized which makes each bit almost independent from another. It was observed that the narrowest SFD at a pressure of 1 Pa for top layer possibly because of good crystalline texture and reduced magnetostatic interaction. This result is significant, as there is a need to minimize SFD in order to minimize writing errors that are facing BPM technology. On the other hand it can be highlighted that SFD was reduced by 20% using granular type stabilizing layer ($CoCr:SiO_2$), while only 5% reduction was observed when CoPt was used. This is due to the different remanent states and their effect on magnetostatic interaction. Moreover, AFC configuration, which reduces magnetostatic interaction, reduces the SFD and top layer properties indeed affect the SFD.

In next chapter, the effect of different exchange coupling fields will be discussed on SFD of AFC patterned media. It can be notice that all of SFD curves in chapters 2 and 3 were based on remanence curves which they were obtained by MFM measurements. This method is very time consuming and it can get just remanence curve for a small area of patterned dots. In chapters 4, In order to observe the AFC kink at remanence state, patterned dots were fabricated by Nano imprinting lithography (NIL) method over a large area (20 mm by 20 mm). Therefore, full M-H loops of patterned structures can be measured by using AGM.

References

1. S. Iwasaki and K. Takemura, IEEE Trans. Magn. **11**, 1173 (1975).
2. Y. Ikeda, Y. Sonobe, G. Zeltzer, B.K. Yen, K. Takano, H. Do, E.E. Fullerton, P. Rice, IEEE Trans. Magn. **37**, 1583(2001).
3. K. Hayashi, M. Hayakawa, H. Ohmori, A. Okabe, K. Aso, J. Appl. Phys. **67**, 5175 (1990).
4. T. Hikosaka, T. Komai, Y. Tanaka, IEEE Trans. Magn. **30** , 4026 (1994).
5. T. Oikawa, M. Nakamura, H. Uwazumi, T. Shimatsu, H. Muraoka, Y. Nakamura, IEEE Trans. Magn. **38**, 1976 (2002).
6. H. Uwazumi, K. Enomoto, Y. Sakai, S. Takenoiri, T. Oikawa, S.Watanabe, IEEE Trans. Magn. **39**, 1914(2003).
7. E. Girt, S. Wu, B. Lu, G. Ju, T. Nolan, S. Harkness, B. Valcu, A. Dobin, J.D. Risner, M. Munteanu, R. Thangaraj, C.-H. Chang, T. Tran, X. -Wu, O. Mryasov, D. Weller, S. Hwang, J. Appl. Phys. **99**, 08E715(2006).
8. S.H. Park, S.O. Kim, T.D. Lee, H.S. Oh, Y.S. Kim, N.Y. Park, D.H. Hong, J. Appl. Phys. **99,** 08E701(2006).
9. I. Takekuma, R. Araki, M. Igarashi, H. Nemoto, I. Tamai, Y. Hirayama, Y. Hosoe,J. Appl. Phys. **99,** 08E713(2006).
10. S.N. Piramanayagam, J. Appl. Phys. **102**, 011301(2007).
11. S. S. P. Parkin, N. More, and K. P. Roche, Phys. Rev. Lett, **64**, 2309 (1990).
12. S.N. Piramanayagam, S.I. Pang, and J.P. Wang, IEEE Trans. Magn., **39**, 657 (2003).
13. S. N. Piramanayagam, K. O. Aung, S. Deng, and R. Sbiaa, J. Appl. Phys.**105**, 07C118(2009) .
14. E. Girt, and H.J. Richter, IEEE Trans. Magn. **39**, 2306 (2003).

15. V. Parekh, E. Chunsheng, D. Smith, A. Ruiz, J. C. Wolfe, P. Ruch hoeft, E. Svedberg, S. Khizroev, and D. Litvinov, Nanotechnology, **17**, 2079 (2006).
16. J.M. Shaw, W.H. Rippard, S.E. Russek, T. Reith, and C.M. Falco, J. Appl. Phy. **101**, 023909 (2007).
17. M. Ranjbar, S. N. Piramanayagam, D. Suzi, K. O. Aung, R. Sbiaa, Y. S. Key, S. K. Wong, and T. C. Chong, IEEE Trans. Magn, **46**, 1787 (2010).
18. R. Sbiaa, C.Z. Hua, S.N. Piramanayagam, R. Law, K.O. Aung, and N. Thiyagarajah, J. Appl. Phys. **106**, 023906 (2009).

Chapter 5. Effect of low and high AFC exchange coupling field on SFD of patterned media

5.1 Introduction

Antiferromagnetically coupled (AFC) patterned media technology as one approach to reduce dipolar interactions and thus minimize the switching field distribution (SFD) in bit-patterned media (BPM) has been investigated in chapters 2 and 3. In chapter 4, AFC patterned media has been studied with emphasis placed on the effect of the top layer coercivity. It is noticed that achieving anti-parallel alignment of magnetic moments at remanence requires a large exchange coupling field (H_{ex}), especially in patterned nanostructures which exhibit a large enhancement in coercivity after patterning. Therefore, tailoring the H_c of the stabilizing layer is important to fulfil the condition $H_{ex} > H_c$. With this particular focus in mind in present chapter, we have investigated the magnetization switching of two kinds of patterned AFC structures; a multilayer such as [Co (0.4 nm)/Pd (0.8 nm)]$_{\times 3}$ antiferromagnetically coupled to another [(Co (0.3 nm)/Pd(0.8)]$_{\times 10}$ multilayers which is called (AFC type 1 with low exchange coupling field), and AFC structure with high exchange coupling field when thin Co (t nm) is antiferromagnetically coupled to [Co(0.3 nm)/Pd(0.8 nm)]$_{\times 15}$ multilayers (called AFC type 2).

The observation of PMA in two above mentioned types of complex structures is mainly because of an antiferromagnetic coupling which causes a spin reorientation transition from in-plane direction to out- of- plane direction [1]. Therefore, we tried to understand the spin reorientation transition in these structures from a fundamental point of view before studying their effects on patterned structures.

In previous chapter, our studies of magnetization reversal were based on MFM measurements at remanence state, which do not give a quantified evaluation of H_{ex} magnitude after patterning [2, 3]. In order to compare H_{ex} and H_c meaningfully, it is necessary to study magnetization reversal by measuring the full hysteresis loops. As the conventional magnetometeric techniques such as alternating gradient force magnetometer or vibrating sample magnetometer require samples larger than 3 mm or 7 mm, respectively, it is necessary to prepare a large coupon sample to study the SFD of the patterned dots. In order to get full hysteresis loop of patterned films in this chapter, nanoimprint lithography (NIL) is employed to fabricate magnetic nanostructures over large area 2 cm by 2 cm.

5.2 AFC configurations with low exchange coupling field (type1)

Nowadays, the physics and applications of ultrathin multilayers including thin ferromagnetic and nonmagnetic layers have been studied extensively. The competitions between magnetic energies such as magnetostatic, interface anisotropy, bulk anisotropy and exchange energies in multilayers are crucial challenges to induce perpendicular magnetization direction in multilayer systems. Perpendicular magnetic anisotropy (PMA) in the Co/Pd multilayer systems was first observed in 1985 by Carcia et al. [4] and later on in several other Co-based multilayers such as: Co/Pt [5], Co/Au [6], Co/Ru [7] and Co/Ir [8]. Since the thickness of Co layer has an important role to induce PMA in multilayers, it is observed that when the Co thick layer in a multilayer system become thicker (above certain thickness), the effects of volume anisotropy can dominate the interface anisotropy. Therefore, at this condition magnetization direction can change from perpendicular to in plane direction of the film surface [9, 10].

Several approaches are studied to induce PMA in thick Co layer. The observation of PMA was limited to Co sublayer thickness below 0.8 nm in the multilayer structure; in fact, in most cases below 0.6 nm. Beyond this thickness, the demagnetizing field dominates over the surface anisotropy, resulting in the loss of PMA. Such films with thinner Co layers (0.3-0.6 nm) are still extensively studied for magnetic data storage applications and spintronics devices [11-18].

It was observed that spin reorientation transition is helpful to induce a perpendicular magnetic anisotropy in both thin film and patterned film by *Sbiaa et al* [1]. By using AFC configuration in multilayers system, the spin reorientation transition can be achieved even in thicker Co layer. Thus in this chapter, the concept of spin reorientation is utilized to induce the low and high exchange coupling filed in AFC structures based on Co/Pd multilayers and their effects on SFD of patterned films.

Although AFC was demonstrated in CoCrPt:Oxide for patterned media application, Co/Pd multilayers are other candidates to achieve single domain magnetic dots [14-16]. However, achieving AFC configuration is challenging in Co/Pd multilayers based patterned media. The typical H_{ex} values are in the order of 1 to 2 kOe, whereas the coercivity of patterned Co/Pd multilayers is as high as 7 to 13 kOe [19, 20-22]. Under this circumstance, it is expected that the recording layer as well as the stabilizing layer will be oriented in the same direction at remanence. To overcome this challenge, there is a need to find out suitable materials or methods to achieve $H_{ex}>H_c$. In the section 5.2, we attempted to have lower H_c of stabilizing layer by increasing the thickness of Co in the Co/Pd multilayer.

In order to study the effect of low H_{ex} field of AFC structures on SFD, AFC1 structures were deposited at room temperature using dc magnetron sputtering system. Thin films of the type AFC1 is: Si substrate/Ta (5 nm)/Cu(5 nm)/Pd(3 nm)/$[$Co (0.3 nm)/Pd (0.8 nm)$]_{\times 10}$ /Ru(0.8 nm)/$[$Co(t nm)/Pd(0.8 nm)$]_{\times 3}$ /Pd(3 nm)/Ta (3 nm). The thickness of Co in $(Co/Pd)_{x3}$

was varied from 0.4 to 1.4 nm. The Ta, Cu and Pd layers below the first Co layer help to achieve a fcc (111) texture in the layers above. The schematic of AFC1 structures is shown in figure 5.1

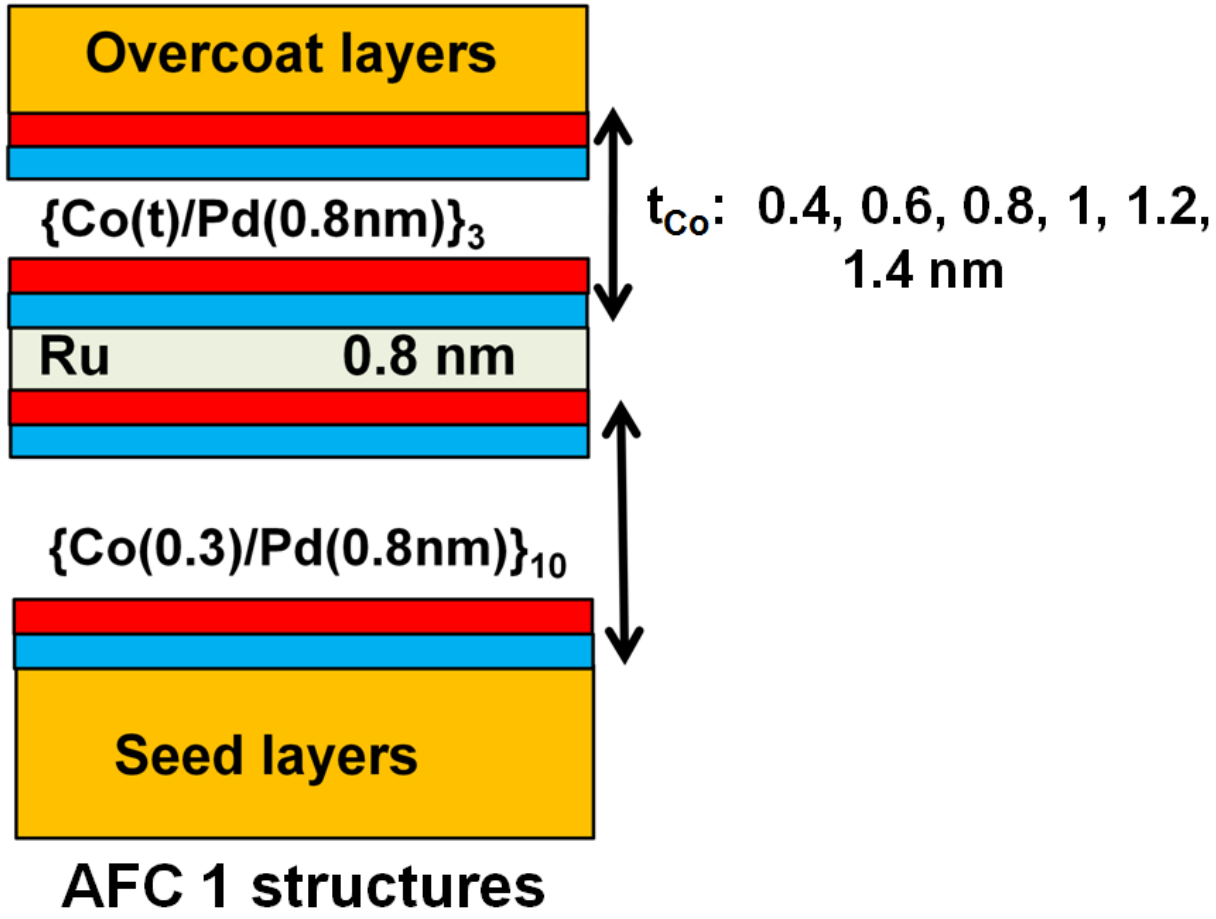

Figure 5.1. Schematic of AFC structured Co/Pd multilayers (type1).

Co/Pd multilayers with 3-bilayers $(Co/Pd)_{\times 3}$ that were antiferromagnetically coupled to $(Co/Pd)_{\times 10}$ were fabricated and their magnetic properties were investigated.

5.2.1 Magnetic properties of AFC thin films (type 1)

Alternating gradient magnetometer (AGM) is utilized to characterize the magnetic properties of AFC1 thin films. Figure 5.2 shows the perpendicular hysteresis loops of AFC1 structures with different thickness of Co sublayer. It was noticed that the AFC is clearly observed for all values of Co thickness up to 1 nm. The minor loops of these films were also

shown and represented by dotted lines. For t > 1 nm, the minor loop is not observed, indicating the absence of PMA. The observation of slope in the field range of 2-4 kOe, further confirms that there is no PMA for t > 1nm.

It can also be noticed that there is a PMA even when the Co sublayers had a thickness of 1 nm. This is quite surprising as there is no prior observation of PMA for such large values of sublayer thickness. While PMA has been reported only below 0.6 nm of Co thickness by Shin *et al.* [24] PMA has been reported for 0.82 nm thick Co layer by Lee et al [23]. However, in the samples of Lee et al., the loop was tilted and the squareness was only around 0.5, indicating that the PMA is not strong with an in-plane component of magnetization. In our films, however, the reversal of magnetization is quite sharp even at t=1 nm, indicating a strong PMA. It is postulated that the observation of PMA arises from the antiferromagnetic coupling between the recording layer and the stabilizing layer.

Although this result is very interesting, further discussion is postponed for a while and the attention is paid at first on the potential of the structures towards AFC patterned media applications.

Figure 5.3 shows the coercivity (H_c) and exchange field (H_{ex}) of [Co (t)/Pd(0.8 nm)]$_3$ in AFC multilayers with 0.4 nm to 1 nm thick Co layer. As the thickness of Co layer increases from 0.4 nm to 1 nm, the coercivity field from minor loops is reduced from 490 Oe to 120 Oe as reported [25]. The exchange field also was reduced from 1050 Oe to 310 Oe. However, this decrease of H_{ex} with Co thickness is mainly due to the fact that the H_{ex} is inversely proportional to $M_s \times t$. The AFC type1 samples were not designed to have same $M_s \times t$ in the stabilizing layers. It is reasonably straightforward to say that the H_{ex} values will be identical if the samples were designed to have same value of $M_s \times t$ by varying the number of bilayers. This is particularly so, as all the samples exhibited almost similar values of J (about 2

erg/cm^2). Such a design will be more practical for patterned media application in achieving a suitable signal from the media. Nonetheless, these results indicate that AFC patterned media based on Co/Pd multilayers can be achieved by designing the stabilizing layer with thicker Co sublayers.

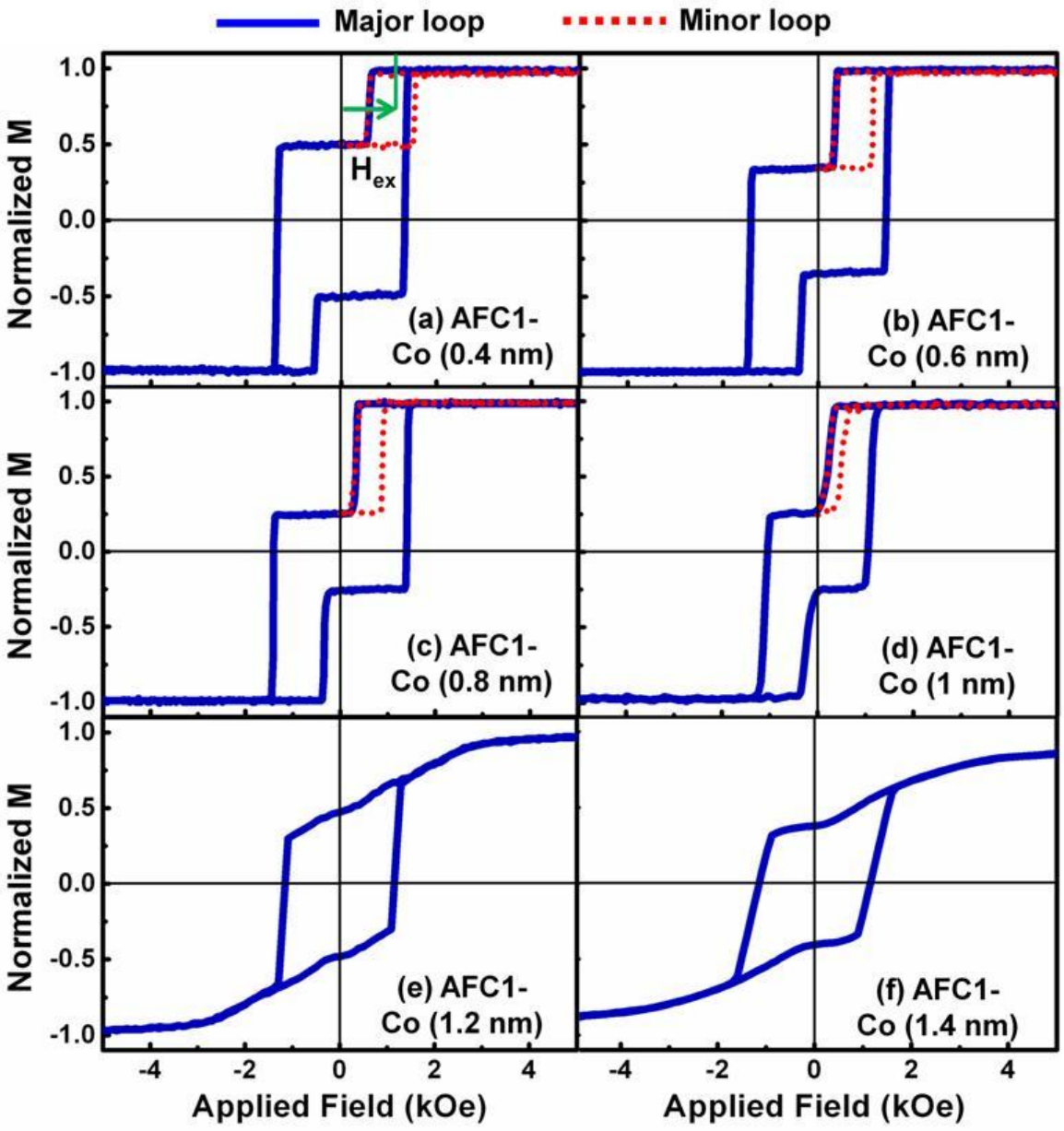

Figure 5.2. Major (solid lines) and minor (dotted lines) out-of-plane hysteresis loops of antiferromagnetically coupled complex structures (AFC 1).

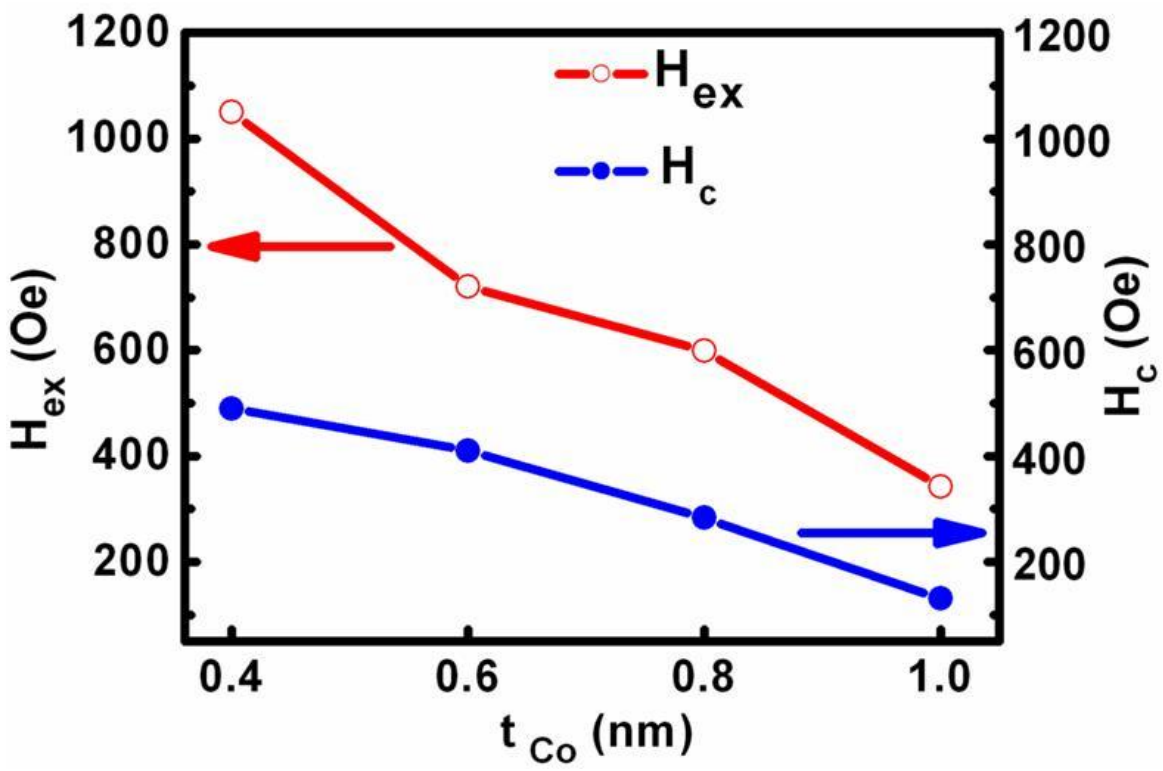

Figure 5.3. Exchange coupling field (H_{ex}) and coercivity field (H_c) versus Co thickness field for AFC system (type1).

In order to further understand if the perpendicular orientation and the exchange field were observed due to antiferromagnetic coupling or to the effect of seed layers, a set of thin film samples Ta (5 nm)/ Pd(10 nm)/ [Co(t nm)/Pd(0.8 nm)]$_3$ /Pd(3 nm)/Ta (3 nm) were deposited as a single layer type1. These structures are identical to the stabilizing layer in AFC type1, without antiferromagnetic coupling. An illustration of single layers structure type1 is shown in figure 5.4.

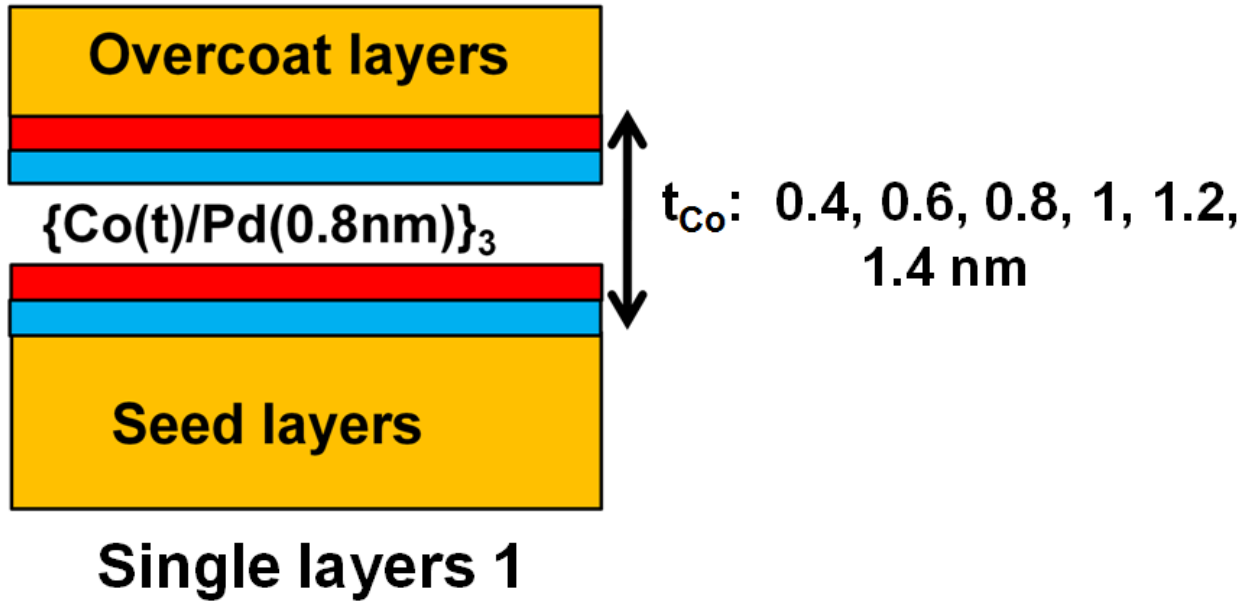

Figure 5.4**.** Schematic of sample structures single layers type1 as reference Co/Pd multilayers without AFC (type1).

5.2.2 Magnetic properties of single layers (type1)

The out of plane and in-plane magnetizations of single layers type1 were measured with AGM. Figure 5.5 shows the hysteresis loops of these samples. It can be seen that the samples with 0.4 nm thick Co show a perpendicular hysteresis loop and those with 0.8 nm to 1.4 nm thick Co show in-plane hysteresis loops. At t of 0.6 nm, the in-plane and perpendicular loops look almost identical, indicating the onset of a loss of PMA. The PMA in thin Co layers (0.4 nm) has been well understood to be arising from surface anisotropy. However, for Co thickness of 0.8 nm, the out of plane component of magnetization decreases due to a domination of volume magnetic anisotropy in comparison to surface anisotropy. Such a result is quite well known in Co/Pd multilayers and is arising from the decrease of interface anisotropy and the dominance of dipolar energy in films with thicker sublayers. Although AFC1 samples with a Co thickness of 0.8 nm in the bilayer showed a perpendicular magnetic anisotropy, the magnetization direction of single Co/Pd multilayers with thick Co (0.8 nm) as

a reference structure (without AFC1) was observed to be in plane. Therefore, by comparing the results of figure 5.2 and figure 5.5, it can be highlighted that the Co/Pd multilayers with 0.8 nm Co acquire a perpendicular anisotropy due to the additional energy from antiferromagnetic coupling with the hard magnetic layer.

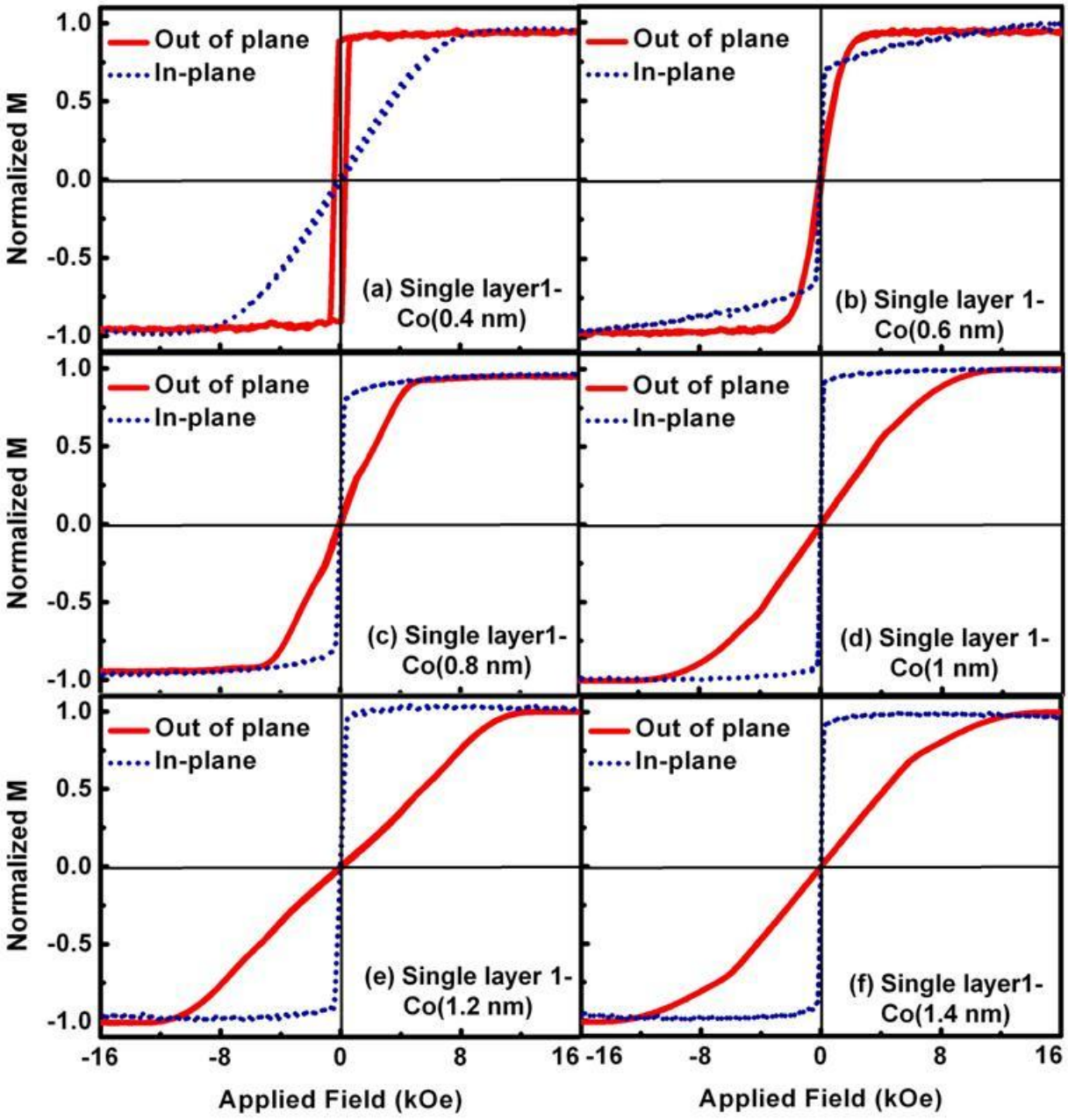

Figure 5.5. Out-of-plane and in-plane hysteresis loops of single layers $[Co(t)/Pd(0.8\ nm)]_{\times 3}$ with 0.4 nm to 1.4 nm thick Co layer.

In order to understand the changes in the coercivity and exchange field as a function of Co thickness in $[Co(t\ nm)/Pd(0.8\ nm)]_{\times 3}$, an estimation of anisotropy constant values were made in unpatterned thin films without AFC coupling. It is well understood that the perpendicular magnetic anisotropy energy K_u in (Co/Pd) multilayers system is the result of the competition between the demagnetization energy and the interface anisotropy energy. The K_u in these systems can be described by the following formula [26, 27]:

$$K_u = K_b + \frac{K_{interface}}{t} - 2\pi M_s^2 \qquad 5.1$$

Where K_b is volume anisotropy energy density, which is negligible, $K_{interface}$ is the interface anisotropy density, t and M_s are the thickness and saturation magnetization of $[Co(t\ nm)/Pd(0.8\ nm)]_{\times 3}$, respectively. The negative or positive sign of K_u imply in-plane or out of plane anisotropy respectively. K_u can be experimentally obtained from M-H loops by comparing the difference of energy to saturate the film along in-plane and out of plane directions as indicated by equation 5.2 [26].

$$K_u = \int_0^{M_s} \mu_0 H_{in}\, dM - \int_0^{M_s} \mu_0 H_{out}\, dM \qquad 5.2$$

Where H_{in} and H_{out} are in-plane and out-of-plane magnetic fields, respectively. The μ_0 is permeability which is the degree of magnetization that a material obtains in response to an applied magnetic field. The value of μ_0 is $4\pi\times10^{-7} \approx 1.2566370614\ldots\times10^{-6}$ $H{\cdot}m^{-1}$ or $N{\cdot}A^{-2}$.

In order to measure out of plane and in-plane energies, an integration has been carried out from both M-H loops. The net area from hysteresis loops was calculated. Then, difference between both areas is magnetic anisotropy energy.

Figure 5.6 shows the K_u and M_s values of reference structures $[Co(t\ nm)/Pd(0.8\ nm)]_{x3}$, without the $(Co/Pd)_{10}$ bilayers. It can be seen that by increasing the thickness of Co from 0.4

nm to 1.4 nm, the saturation magnetization is increased from 344 emu/cc to 760 emu/cc and K_u is reduced from 2.5×10^6 erg/cc to -0.27×10^6 erg/cc. This result explains the lack of PMA in reference sample with t = 0.8 nm. In the AFC samples, it may be postulated that the energy from the antiferromagnetic coupling between the $[Co/Pd]_{10}$ and the $[Co/Pd]_3$ helps to align the easy axis in the perpendicular direction for thick Co 0.8 nm layer, as per the following relation:

$$K_u = K_b + K_{AFC} + \frac{K_{interface}}{t} - 2\pi M_s^2 \quad (5.3)$$

Where K_{AFC} is the additional term arising from the antiferromagnetic coupling. Although, the exact form of K_{AFC} needs to be derived after a detailed analysis, it is most likely proportional to J – the antiferromagnetic coupling constant and inversely proportional to thickness, t.

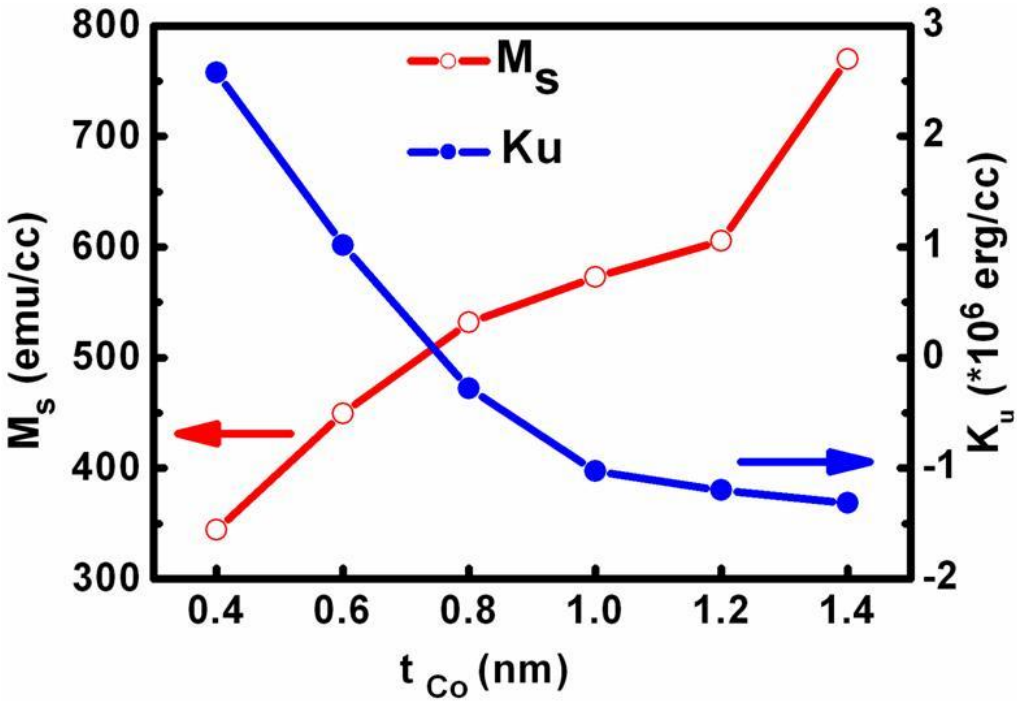

Figure 5.6. Anisotropy constant (K_u) and saturation magnetization (M_s) values of $(Co_{t=0.4,\ 0.6,\ 0.8,1,\ 1.2,\ 1.4\ nm}/Pd_{0.8\ nm})_3$ structures.

Another point that can be highlighted by comparing the observations from figure 5.2 and figure 5.5 is the following: M_s for the film with t=1.2 nm Co thick layer is around 600

emu/cc. When the magnetization is oriented in-plane, the perpendicular hysteresis loop will saturate at $4.\pi.M_s$, which is about 7.6 kOe. In fact, in figure 5.5, the saturation field of such a film in the perpendicular direction is observed at field of about 10 kOe. In contrast, the slope in the hysteresis loop of AFC structure with t=1.2 nm vanishes at a saturating field below 4 kOe. This seems to indicate that the AFC sample with t=1.2 nm may have a weak perpendicular anisotropy.

5.2.3 Crystallographic properties

XRD results of AFC1 thin films are shown in figure 5.7. From XRD measurements only one clear peak at around 40.92° was observed for the entire AFC multilayer which is an indication of the growth of fcc (111) of CoPd. There was no change in the fcc (111) peak position by increasing the thickness of Co layers. Furthermore, rocking curve scans were carried out to measure the full width at half maximum (FWHM) of (Co/Pd) multilayers peaks and it was found to be in the range of 4° to 5° indicating that the crystallographic growth of the (Co/Pd) multilayers was not affected.

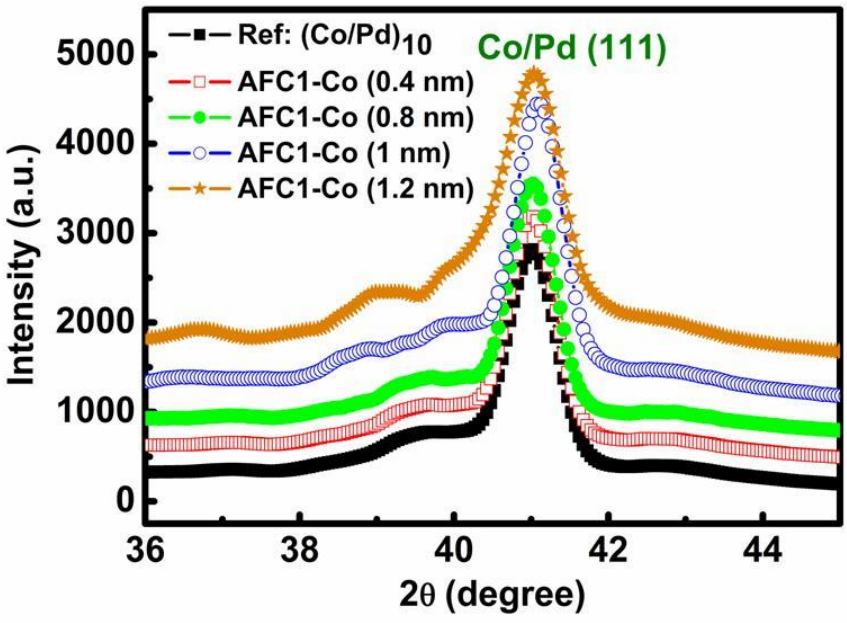

Figure 5.7. XRD patterns of AFC1 thin films.

The results indicated that the observation of AFC configuration in Co/Pd multilayers for Co sublayer thickness of 1 nm is based on magnetic origin. Therefore, AFC could help to induce spin reorientation from in plane direction to perpendicular direction at 1 nm Co thick layer.

Before discussion on the effect of low exchange coupling field in AFC1 samples on SFD of patterned films, we introduce the other type of AFC 2 structures with high exchange coupling field in section 5.3. Then, the effect of pattering for both AFC1 and AFC 2 will be discussed in section 5.4.

5.3 High AFC exchange coupling field structures (type 2)

In order to achieve AFC after patterning, it is important to have higher antiferromagnetic exchange coupling field (H_{ex}) than the coercivity of stabilizing layer. Therefore, materials which show a high H_{ex} are desired. In this section, other type of AFC structures with high exchange coupling field fabricated.

AFC thin films (type2) were deposited using dc magnetron sputtering system at 1.5 mTorr Ar pressure on thermally oxidized Si (100) substrates. The base pressure prior to the deposition was below 5×10^{-9} Torr. The samples had a structure of Ta (5 nm)/Cu(5 nm)/Pd(3 nm)/Co(t)/Ru(0.8 nm)/ Co(0.5 nm)/$[$Co(0.3 nm)/Pd(0.8 nm)$]_{\times15}$/Pd(3 nm)/Ta (3 nm). The thickness, t was varied from 0.75 nm to 2.4 nm and a schematic of the film structures is shown in figure 5.8.

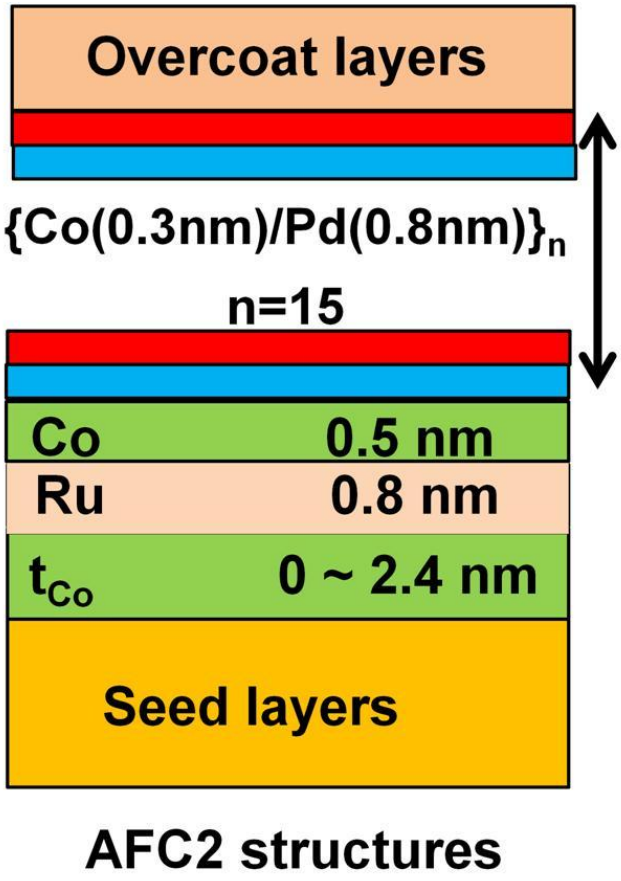

Figure 5.8. Schematic illustration of AFC (type2) structures with different thickness of Co thin film (0-2.4 nm).

5.3.1 Magnetic properties of AFC and single layers thin films (type2)

Figure 5.9 shows the perpendicular hysteresis loops of exchange coupled AFC 2 structures with different thickness of Co bottom layer as measured by AGM. A very high exchange coupling field of 15 kOe can be observed for 0.75 nm thick Co. With the increase of Co thickness to 1 nm, the exchange field reduces to a value of about 10 kOe. For relatively high values of Co thickness (e.g., 2.4 nm), no antiferromagnetic exchange coupling was observed. These results are, to some extent, very similar to Sbiaa et al. [1] observations where—at Co thickness of 1nm—they reported magnetization reorientation of Co magnetization from in plane to out of plane direction. For a Co layer thickness of about 2.4 nm, no magnetization reorientation could be observed. While the reversal characteristics of the 1 nm Co layer is

very similar to that in earlier work, the obvious difference in the present study is the sharp magnetization reversal characteristics of the 0.75 nm Co layer.

In order to understand this effect further, thin film samples of the type Ta (5 nm)/Cu(5 nm)/Pd(3 nm)/Co(t)/Ru(0.8 nm)/Pd(3 nm)/Ta (3 nm) were made. The schematic of single layers (type2) is shown in figure 5.10.

This sample structure, without the complexity of the multilayers on the top, helps to understand the anisotropy of the thin Co layer per se. Figure 5.11 shows the hysteresis loops of the single layered Co films, measured when field was applied in perpendicular and in-plane directions.

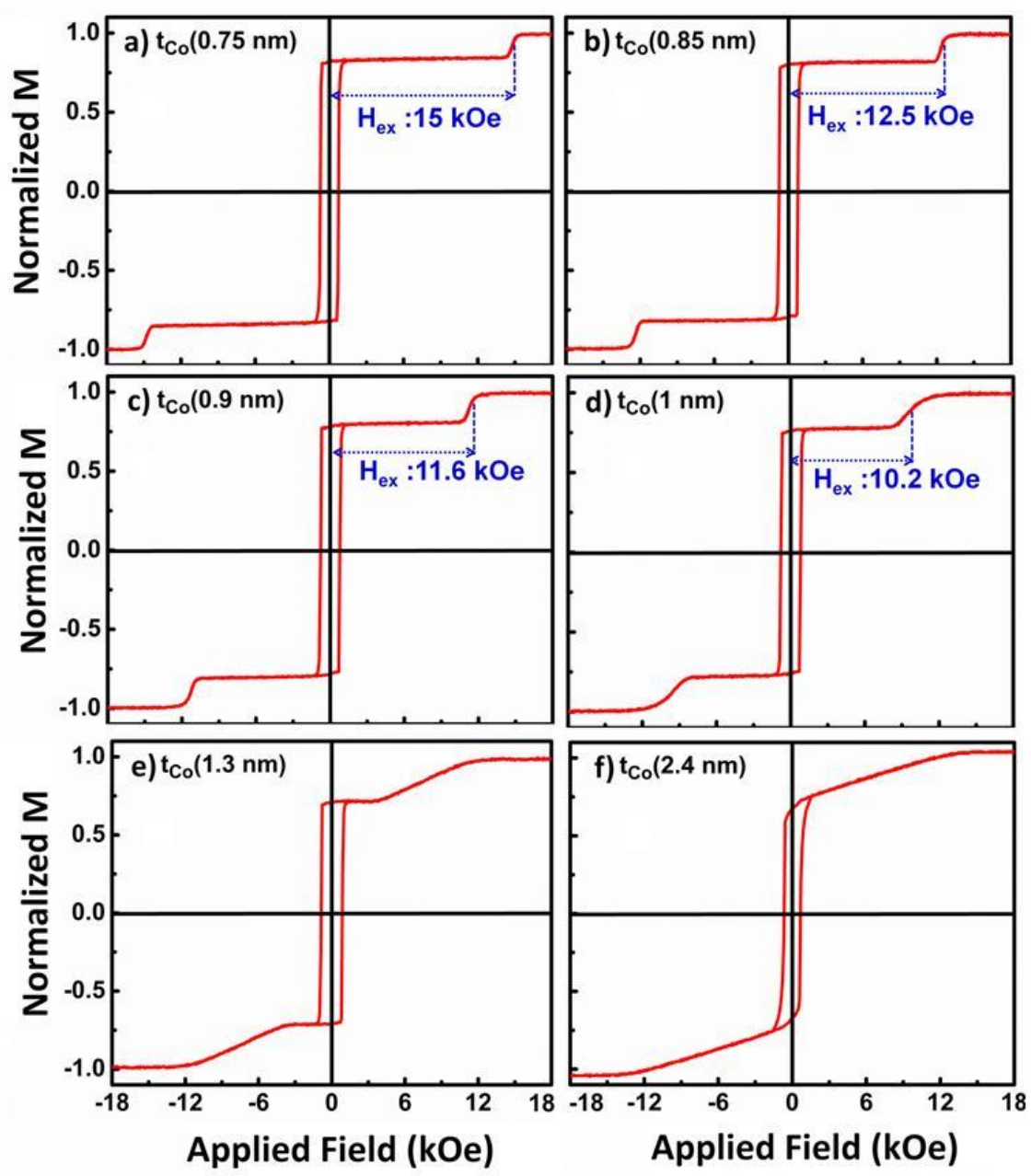

Figure 5.9. Hysteresis loops of AFC multilayer systems (type2).

It can be seen that the single layer samples (type2) with 0.75 nm thick Co show a perpendicular hysteresis loop and those with 0.8 nm to 1 nm thick Co show in-plane hysteresis loops.

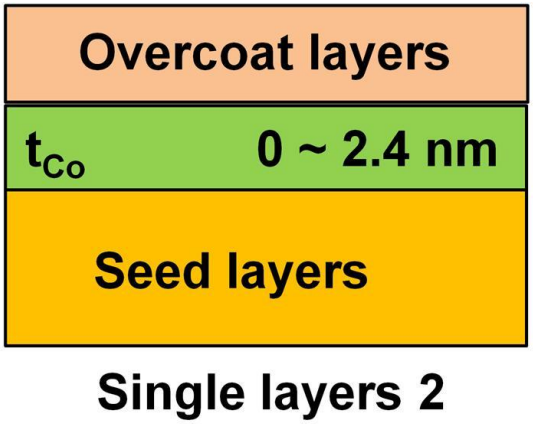

Figure 5.10. Schematic illustration of single layer structures (type2) with different thickness of Co thin film (0-2.4 nm).

Table 5.1 summarizes the switching field distribution, as measured from the width of the peaks in differentiated M-H loops. It can be noticed that the SFD increases from 0.6 kOe for t of 0.75 nm to a value of 1.6 kOe for t larger than 0.9 nm. While the SFD in our earlier work is as high as 1.6 kOe, the relatively sharp switching and a large exchange coupling in 0.75 nm was not observed. It can be noticed that the sample with t_{Co} (0.75 nm) shows a PMA with a narrow SFD (as seen from Table 5.1), possibly induced by a contribution of surface and magneto-crystalline anisotropy arising from the Pd(111) seedlayer below. The PMA vanishes for thickness greater than 0.9 nm, and the films show in-plane magnetization orientation. The SFD of the films greater than 0.9 nm is larger in the perpendicular direction and narrower in the in-plane direction

Table 5. 1. Switching field distribution, as measured by the full width at half-maximum of the derivatives of the M-H loops Co layers in perpendicular and in-plane magnetization direction, in single-layer and complex multilayer system.

	Switching Field Distribution (kOe)		
Co Thickness (nm)	**AFC2**	**Single layer2 (Perpendicular)**	**Single layer2 (In-plane)**
0.75	0.6	0.35	2
0.9	0.6	1	0.37
1	1.6	2.2	0.37

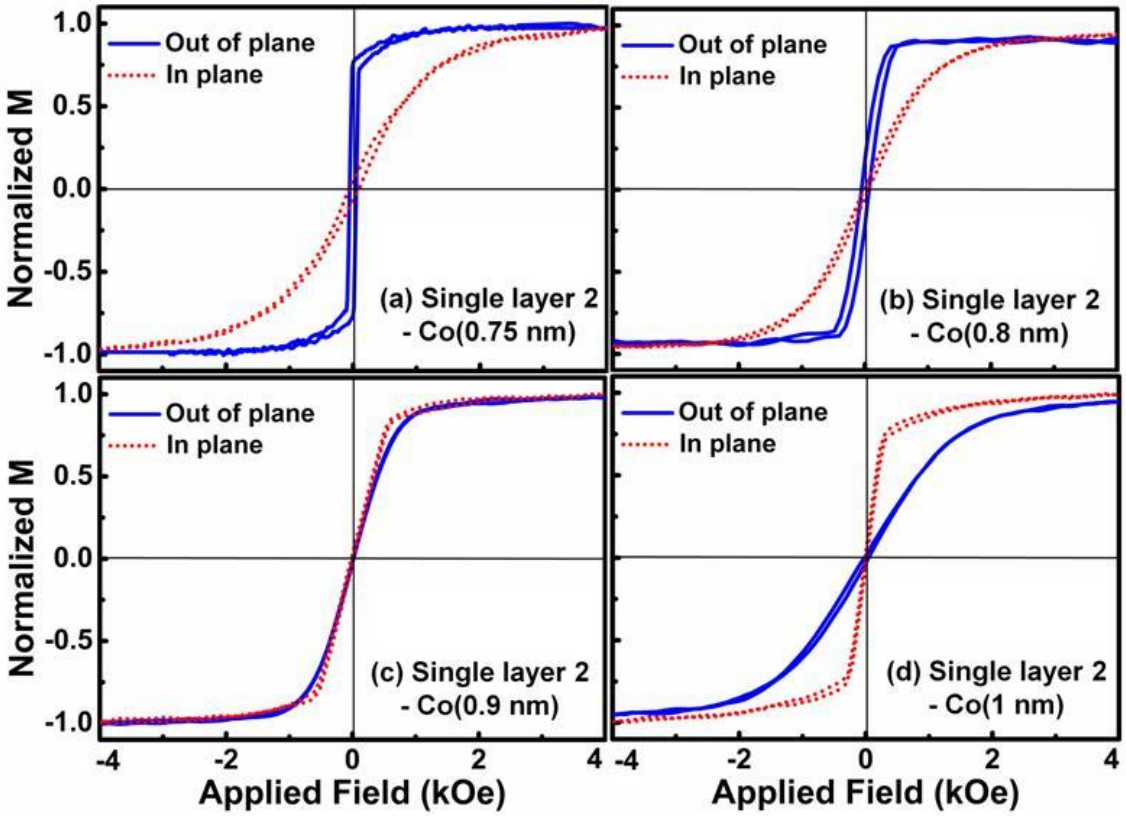

Figure 5.11. Out of plane and in-plane magnetizations of Co thin film with thickness of (a) 0.75 nm, (b) 0.8 nm, (c) 0.9 nm, and (d) 1 nm, respectively.

The following discussion can be made from the results shown in figures 5.9 and 5.11. In the AFC2 multilayers, the Co layer at the bottom has a texture-induced PMA for a maximum thickness of about 0.85 nm. The bottom layer is antiferromagnetically coupled to the top

Co/Pd multilayer through the Ru layer, as shown in several other studies [2, 3, 28]. For the films with a Co layer thickness of 0.9 and 1 nm, the PMA is mainly due to the antiferromagnetic coupling which causes a spin reorientation. As the sample has a PMA until 1 nm due to AFC or crystallographic texture, an exchange field can be observed until 1 nm.

For too large values of Co layer thickness (~2.4 nm), the antiferromagnetic coupling is not strong enough to cause reorientation, and hence, the magnetization simply lies in the film-plane in the absence of an external magnetic field.

5.3.2 Spin reorientation versus surface anisotropy

In order to further illustrate the physics behind our observation, we defined three regions corresponding to the different behavior of bottom Co layer which itself is dependent on the thicknesses of Co layer. Figure 5.12 shows the values of H_{ex} as a function of thickness of the bottom Co layer. The H_{ex} shows a steady decrease until a thickness of about 1 nm, beyond which the exchange coupling cannot be observed. In region (I), Co thin layer (in the thickness range up to 0.8 nm) has a PMA due to interface effects and is antiferromagnetically coupled to (Co/Pd) multilayer. In region (II), where the bottom Co layer thickness is between 0.9 nm and 1.2 nm, the magnetization of the film as such had no PMA due to crystallographic texture but was reoriented due to the antiferromagnetic coupling with the Co/Pd multilayers on the top. In the third region, for large values (>1.2 nm) of thickness, H_{ex} vanishes due to the in-plane orientation of the Co layer. This result is in contrast with the case of conventional AFC1 system, where the value of H_{ex} decreases monotonically as a function of thickness. Another interesting point to notice from this study is that the value of H_{ex} in the AFC 2 system is much larger than that observed in our earlier AFC 1 systems.

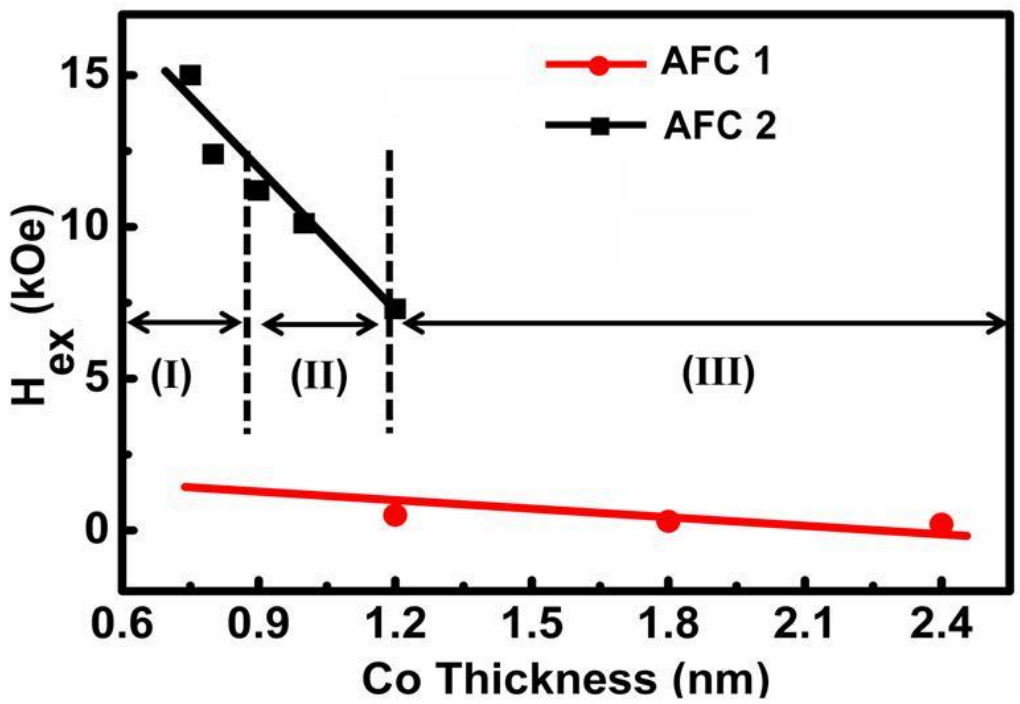

Figure 5.12. Exchange coupling field (H_{ex}) versus Co thickness field for AFC 2 system in this study and AFC 1 system.

As the value of H_{ex} increases inversely proportional to the thickness, it is meaningful to look at the value of exchange coupling energy J. In our samples, J was found to be close to 1.24 erg/cm^2 for a sample with 0.75 nm thick Co layer. In the case of longitudinal recording media, an increase of J from 0.08 to 0.32 erg/cm^2 has been reported by the introduction of thin Co layers at the Ru interface [28-30]. In the case of perpendicular media with antiferromagnetically coupled configuration, J was found to be in the range of 0.2 to 0.44 erg/cm. In the pioneering work on oscillatory coupling in Co/Ru/Co, Parkin et al. have reported a value of J of about 5 erg/cm^2. From the hysteresis loops plotted in figure 5.13, a saturation field of about 14 kOe for 2.4 nm thick Co layer can be observed. Using the method of Parkin et al., this yields a J value of 4.7 erg/cm^2, which is very close to the reported value [31].

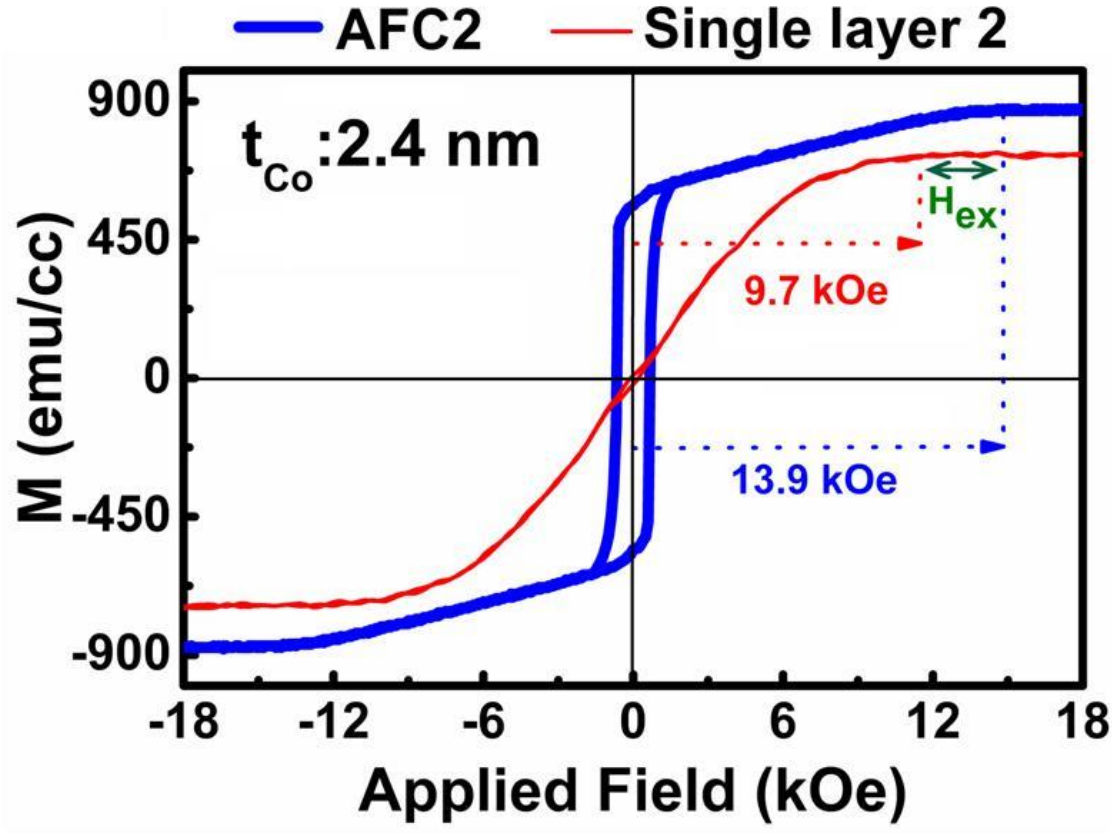

Figure 5.13. M-H loop of complete AFC 2 system with 2.4 nm thick Co layer and only 2.4 nm Co layer without Co/Pd as a single layer type2.

In order to confirm if this high value of saturation field is due to AF coupling, hysteresis loop of 2.4 nm Co layer without Co/Pd multilayers was measured by AGM for comparison. Figure 5.13 shows the hysteresis loops for the two cases. A saturation field of 9.7 kOe was observed for single Co layer which is smaller compared to the case (14 kOe) when it is exchange coupled antiferromagnetically to (Co/Pd) multilayer. This result is in contrast to what was observed in case of two ferromagnetically coupled layers [32, 33]. In the case of two magnetic layers that were coupled ferromagnetically, the saturation field was lower as compared to a single layer. These results indicate that the difference of 4.3 kOe is the magnitude of field needed to overcome the antiferromagnetic coupling.

5.3.3 Structural characterization

In order to further confirm that the differences in the crystallographic structure for different thickness of Co layers are not the cause of the observed phenomenon, rocking curves were measured by XRD as shown in figure 5. 14a. The full width at half maximum (FWHM) was found to be in the range of 4° to 5° (shown in Fig. 5.14(b)) indicating that the crystallographic growth of the (Co/Pd) multilayer was not affected. The absence of any significant trend with Co thickness (0.9–1.2 nm) indicates that the reorientation is essentially magnetic in origin.

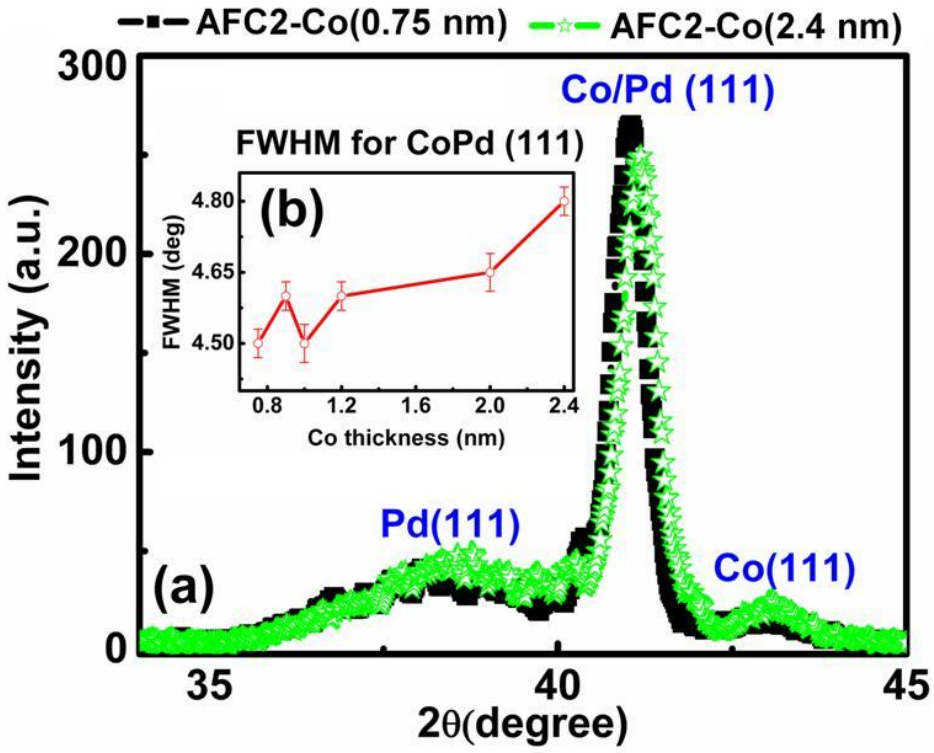

Figure 5.14. (a) X-ray θ-2θ scan of AFC2 with thickness of Co thin film 0.75nm and 2.4 nm, (b) FWHM of Co (FCC:111) peak for complete AFC2 multilayer.

5.3.4 Angular dependency of coercivity and temperature dependency of H_{ex} for AFC 2 films

Angle dependence of perpendicular coercivity was measured for AFC2 thin films with different Co thickness, and it was observed that the coercivity increases with the angle

between magnetization and applied magnetic field (shown in figure 5.15). This behavior indicated that the magnetization reversal in these films is due to domain wall motions. In order to understand the interlayer exchange coupling further, the temperature dependency of magnetization in AFC2 structures with different Co thickness film thicknesses (0.75 nm and 2.4 nm) was studied using superconducting quantum interference device (SQUID). The minor loops of these samples were measured with field increment of 150 Oe at different temperatures ranging from 5 K to 300 K as shown in figures 5.16(a) and 5.16(b). It can be noticed that the sample with 0.75 nm Co, in general, switches in a narrower range of field, indicating spin reorientation.

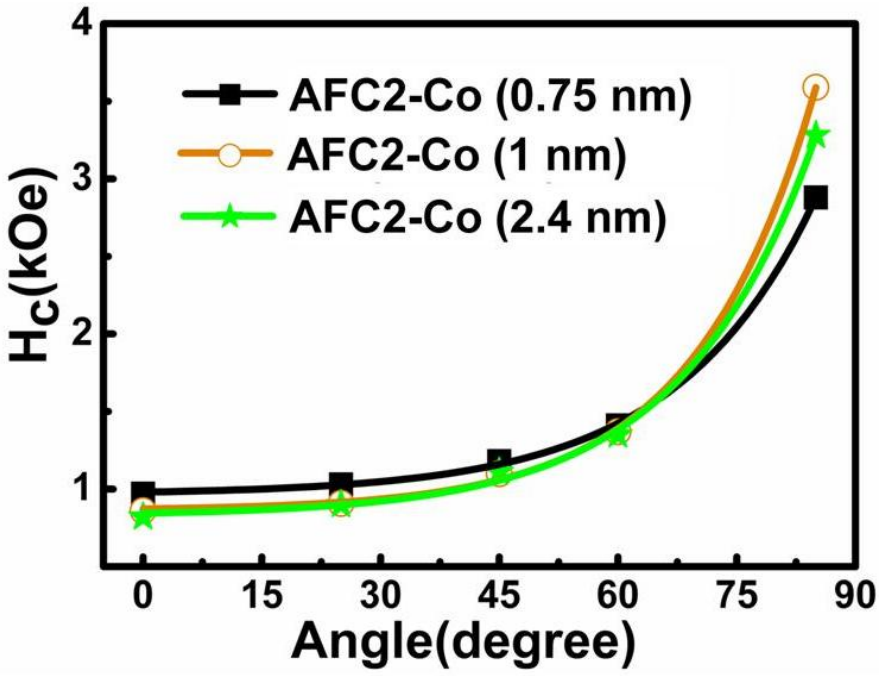

Figure 5.15. Variation of coercivity as a function of applied magnetic field direction in AFC2 structures for selected Co thin film thicknesses (0.75, 1, and 2.4 nm).

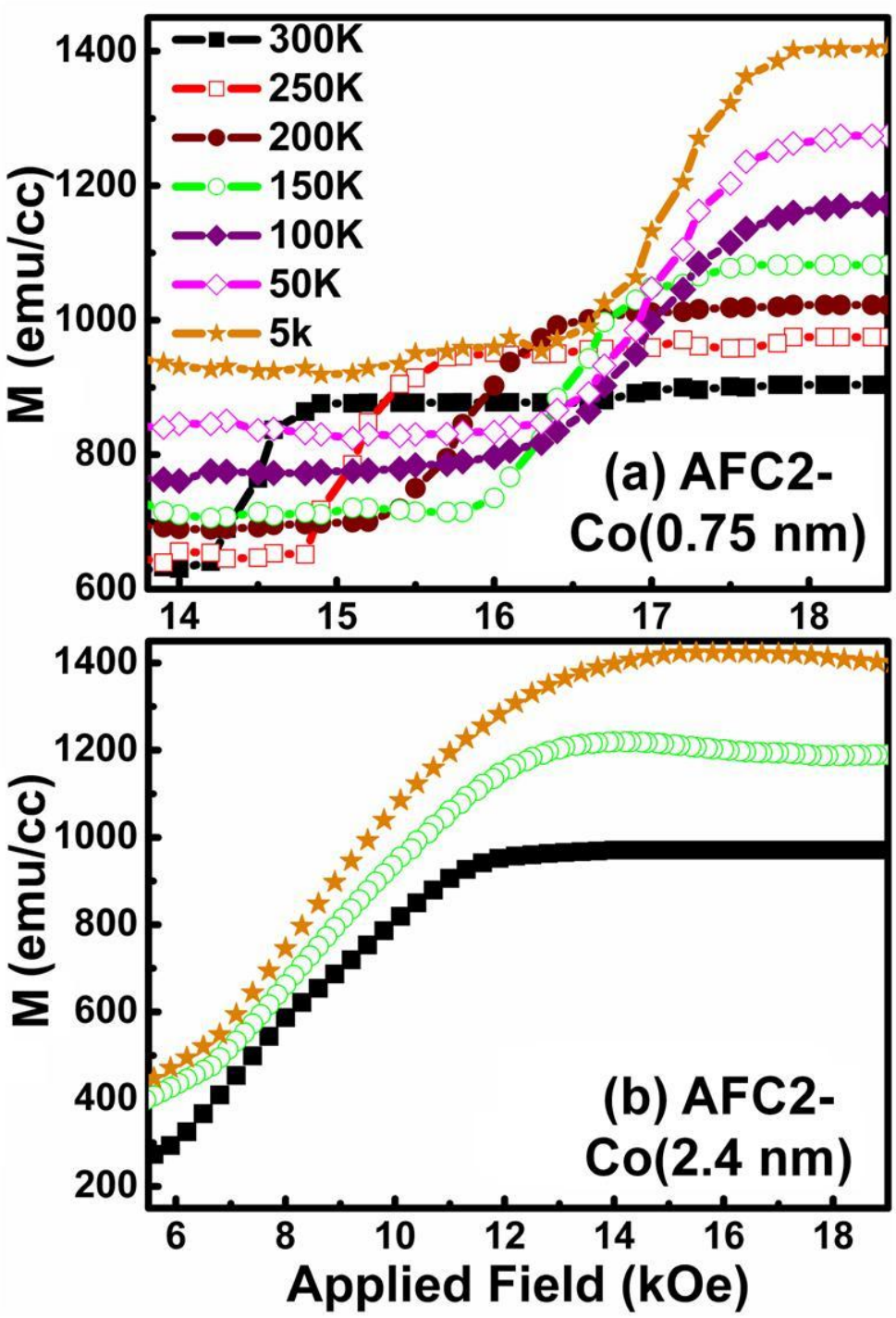

Figure 5.16. Magnetization of AFC2 multilayer system with (a) Co film of 0.75nm in thickness and (b) Co film with 2.4 nm in thickness measured at different temperatures ranging from 5K to 300 K.

On the other hand, the sample with 2.4 nm thick Co does not show a reversal at all temperatures, indicating the absence of spin reorientation even at 5K. For sample with 0.75

nm thick Co layer, the measured FWHM of the derivative of M-H loop (SFD) is 0.51 kOe at 300 K and 0.89 kOe at 5 K. This is attributed to the increase of saturation magnetization at reduced temperatures [34]. It can also be seen from figure 5.16(a) that the exchange coupling field of a complex structure with 0.75 nm Co thin film increases to 17.2 kOe at 5 K. The enhancement in H_{ex} (as temperature decreases) may arise from an increase in J or a decrease in M_s. However, our measurements indicated an increase of saturation magnetization of Co, as reported by Gong et al.,[35] from about 800 emu/cc at 300 K to about 1300 emu/cc at 5 K.

Therefore, the increase in H_{ex} is expected to arise from an increase in J. The value of exchange coupling energy J, calculated using the experimentally measured values of M_s, H_{ex}, and t shows an increase from 1.22 erg/cm^2 at room temperature to 2 erg/cm^2 at 5K. Moreover, it was observed that the saturation field increases from 13.6 kOe and 15.11 kOe at room temperature to 18.1 kOe and 18.25 kOe at 5K for a multilayer system with 2.4 nm and 0.75 nm Co thin film, respectively. These enhancements of saturation field for the films indicate that a large interlayer coupling is induced between ferromagnetic layers [35, 36].

5.4 Magnetic properties of patterned films

As the main objective of this chapter is to understand the effect of low exchange coupling fields and the remanent magnetization on the SFD, patterned magnetic nanostructures over a large area (20 mm by 20 mm) were fabricated with nano imprinting lithography method. For the fabrication of nanostructures, the magnetic films were coated with a UV resist and imprinted using a positive nano-imprinting process described in section (3.4). The patterns from the mold that had holes with a diameter of 200 nm at 400 nm pitch were transferred to

the magnetic films using reactive-ion etching and ion-milling. Figure 5.17 shows the atomic force microscopy (AFM) image from magnetic nanostructures.

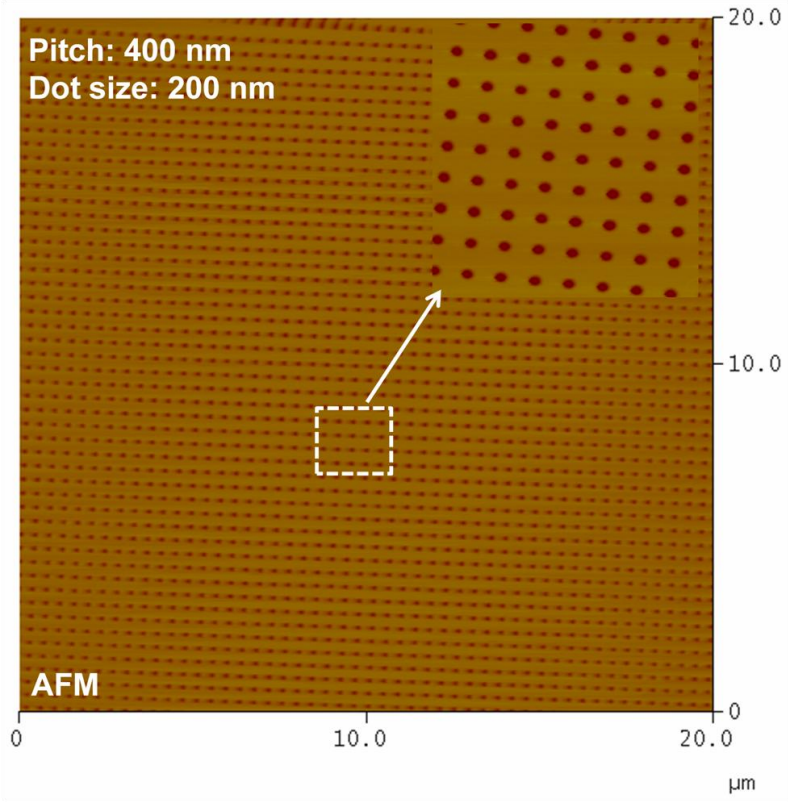

Figure 5.17. Atomic force microscopy image (AFM) of magnetic nanostructures with 400 nm pitch size and 200 nm diameter, respectively.

The patterned nanostructures were characterized using alternating gradient magnetometer, and atomic force microscopy. The details of magnetic properties and SFD of both AFC1 and AFC2 nanostructures will be discussed in section 5.4 and 5.5, respectively.

5.4.1 M-H loops of nanostructures with low exchange coupling field

The magnetic nanostructures of AFC1 samples were also characterized using AGM. Figure 5.18 shows the hysteresis loops of the patterned films of $(Co/Pd)_{10}$ multilayers as reference sample, AFC1 multilayers with Co thickness ranging from 0.4 nm to 1.4 nm. The coercivity

values of the patterned samples are higher than those in thin films. This can be understood to be arising from the possible reduction of nucleation sites with lower reversal fields due to patterning. In continuous films, the magnetization reversal nucleates at sites with lower anisotropy and progresses in a rapid sweep of domain wall. In the case of patterned films, the patterning process removes several of such nucleation sites, resulting in an increased coercivity.

AGM was also used to measure the minor loops as shown in figure 5.19 to understand more about the reversal of $[Co\ (t\ nm)/Pd(0.8\ nm)]_{\times 3}$. It can be noticed that the minor loop coercivity of sample with 0.4 nm Co is much larger and that the kink is observed in the second quadrant. No reduction in the $M_r \times t$ is observed for t=0.4 nm. On the other hand, for 1 nm thick Co, the minor loop coercivity is much lower and a kink is observed in the first quadrant. As mentioned earlier, for a suitable $M_s \times t$ of the stabilizing layer, the kink would be further moved to the right side of the first quadrant. These results indicate that AFC patterned Co/Pd multilayers can be prepared with thicker Co sublayers in the stabilizing layer.

In other respects, the coercivity of the samples with 1 nm Co is not significantly enhanced even after patterning. In these samples, the H_{ex} (255 Oe) is slightly larger than Hc (240 Oe), even after patterning. Although the nucleation of $(Co/Pd)_{\times 3}$ occurs in the first quadrant, the remanent moment is not significantly reduced due to the switching field distribution. However, this is not a serious disadvantage, as significant reduction of M_r can be achieved using Co layers with t= 1 nm, by using only 2 bilayers instead of 3. As H_{ex} is inversely proportional to the thickness, reducing the bilayers from 3 to 2, can help to achieve a larger H_{ex} and an antiferromagnetically coupled remanent moment configuration.

Figure 5.19 shows the coercivity and exchange field obtained from the minor loop. It can be noticed that the H_c decreases from about 4000 Oe to about 200 Oe. Moreover, coercivity of

the thinner layer, especially in samples with 0.4 nm thick Co, increases significantly after patterning. At the same time, patterning also reduces H_{ex}. This leads to a situation where $H_{ex} < H_c$, where there is no antiparallel alignment of moments at remanence. These results confirm the hypothesis with which this work was initiated. In the case of AFC patterned media, such an increase of H_c (together with the decrease of H_{ex}) invalidates the benefit of AFC.

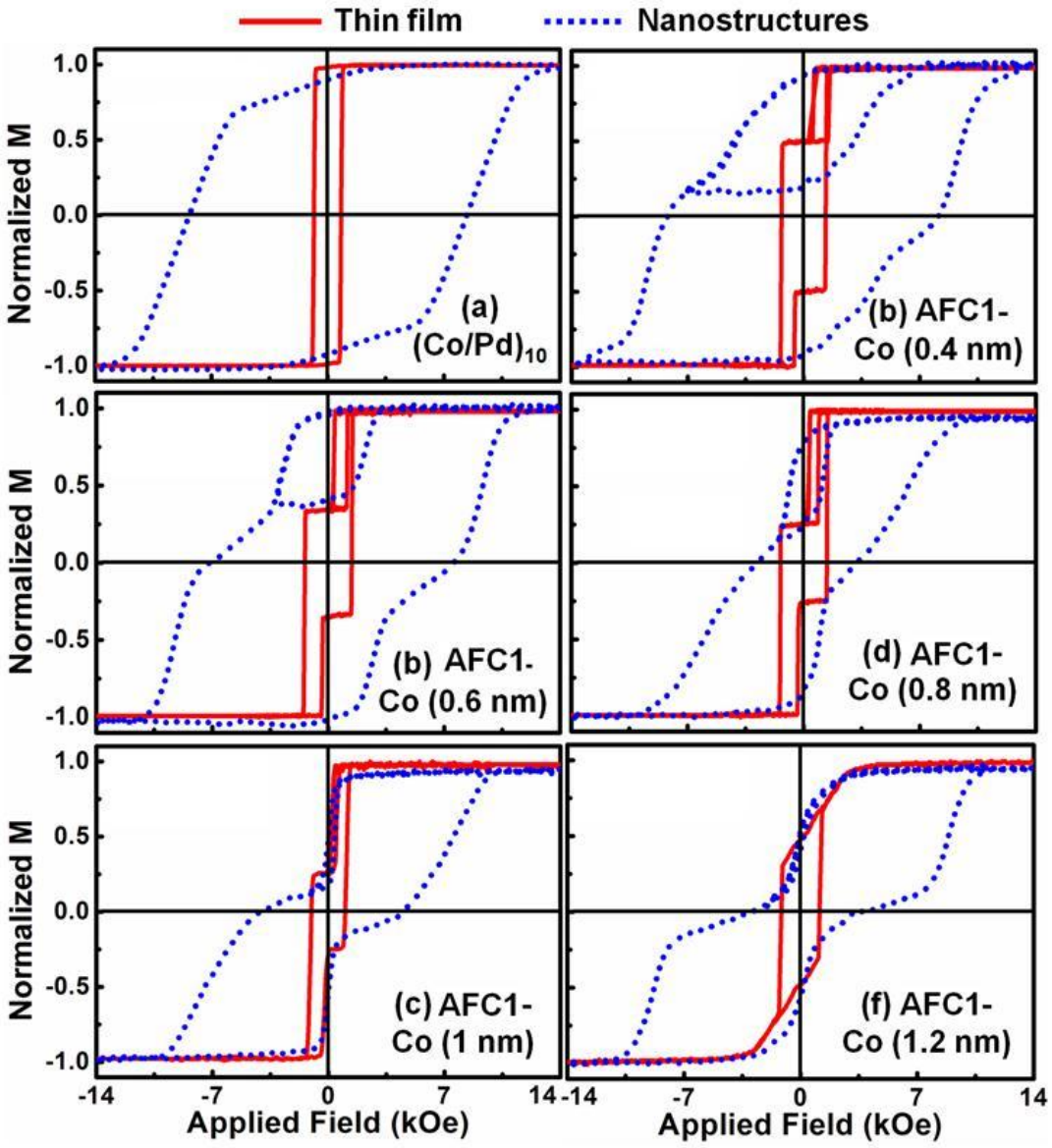

Figure 5.18. Hysteresis loops of thin film and patterned films of Co/Pd multi layers and AFC1-Co/Pd multilayers with Co thickness from 0.4 nm to 1.4 nm.

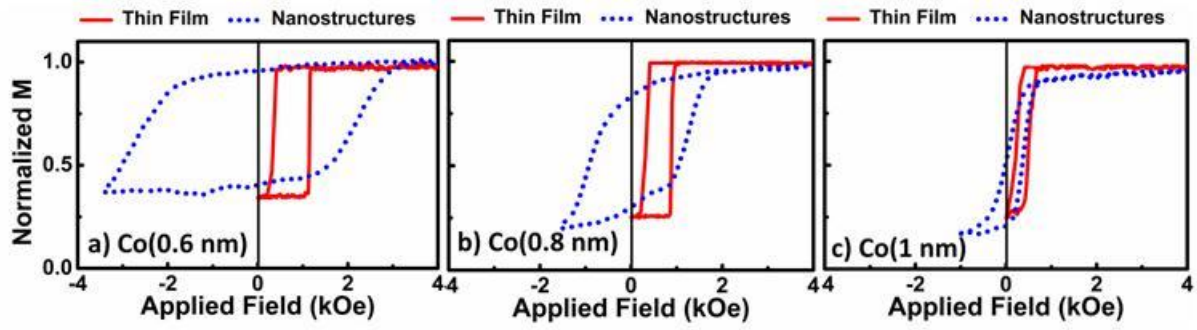

Figure 5.19. Minor hysteresis loops of thin film and patterned films of Co/Pd multi layers and AFC1-Co/Pd multilayers with Co thickness from 0.6 nm to 1 nm.

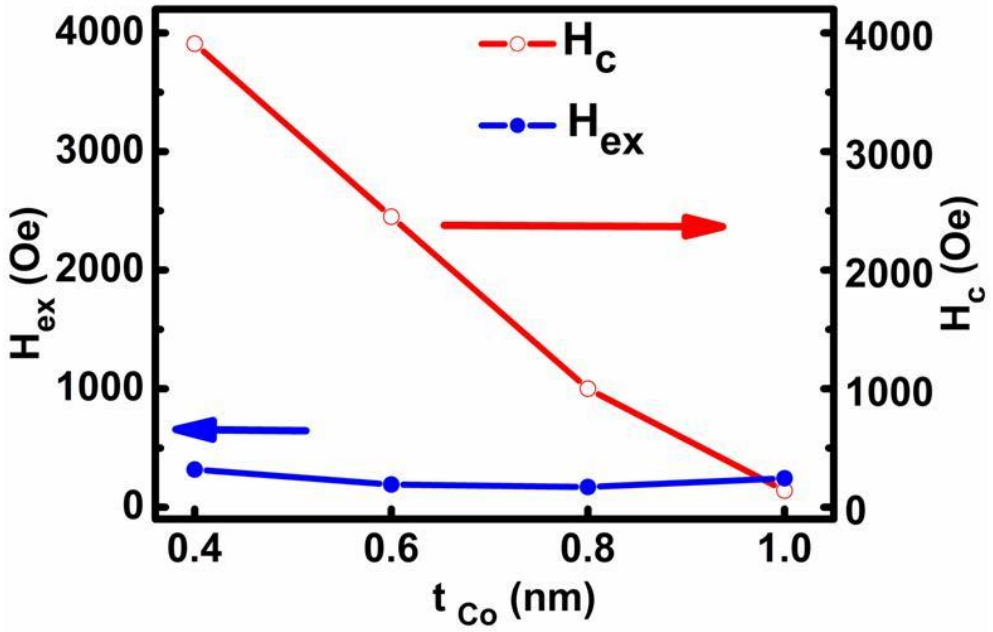

Figure 5.20. H_{ex} and H_c of minor loops from AFC1 patterned samples as a function of thickness of Co sublayer in the stabilizing layer.

Another observation that can be made from figure 5.20 is that the coercivity of the minor loops in nanostructured samples reduces with the increase in Co sublayer thickness. Such a decrease of coercivity can be explained by the reduction in the anisotropy of the $(Co/Pd)_{\times 3}$ multilayers. The key highlight of figure 5.19 is that the H_c reduces to a value lower than H_{ex} with an increase of t. It has to be mentioned that the H_{ex} in this sample can be further increased if the number of bilayers is reduced to 2. These results indicate that the AFC configuration at remanence can be tailored in patterned media with Co/Pd multilayers.

5.4.2 M-H loops of AFC2 nanostructures with high exchange coupling field

The magnetic properties of AFC2 patterned samples with high exchange coupling filed were also measured by AGM. Figure 5.21a shows the hysteresis loops of the thin films and the patterned films (Co (0.3 nm)/Pd (0.8 nm)]$_{\times 15}$ multilayers without exchange layer as a reference structure , and figure 5.23 (b-d) show M-H loop of thin film and AFC2 patterned samples with 0.75 nm to 2.4 nm thick Co layer. It can be seen that the values of the coercivity of the patterned samples are higher than those in thin films. As mentioned earlier, this increment in coercivity of patterned films can be understood to be arising from the possible reduction of nucleation sites with lower reversal fields due to patterning.

It was expected that after patterning the films, demagnetizing field will be reduced and H_{ex} increased. However, surprisingly, H_{ex} remained at about 15 kOe, even after patterning of AFC2 with 0.75 nm thick Co layer. This is understood to be arising from competing effects from patterning which reduces the demagnetization field, and at the same time, the ion milling process which reduces J. With an increase of Co thickness, H_{ex} decreased as expected and beyond certain thickness (1.3 nm), surprisingly, exchange coupling field was not observed.

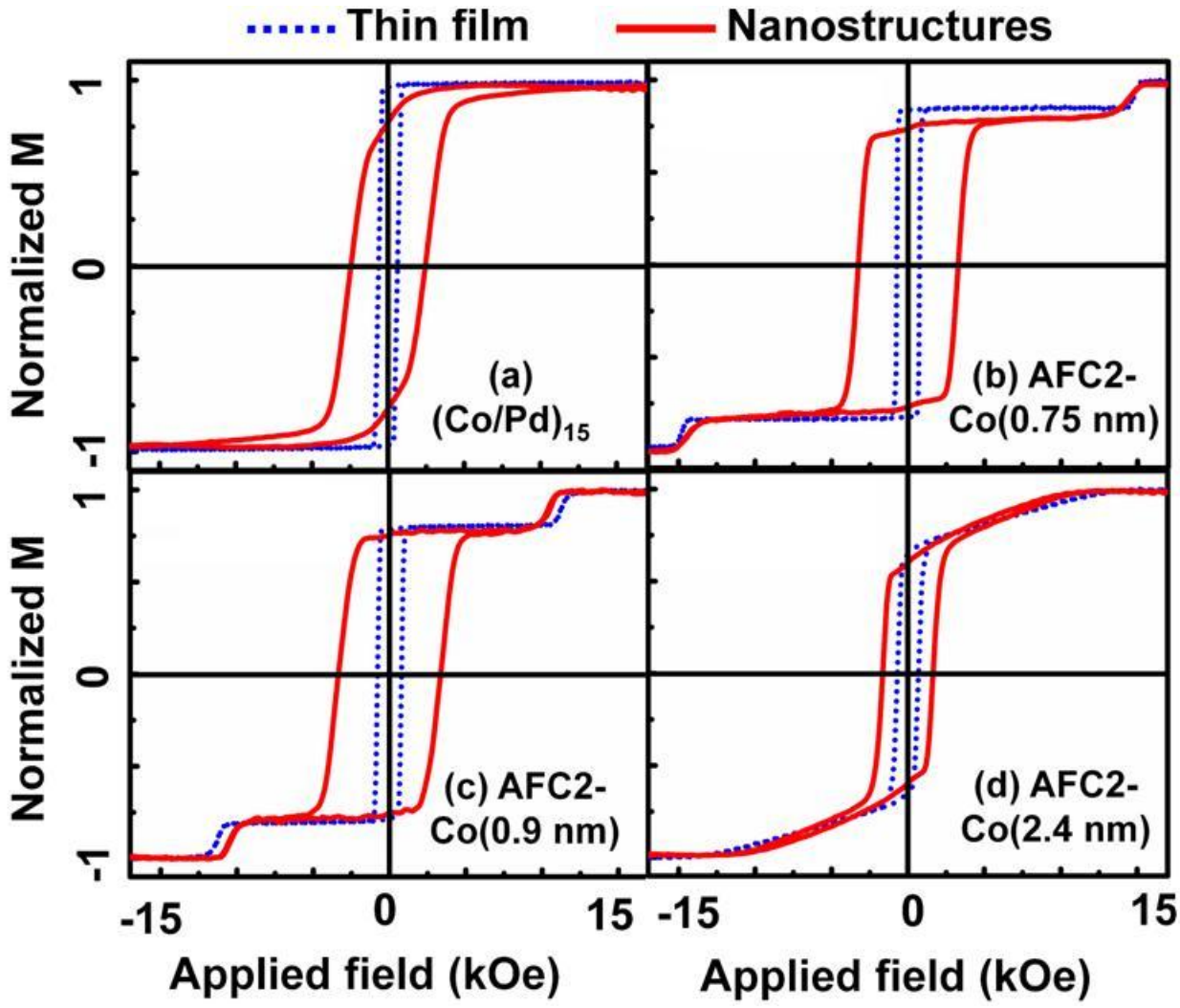

Figure 5.21. M-H loops of the thin films and the patterned samples a) for $(Co/Pd)_{15}$ multilayers without AFC2 configuration as a reference layer, AFC2 structures with thick b) 0.75 nm, c)0.9 nm and d) 2.4 nm Co layer, respectively.

As the main objective of the work is to understand the effect of H_{ex} on the SFD of patterned films, the derivative of the hysteresis loop of AFC1 and AFC2 patterned films was used to measure SFD. The details of SFDs study in section 5.5.

5.5 Measurement of SFD curves

Figure 5.22 shows normalized SFD of $(Co/Pd)_{\times 15}$ without exchange coupling layer, (AFC2) composed of $(Co/Pd)_{\times 15}$ multilayers coupled with 0.75 nm and 2.4 nm thick Co layer. It can

be noticed that the SFD of 0.24 is the smallest for the AFC2 structure with 0.75 nm thick Co layer. These results indicate that the media with a high H_{ex} provides lower SFD. This result is closer to our prediction which laid the objective of this work. When the exchange coupling field is larger than the coercivity after pattering, the magnetization of stabilizing layer can be antiferromagnetically coupled with the recording layer. Therefore, the AFC2 media with 0.75 nm thick Co stabilizing layer that possesses an antiferromagnetically coupled configuration at remanence provides the lowest SFD.

In addition, reduction in SFD by 22.5% in AFC1 patterned film can be related to antiparallel alignment at remanence state which reduces dipolar interactions. However, no reduction in the remanent magnetization is observed in AFC2 patterned structure. It was found that achieving the antiferromagnetically coupled configuration at remanence plays an important role in minimizing the SFD. The high H_{ex} can be used for AFC bit patterned media and magnetic memory.

Another interesting observation can be made from figure 5.23, which shows the trend of H_{ex} as a function of thickness in stabilizing layer. The trend of H_{ex} in the AFC2 nanostructures is almost same as in thin films. The AFC2 structure shows a large H_{ex} for t less equal to 1.2 nm (region I), beyond which (region II), no exchange coupling can be observed (H_{ex} ~0), in the case of both thin film and patterned samples. This can be explained as a consequence of the lack of spin-orientation in films with thicker Co layers [39]. In other ways, the AFC1 structure shows a decrease of H_{ex} with t, as per the relation $H_{ex} = J/M_S \times t$. These results illustrate the difference between conventional synthetic antiferromagnets and spin-reoriented synthetic antiferromagnets. Moreover, it can be noticed that a high value of H_{ex} is observed in a complex multilayer system because of the high perpendicular anisotropy induced by seed layers below Co thin layers. However, above a certain thickness of Co layer

(> 1.3 nm) the bulk anisotropy is more dominant than interface anisotropy and high H_{ex} was not observed.

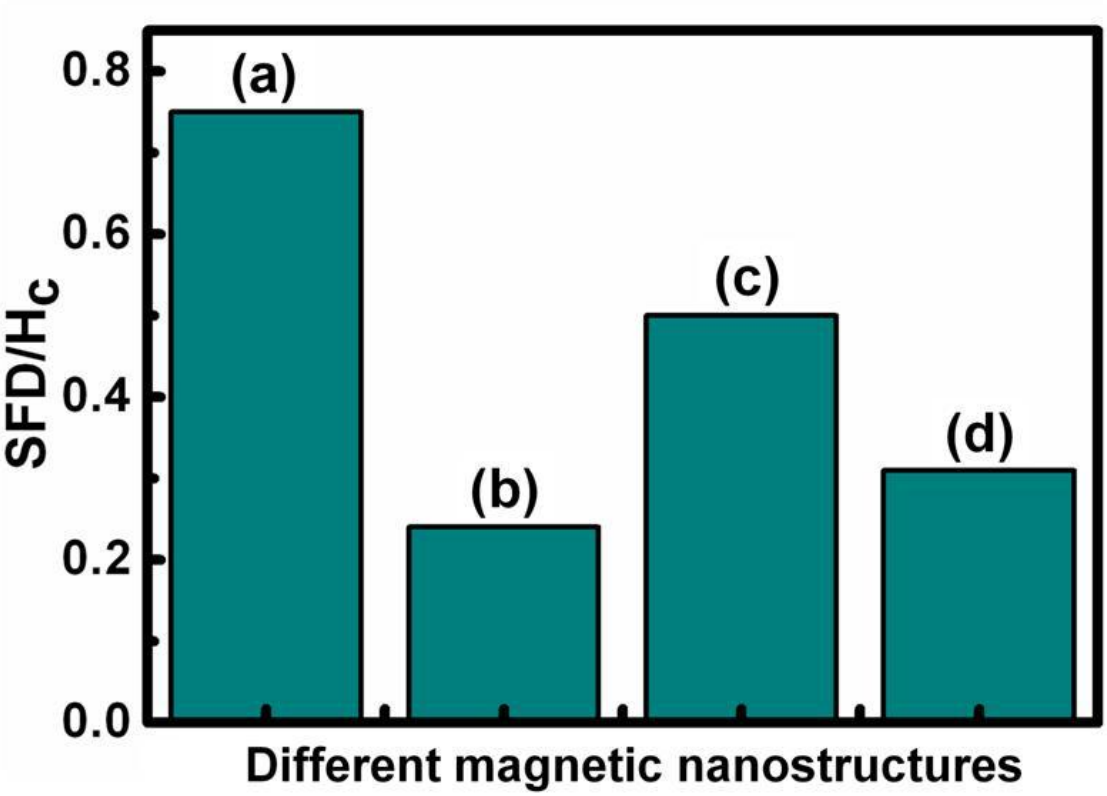

Figure 5.22. Normalized SFD of (a) $(Co/Pd)_{\times 15}$ without exchange coupling layer, (AFC1) composed of $(Co/Pd)_{\times 15}$ multilayers coupled with (b) 0.75 nm, (c) 2.4 nm thick Co layer, and (d) (AFC2) composed of $(Co/Pd)_{\times 10}$ coupled with $[Co\ (0.4\ nm)/Pd\ (0.8\ nm)]_{\times 3}$ bilayers, respectively.

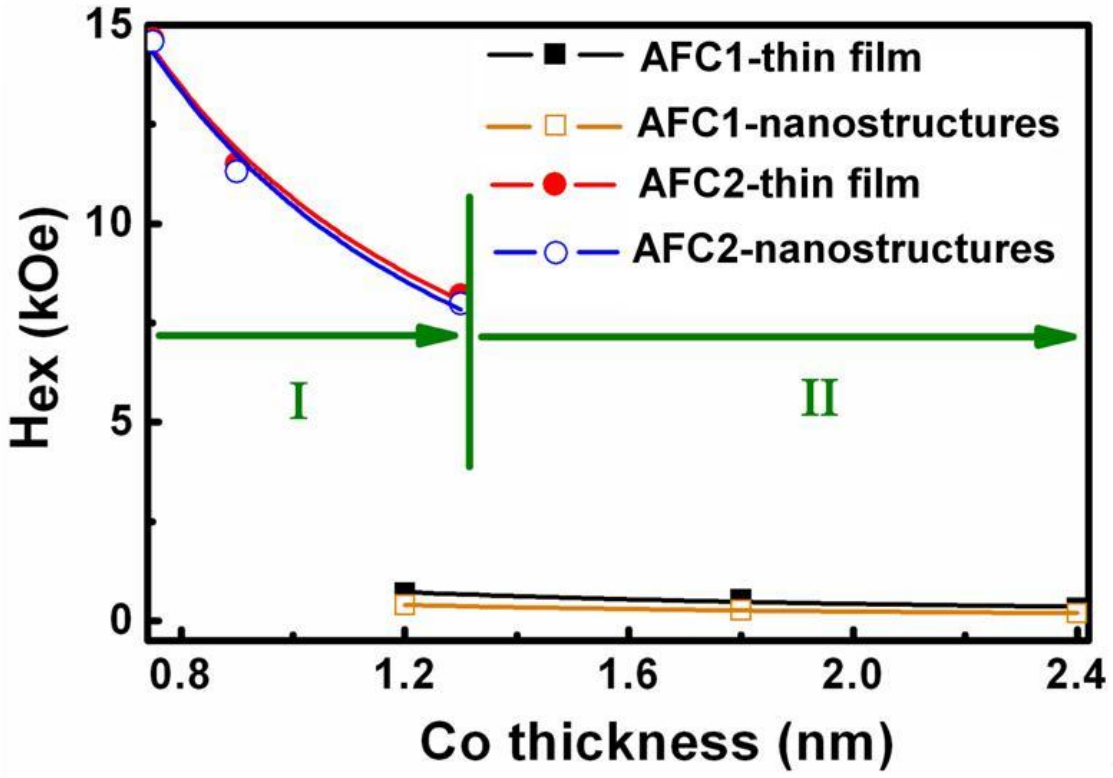

Figure 5.23. Exchange field of thin film and patterned films versus Co thickness (nm) for AFC1 and AFC2 structures.

In addition, reduction in SFD by 22.5% in AFC1 patterned film can be related to antiparallel alignment at remanence state which reduces dipolar interactions. However, no reduction in the remanent magnetization is observed in AFC2 patterned structure. It was found that achieving the antiferromagnetically coupled configuration at remanence plays an important role in minimizing the SFD. The high H_{ex} can be used for AFC bit patterned media and magnetic memory.

Summary

In summary, spin-reorientation in antiferomagnetically coupled structures was studied in thin films and nanostructures. A high value of H_{ex} is observed in a complex multilayer system because of the high perpendicular anisotropy induced either by seed layers or because of a

spin-reorientation caused by antiferromagnetic coupling. However, above a certain thickness of Co layer (> 1.3 nm) the volume anisotropy is more dominant than interface anisotropy and high H_{ex} was not observed. Moreover, the effect of high and low exchange coupling fields on the magnetostatic interaction and hence on the SFD of the patterned structure has been investigated. In addition, reduction in SFD by 22.5% in AFC2 patterned film can be related to antiparallel alignment at remanence state which reduces dipolar interactions. It was found that achieving the antiferromagnetically coupled configuration at remanence plays an important role in minimizing the SFD. The high H_{ex} can be used for AFC bit patterned media and magnetic memory.

Until now, the SFD was controlled using antiferromagnetic coupling as a main mechanism. In chapter 6, our second approach to reduce the SFD of patterned media based on capped bit-patterned media (CBPM) will be discussed. In CBPM, a continuous ferromagnetic layer is added to patterned nano structures. The thin film layer can introduce exchange coupling to compensate magnetostatic interactions as a way to tailor the SFD. In addition, anomalous Hall effect (AHE) measurement is utilized to study the magnetic properties of patterned film with 50 nm pitch size and also capped layer.

References

1. R. Sbiaa, S. N. Piramanayagam, and R. Law, Appl. Phys. Lett. **95**, 242502 (2009).
2. S.N. Piramanayagam, K.O. Aung, S. Deng, and R. Sbiaa, J. Appl. Phys. **105**, 07C118 (2009).
3. M. Ranjbar, S. N. Piramanayagam, D. Suzi, K. O. Aung, R. Sbiaa, Y. S. Key, S. K. Wong, and T. C. Chong, IEEE Trans. Magn, **46**, 1787 (2010).

4. P. F. Carcia, A. D. Meinhaldt, A. Suna, Appl.Phys.Lett. **47,** 178 (1985).

5. P. F. Carcia, J.Appl.Phys. **63**, 5066 (1988).

6. F. J. A . denBroeder, D . Kuiper, A. P.Vande Mosselaar,W. Hoving, Phys. Rev. Lett. **60**, 2769 (1988).

7. M. Sakurai, T. Takahata, I. Moritani, J. Magn. Soc. Jpn.**15**, 411 (1991).

8. F. J. A. denBroeder,W. Hoving, P. J. H. Bloemen, J.Magn.Magn.Mater.**93,** 562 (1991).

9. Y. Kawada,Y. Ueno, K. Shibata, IEEETrans.Magn.**38**, 2045 (2002).

10. H.Ohmori, A. Maesaka, IEEETrans.Magn.**36,** 2384 (2000).

11. S.N. Piramanayagam, M. Matsumoto, A. Morisako, S. Takei and D. Kadowaki, IEEE Trans. Magn. **33**, 3247 (1997).

12. D. Weller, L. Folks, M. Best, E. E. Fullerton, B. D. Terris, G. J. Kusinski, K. M. Krishnan, and G. Thomas, J. Appl. Phys. **89**, 7525 (2001).

13. H-S. Oh, S-K. Joo, IEEE Trans. Magn. **32,** 4061 (1996).

14. B. Terris, T. Thomson, G. Hu, Microsyst. Technol. **13**,189 (2007).

15. R. Sbiaa, C. Z. Hua, S. N. Piramanayagam, R. Law, K. O. Aung, and N. Thiyagarajah, J. Appl. Phys.**106**, 023906 (2009).

16. O. Hellwig, A. Berger, T. Thomson, E. Dobisz, Z. Z. Bandic, H. Yang, D. S. Kercher, E. E. Fullerton, Appl. Phys. Lett. **90**, 162516 (2007).

17. M. Ranjbar, A. Tavakkoli K. G, S. N. Piramanayagam, K. P. Tan, R. Sbiaa, S. K. Wong and T. C. Chong, J. Phys. D: Appl. Phys. **44,** 265005 (2011).

18. J. M. Shaw, W. H. Rippard, S. E. Russek, T. Reith, and C. M. Falco, J. Appl. Phy. **101**, 023909 (2007).

19. B. D. Terris, M. Albrecht, G. Hu, T. Thomson, and C. T. Rettner, IEEE Trans. Magn. **41**, 2822 (2005).

20. A. Moser, O. Hellwig, D. Kercher, and E. Dobisz, Appl. Phys. Lett. **91**, 162502 (2007).

21. S.N. Piramanayagam, J.P. Wang, C.H. Hee, S.I. Pang, T.C. Chong, Z.S. Shan and L. Huang, Appl. Phys. Lett. **79**, 2423 (2001).

22. T. Thomson, G. Hu, and B. D. Terris, Phys. Rev. Lett. **96**, 257204 (2006).

23. Y.P. Lee, S.K. Kim, J.S. Kang, J.I. Jeong, J.H. Hong, Y.M. Koo and H.J. Shin, J. Vac. Sci. Technol. A, **12(5),** 2672 (1994).

24. S-C. Shin, Appl. Surf. Sc. **65/66**, 110 (1993).

25. R. Sbiaa, Z. Bilin, M. Ranjbar, H. K. Tan, S. J. Wong, S. N. Piramanayagam, and T. C. Chong, J. Appl. Phys. **107**, 103901 (2010).

26. S. Ikeda, J. Hayakawa, Y. Ashizawa, Y. M. Lee, K. Miura, H. Hasegawa, M. Tsunoda, F. Matsukura, and H. Ohno, Appl. Phys. Lett. **93**, 082508 (2008).

27. H. Meng, W. H. Lum, R. Sbiaa, S. Y. H. Lua, and H. K. Tan .J. Appl. Phys. **110**, 033904 (2011).

28. S. I. Pang, S. N. Piramanayagam, and J. P. Wang, Appl. Phys. Lett. **80**, 616 (2002).

29. N. Kikuchi, S. Okamoto, O. Kitakami, Y. Shimada, and K. Fuakmichi, Appl. Phys. Lett. **82**, 4313 (2003).

30. E. Girt and H. J. Richter, IEEE Trans. Magn. **39**, 2306 (2003).

31. S. S. Parkin, N.More, and K. P. Roch, Phys. Rev. Lett.**64**, 2304 (1990).

32. R. Sbiaa, H. Le Gall, Y. Braik, J. M. Desvignes, and S. Yurchenko, IEEE Trans. Magn. **31**, 3274 (1995).

33. H. Le Gall, R. Sbiaa, and S. Pogossian, J. Alloys Compd. **275**, 677 (1998).

34. L. Li, F. Zhang, N. Wang, Y. F. Lv, X. Y. Han, and J. J. Zhang, J. Appl.Phys. **108**, 073908 (2010).

35. W. Gong, H. Li, Z. Zhao, and J. Chen, J. Appl. Phys. **69**, 5119 (1991).

36. Y.P. Lee, S.K. Kim, J.S. Kang, J.I. Jeong, J.H. Hong, Y.M. Koo and H.J. Shin, J. Vac. Sci. Technol. A, **12(5),** 2672 (1994).

37. C.R. Pike, A.P. Roberts and K.L. Verosub, J. Appl. Phys. **85,** 6660 (1999).

38. S. Piramanayagam, M. Ranjbar, J. Appl. Phys. **111**, 07B728 (2012).

39. M. Ranjbar, S. N. Piramanayagam, S. K. Wong, R. Sbiaa, W. Song, H. K. Tan, L. Gonzaga, and T. C. Chong, J. Appl. Phys. **110**, 093915 (2011).

Chapter 6. Reduction of SFD with Capped bit-patterned media (CBPM)

6.1 Introduction

In Chapters 3, 4 and 5, we discussed our first approach to reduce switching field distributions (SFDs) based on antiferromagnetically coupled (AFC) bit patterned media (BPM) with different designs for the stabilizing layer. In previous chapters, our objective to minimize the SFD was through creation of anti-parallel configuration of magnetizations at remanent state. In this chapter, we discuss the role of a small exchange coupling between isolated single-domain magnetic dots and a thin continuous film – in a system called capped bit-patterned media (CBPM).

Since conventional magnetic characterization techniques such as magnetic force microscopy (MFM) can only measure one magnetization direction at a time or alternating gradient magnetometer (AGM) need a large area of patterned area, we used anomalous Hall effect (AHE) measurements which is a capable technique to study the magnetization switching and magnetic properties of patterned dots even for small area. In addition, AHE can distinguish simultaneously the in plane and out of plane components of magnetization. Thus, AHE was used to investigate the SFD for BPM and CBPM based on (Co/Pd) multi layers with 5, 10, 15, 25 repeats. The first part of this chapter explains the magnetic and crystallographic properties of Co/Pd multilayers. The second part studies the effect a continuous layer coupled with BPM structure on SFD.

6.2 Co/Pd multilayers

$(Co/\ Pt)_N$ or $(Co/Pd)_N$ multilayers with 5 to 25 bilayer repeats have been investigated by different groups and it has been reported that magnetization exhibits sharp switching [15,16].

For the case of N equals to 4, the existence of sub microsized domains inside much larger macroscopic “bubble” type domains was observed. For much larger N, magnetization reversal is found to be dominated by nucleation followed by domain wall motion [17–23]. Knepper and Yang [21] investigated (Co/Pt) multilayer with a number of repeats ranging from 2 to 30, but their study focused on the oscillatory behavior of the interlayer coupling of the multilayers as a function of Pt thickness.

In this chapter, magnetization reversal and domain structures in $(Co/Pd)_N$ multilayers with a number of repeats ranging from 5 to 25 have been investigated for patterned media applications. The $(Co/Pd)_N$ multilayers used in our study were deposited on thermally oxidized Si substrates by dc sputtering. A schematic of these structures is shown in figure 6.1. A lamination of Ta (5 nm)/Cu (5 nm)/Pd (3 nm) was used as seed layer to improve the crystallographic growth of the multilayer as was reported in a previous study [8, 24]. The thickness of Co and Pd were fixed to 3 Å and 8 Å, respectively, to achieve a relatively large perpendicular anisotropy.

Magnetization reversal in (Co/Pd) multilayers with perpendicular anisotropy for different numbers of bilayers (N) is investigated experimentally and by theoretical modeling. Before discussion about patterned media properties, firstly we studied the magnetostatic energy in these structures and its effect on the magnetization reversal behavior and the nature of domain formation.

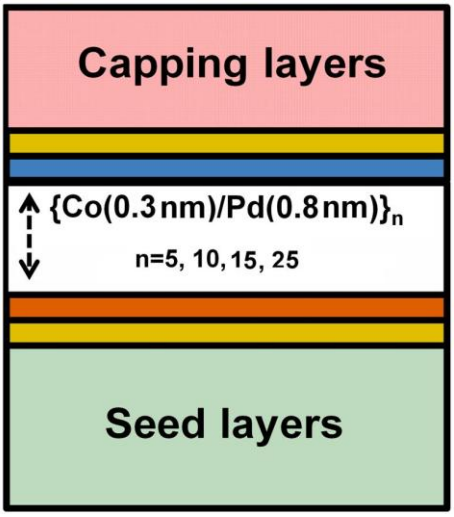

Figure 6.1. An illustration of Co/Pd multilayers with 5, 10, 15 and 25 repeats.

6.2 .1 Magnetization reversal mechanisms in Co/Pd multilayers

The hysteresis loops for $(Co/Pd)_N$ multilayers are shown in figure 6.2 for different number of bilayers. There was no noticeable change in the coercivity H_C with N although the multilayer with ten bilayers shows slightly larger H_C. The most striking behavior is the change in the slope of the hysteresis loop for fields near and exceeding H_C as N varies. For multilayers with less than ten bilayers, a sharp magnetization reversal was observed. This is in contrast to multilayers with 15 and 25 repeats which show a large tail in the hysteresis loop. In all the multilayers deposited with N up to 25, the ratio between remanence magnetization M_r and saturation magnetization M_s is equal to 1. In figure 6.2 for films with more than 15 bilayers, magnetization reversal occurs in two steps: nucleation of a large number of domains followed by a slow domain movement.

From the study on multilayers with 15 repeats, Sbiaa et al. observed that after nucleation of domains, the width of the stripes decreases while the domains expand until saturation [22].

Even though there is no clear trend of H_c as a function of N, the tail of the hysteresis loop is more pronounced for multilayers with N larger than 15. To explain the experimental results presented in figure 6.1, we also conducted MFM studies of these samples. The images, taken at ac-demagnetized state for the different multilayers, show a clear difference in domain size.

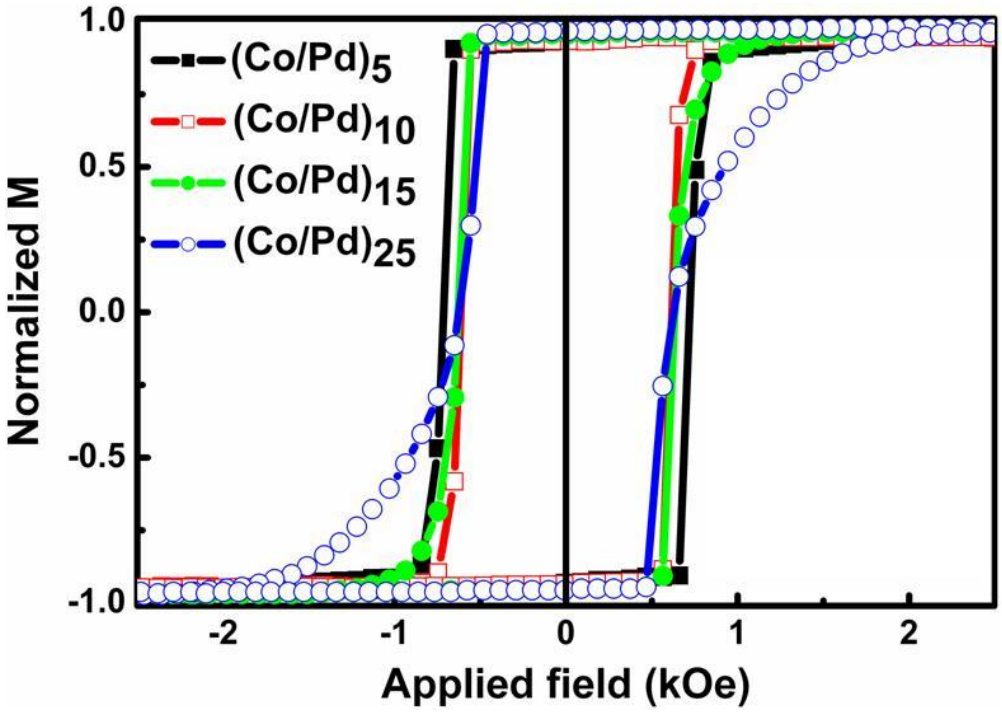

Figure 6.2. Hysteresis loops for (Co/Pd) multilayers with different number of repeats measured by AGM. In the measurement, the magnetic field was applied perpendicular to film plane. A sharp magnetization switching can be seen for five and ten bilayers cases while tails in the hysteresis loops were observed for multilayers with 15 and 25 repeats.

All the MFM images shown in figure 6.3 were taken from a 20 µm by 20 µm area of each multilayer. For five bilayers case, no clear magnetic domains could be observed after demagnetization of the sample. For (Co/Pd) with 10 and 15 bilayers, large domains of more than 3 µm in width can be observed. The same domain patterns were observed for all other multilayers except that the size of the domains becomes smaller as the number of bilayers

increases. To confirm the correlation between the size of magnetic domains and the number of bilayers, each multilayer has been deposited three to four times and similar results as shown in figures 6.1 and 6.3 were obtained. In figure 6.3, for multilayers with 22 and 25 bilayers, we did not see a clear difference in magnetic domain size although the samples were repeated. It is known that magnetostatic interactions influence the domain size in magnetic thin films with perpendicular anisotropy [25–27].

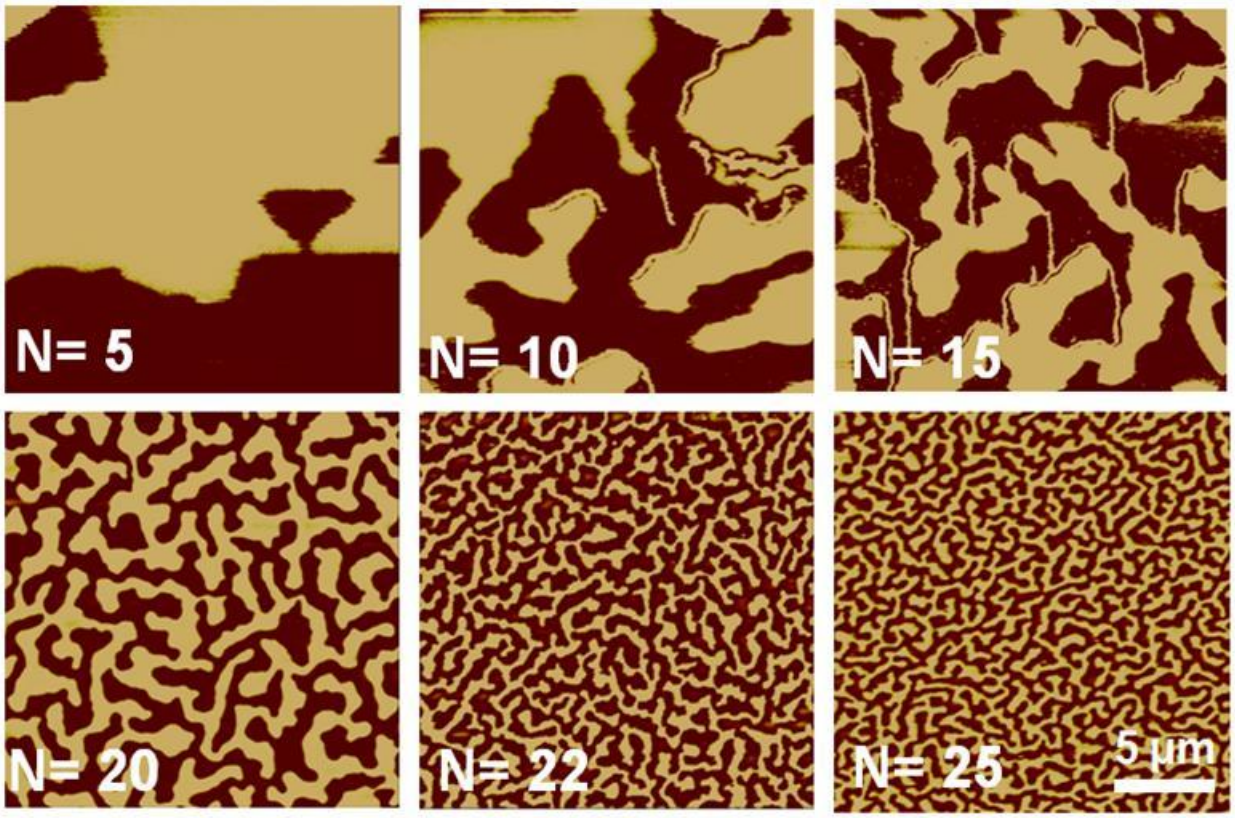

Figure 6.3. MFM images in demagnetized states for (Co/Pd) multilayers with different number of repeats N. The series of images clearly show the reduction in domain size as the number of bilayers increases. The image scale is 20 µm by 20 µm.

Based on theoretical modeling [28] that took into account of the magnetostatic energy from the different magnetic layers, the domain size dependence on the number of bilayers is explained. For large N, the tail in the hysteresis loop is revealed to be the result of an increase

in the magnetostatic energy, which at the same time leads to a drastic reduction in domain width.

6.2 .2 Crystallographic properties of Co/Pd multilayers

From x-ray diffraction measurements shown in figure 6.4, only one clear peak at around 41° was observed for all the multilayers which is a good indication of the growth of fcc (111) of CoPd. There was no change in the fcc (111) peak position by increasing the number of bilayers although the intensity of the x-ray signal increases with the total thickness as expected. Furthermore, we did not observe a difference in signal taken from low angle XRD of these three multilayers. These results confirm that the microstructure and roughness at the interfaces of the (Co/Pd) multilayer did not change by increasing the number of repeats.

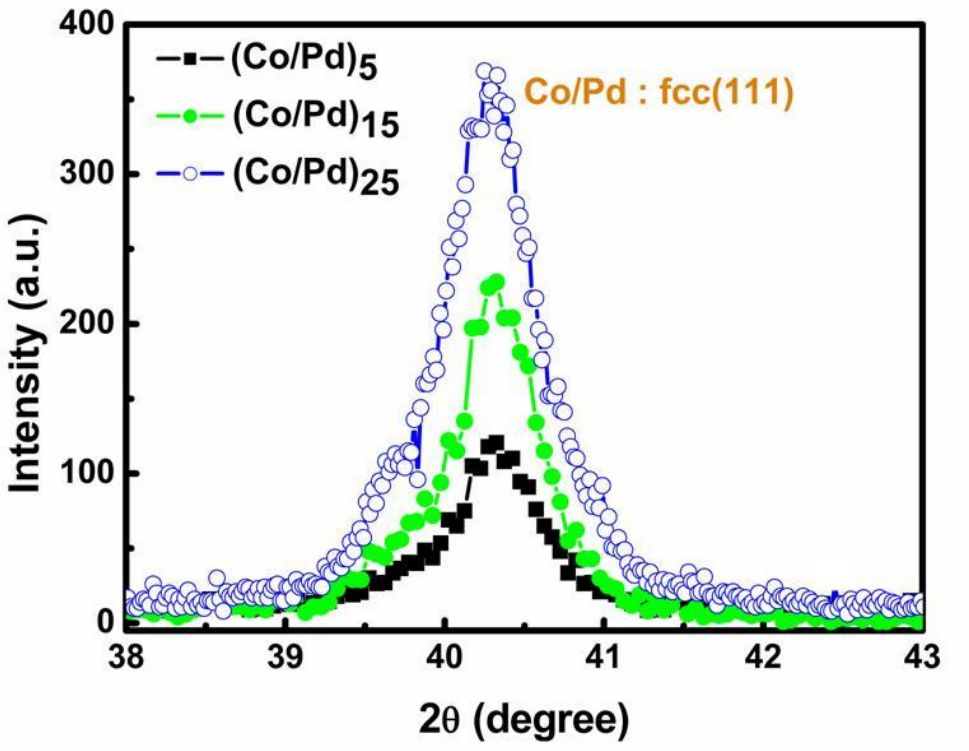

Figure 6.4. X-ray θ-2θ scan of (Co/Pd) multilayers with 10, 15, and 25 bilayers.

Having discussed the magnetic and structural properties of thin films, the discussions in the next sections focus on the magnetic properties of conventional and novel BPM as investigated using AHE measurement.

6.3 Capped bit patterned media (CBPM)

As is discussed in previous chapters, Bit patterned medium is one of the promising candidates to overcome the issue of media trilemma and the switching field distribution (SFD) of the magnetic dots remains as a challenge [33-39]. Since a larger SFD will lead to increased amount of write-in errors, SFD is an important topic studied by several researchers [39-41].

Antiferromagnetically coupled patterned (AFC) media were discussed in chapters 3, 4 and 5 as possible candidates to understand the effect of magnetostatic interaction on the SFD [38, 39]. Recently, magnetically hard patterned islands coupled to a continuous film (capped bit-patterned media which called CBPM) have also been investigated based on micromagnetic simulations [42-44]. In this thesis, we have proposed heterogeneous CBPM - wherein the capping layer is made of another material such as a soft layer - to minimize SFD. We show that a reduction in H_c and SFD can be achieved by using same material for capping layer by carrying out experimental and micromagnetic simulation studies on bit patterned structures.

For experimental demonstration, we deposited Co/Pd multilayers with the following structure: Ta(5nm)/Pd(3nm)/$[Co(0.3nm)/Pd(0.8nm)]_n$ (where n=5,10,15 and 25 repeats) using dc magnetron sputtering on Si substrates with a thermally oxidized SiO_2 surface [29-45]. The patterned dots with 50 nm pitch and 25 nm diameter were achieved using high resolution electron beam lithography (section 2.3).

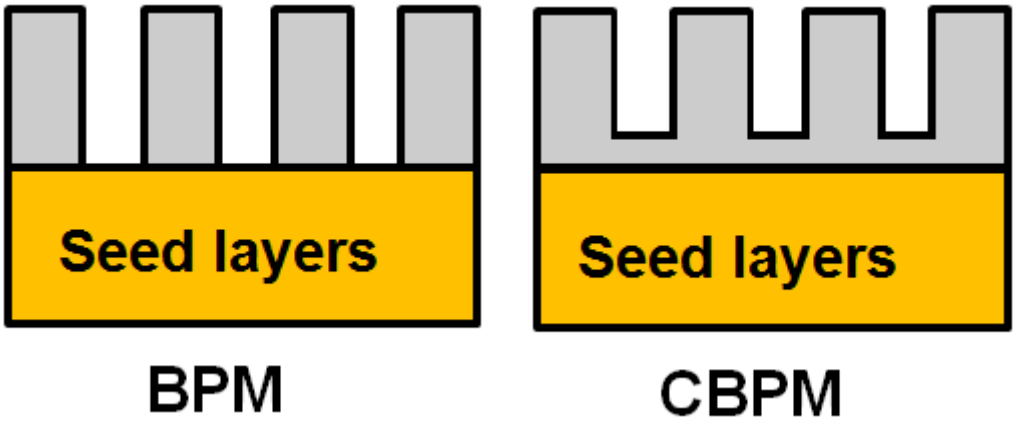

Figure 6.5. The schematic of BPM (left hand side) and CBPM (right hand side).

In order to achieve conventional BPM samples, Co/Pd multilayers with n=5 and 10 layers were completely ion-milled to form discrete magnetic islands. To prepare CBPM sample, ion-milling was carried out partially on Co/Pd multilayers with n=15 and 25 and the ion-milling time (2 minutes) was maintained the same for all samples. The schematic of BPM and CBPM is shown in figure 6.5.

AHE measurements were used to obtain information on the magnetization switching mechanism through measurements with different angles for the applied magnetic field. For this measurement, the Hall bar is necessary to fabricate. The methods of Hall bar fabrication, analysing the Hall voltage and extracting the in-plane and out of plane magnetization signal have been discussed in section (2.6.2).

6.4 Anomalous Hall voltage (AHV)

Figure 6.6a shows a scanning electron microscopy image of a fabricated patterned device ready for AHE measurements. The schematic diagram (as inset in figure 6.6b) shows the relative angles between the external magnetic field H, magnetization M, and the current I.

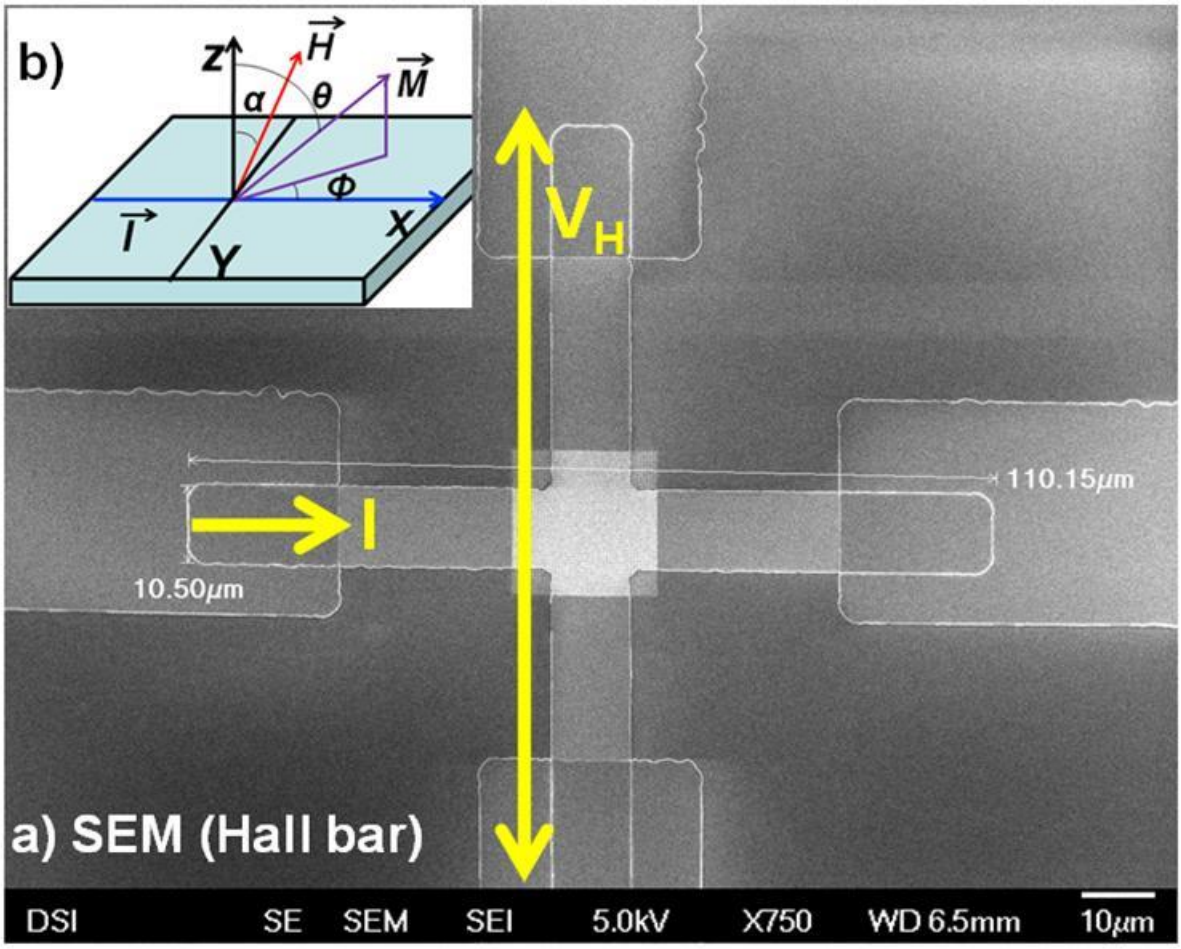

Figure 6.6. a) SEM image from Hall bar, b) schematic diagram showing the relative angles between the external magnetic field H, Magnetization M and the current I are shown as inset files.

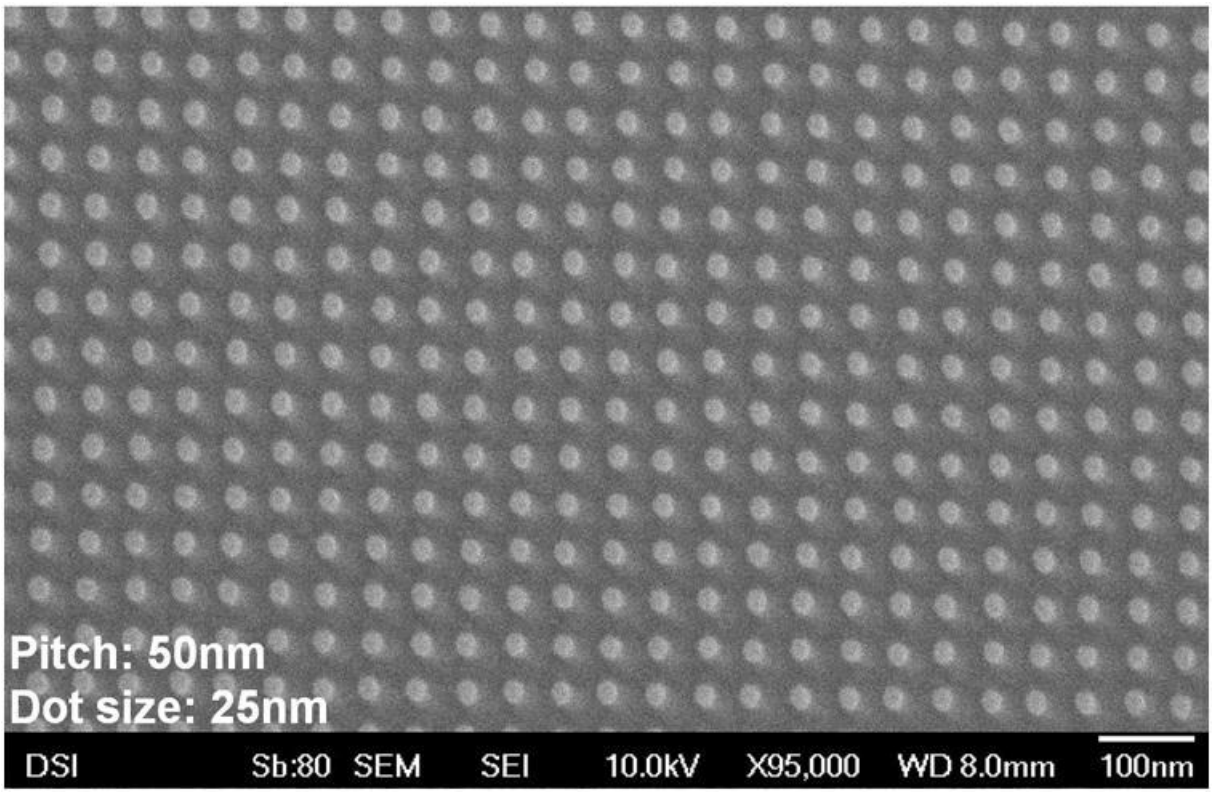

Figure 6.7. SEM image of BPM with 25 nm , 50 nm dot size and pitch size, respectively.

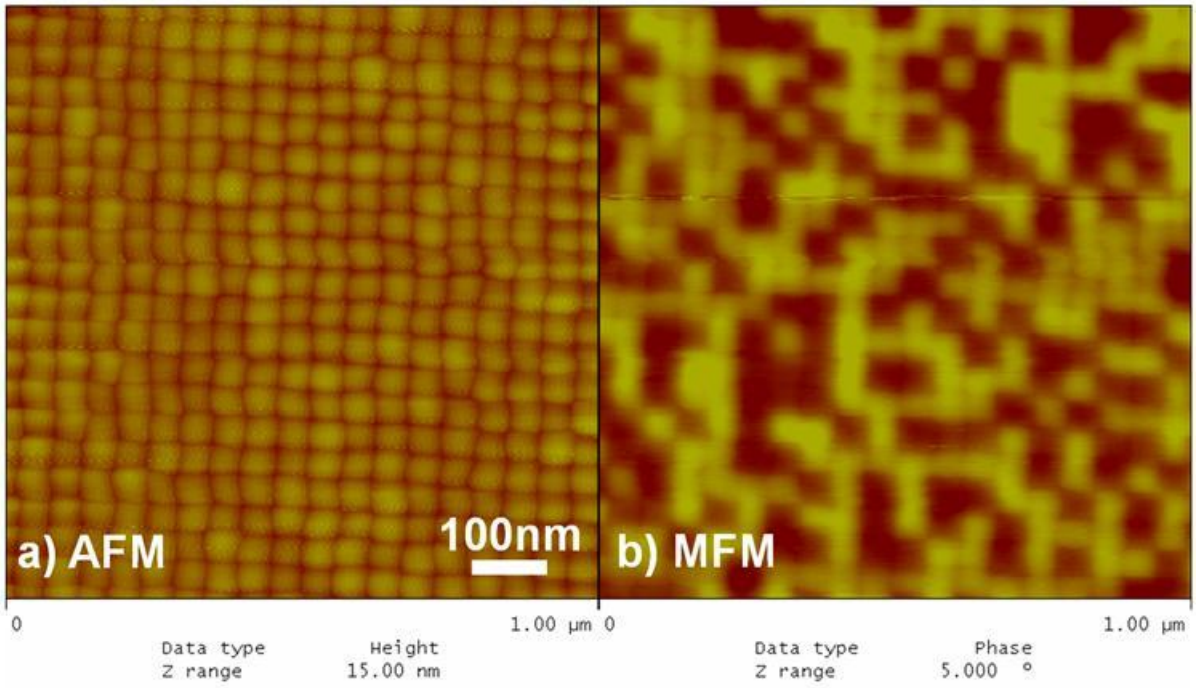

Figure 6.8.a) Atomic force microscopy (AFM), b) Magnetic force microscopy (MFM) image of BPM with 50 nm pitch size at ACD.

The SEM image of the patterned structure is shown in figure 6.7. Figure 6.8 shows that the MFM images of BPM2 after AC demagnetization state. Figure 6.9 shows the anomalous Hall voltage (AHV) loops of the conventional patterned samples and Capped bit patterned media. The legend abbreviations inside figure 6.9 are explained as follow. BPM1 and BPM2 represent fully etched patterned Co/Pd multilayers with 5 and 10 repeats, respectively. Based on ion milling etch rates for different materials, we calculated the thickness of capping layer. For CBPM1 which is corresponding to partially etched $(Co/Pd)_{15}$ mulilayers, the thickness of patterned dots is 14.1 nm and thickness of capping layer is 2.4 nm. The thickness of patterned dots is 14.1 nm and thickness of capping layer is 13.4 nm for CBPM2 which was obtained from $(Co/Pd)_{25}$ multilayers.

The coercivity values of all the patterned samples were found to be larger than that observed in unpatterned films [40, 41, 46, 47]. The conventional BPM samples (with completely decoupled magnetic bits) exhibit a higher coercivity than CBPM samples (with coupled magnetic bits). Among the two conventional BPM samples, the one with a larger number of magnetic bilayers has a higher coercivity. Among the two CBPM samples, the one with the thinnest capping layer (CBPM1) has a higher coercivity. Although the total magnetic layer thickness is larger in CBPM samples, they have a lower coercivity than the conventional BPM sample with 10 bilayers.

It can be seen that, the coercivity of patterned Co/Pd multilayers with 5 and 10 repeats were increased from 750 Oe, and 800 Oe (thin film) to 4.5 kOe and 11 kOe, respectively. The enhancement in coercivity of fully etched patterned dots is well explained earlier. In the case of unpatterned samples, the reversal is by nucleation and domain wall motion. Whereas, the switching mechanism in patterned dots is based on coherent rotation and the applied filed to reverse the magnetization of single domain island should overcome to magnetic anisotropy energy. Despite, it was observed that the coercivity of CBPM 1 and CBPM2 media are

increased to 3.8 kOe and 2 kOe, respectively. The small enhancement in coercivity is related to the contribution from the thin film which is coupled to the patterned islands. Therefore, the mechanism of magnetization reversal is not based on Stoner–Wohlfarth model. The M-H loop is almost square with sharper switching for CBPM1 and CBPM2.

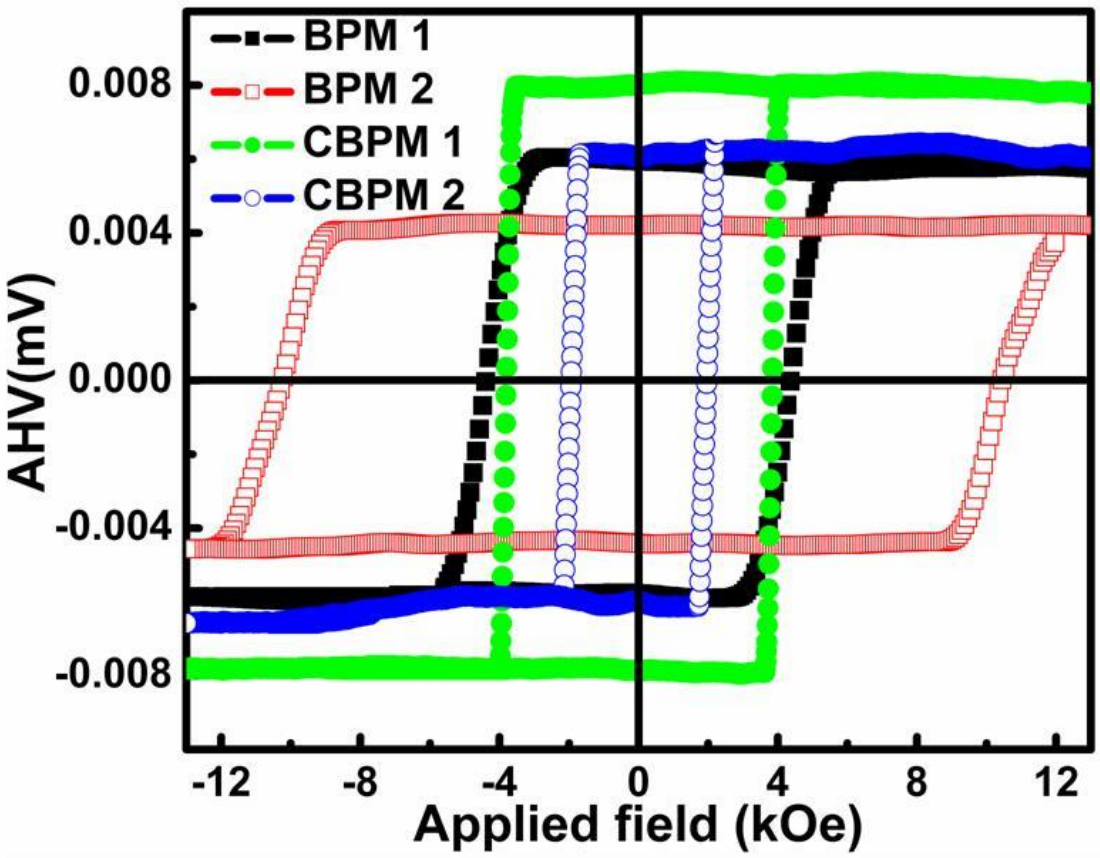

Figure 6.9. Anomalous Hall Voltage (AHV) of (Co/Pd) conventional bit-patterned media with 5 and 10 bilayers and capped bit-patterned media with 15 and 25 bi-layers.

Figure 6.10 shows the MFM images of bit patterned media with a) $(Co/Pd)_5$ as BPM1, b) $(Co/Pd)_{10}$ as multi layers BPM2, c) capped bit patterned media with 2.4 nm as CBPM1 and d)13.4 nm thickness of capping layer (CBPM2) at remanence. The brown (darker) dots indicate the magnetic regions that have reversed and the yellow (brighter) dots indicate the regions that were not reversed. In conventional BPM samples (BPM2), the dots were found to switch independent of each other, indicating the absence of exchange coupling. Just the

opposite, in sample with too thick layer of continuous film (CBPM2), magnetic clusters were observed - indicating the effect of the exchange interaction introduced by the continuous layer. These results also indicate that the exchange interaction must be optimized with a suitable thickness of capping layer in order achieve a reduced SFD and independent switching of dots.

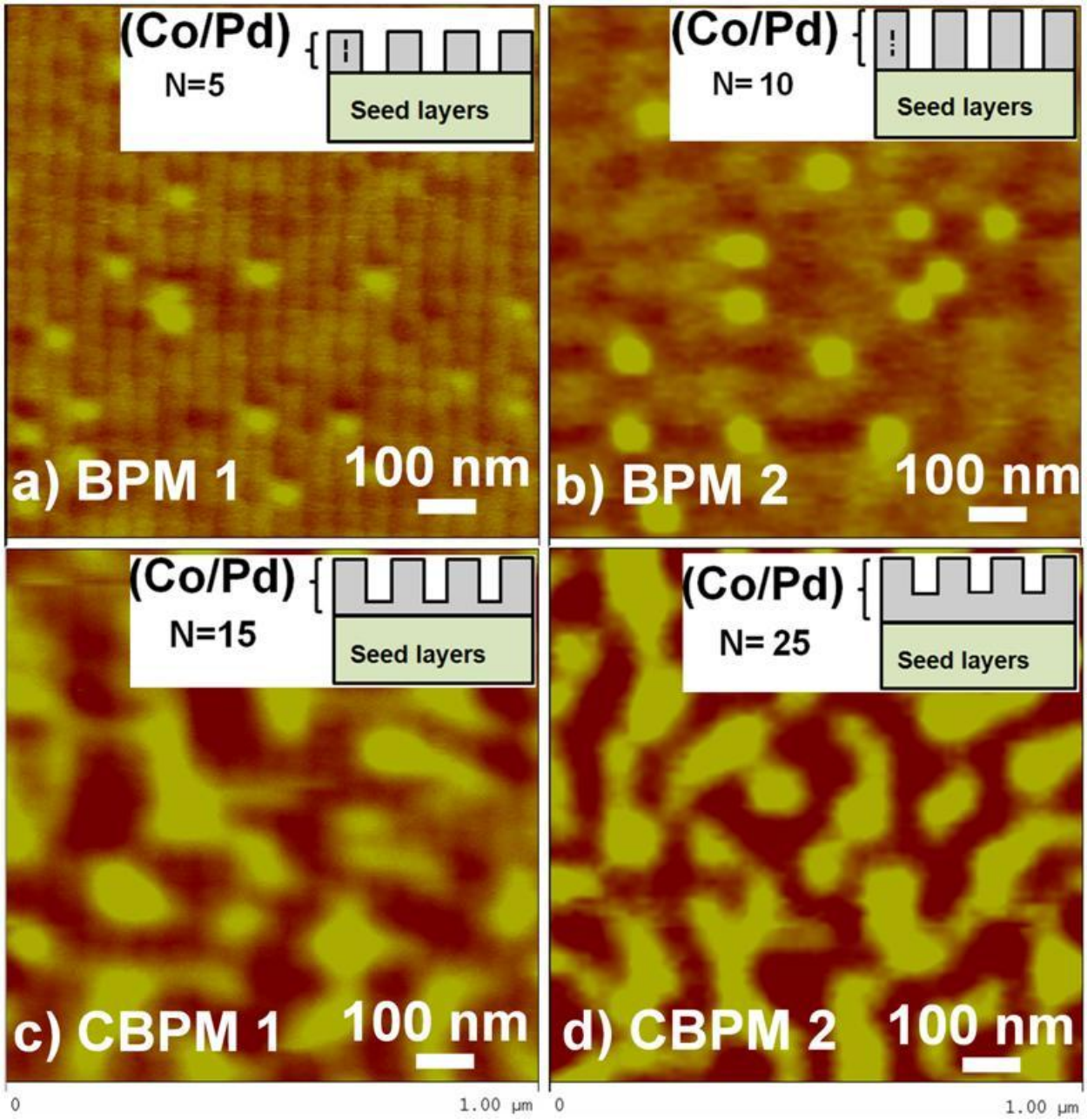

Figure 6.10. Magnetic Force Microscopy (MFM) images of (a) BPM1 with n=5 bilyers, (b) BPM2 with n=10 bilyers, c) CBPM1 with n=15 bilayers and 2.4 nm thick of capping layer and d)CBPM2 with n=25 bilayers and 13.4 nm thick of capping layer.

6.5 Switching field distributions of BPM vs CBPM

In order to understand and minimize the SFD of patterned structures, a derivation has been taken from out of plane hysteresis loops. Moreover, systematic micromagnetic simulations were carried out to compare the simulated and experimental SFDs for BPM and CBPM.

We carried out micromagnetic simulations using commercial software - Advanced Recording Model (ARM) - on different configurations; Co/Pd BPM with 10 bilayers, unpatterned film with a thickness of 2.4 nm (representing the capping layer of CBPM1), CBPM which combines the continuous film (with thicknesses of 6 nm, 10 nm and 13.4 nm) and the BPM dots with 10 bilayers. BPM was simulated based on dots with a diameter of 25 nm and a pitch of 50 nm. Easy axis dispersion, saturation magnetization M_S and exchange constant A were fixed at 4 degrees, 330 emu/cm^3(typical values based on experimental data) and 6×10^{-7} erg/cm, respectively.

In the first step, we made 120 runs to obtain the best fitting between the experimental and simulation results. To simulate CBPM, we used highly exchange coupled continuous thin film as a capping layer. Therefore, after finding the best fitting, we carried out 5 more simulation runs to test the repeatability of results. The standard deviation of normalized SFD and H_c were calculated as shown in table 6.1.

Table 6. 1. Summarized simulation results for CBPM with different thickness of capped layer.

Capping layer thickness (nm)	Hc_1 (Oe)	SFD_1	Hc_2 (Oe)	SFD_2	Hc_3 (Oe)	SFD_3	Hc_4 (Oe)	SFD_4	Hc_5 (Oe)	SFD_5	$Hc\pm\sigma_{Hc}$ (Oe)	$SFD\pm\sigma_{SFD}$
2.4	3836	0.115	3821	0.114	3840	0.116	3821	0.114	3868	0.117	3837±29	0.115±0.002
6	3558	0.111	3580	0.112	3558	0.111	3565	0.112	3558	0.111	3563±16	0.111±0.001
10	2542	0.101	2582	0.103	2578	0.102	2584	0.104	2578	0.102	2573±11	0.102±0.002
13.4	1984	0.094	1943	0.093	1963	0.098	1890	0.073	2033	0.088	1963±70	0.089±0.008

For CBPM with 2.4 nm thick capping layer, the experimental values of normalized SFD and Hc were 0.115 and 3800 Oe respectively. Although for thick 13.4 nm capping layer the normalized SFD is smaller than that of capping layer with 2.4 nm thick, the coercivity of CBPM with 13.4 nm capped layer is closer to the coercivity of thin film – indicating a collective reversal, which is not desired from readback signal perspective.

Figure 6.11a shows the hysteresis loops (normalized magnetization: M) obtained from the micromagnetic simulations for the three configurations. The simulation results closely mirror the experimental measurements. Figure 6.11b shows the SFD from simulations and experiments for the BPM and CBPM samples obtained from the derivative of the hysteresis loops. The BPM sample with 10 bilayers shows the largest SFD in both simulation and experimental measurements. On the other hand, the CBPM sample shows a reduction in H_c as well as SFD. The reduction in SFD and H_c were understood to be arising from the introduction of an optimum exchange coupling field originating from the capping layer to compensate the magnetostatic field between the magnetic dots as shown in figure 6.12 [42-44]. It can be mentioned that in the case of CBPM, there is a lateral exchange coupling energy in capped layer and conversely dipolar interactions between patterned dots. Therefore, this lateral exchange coupling can reduce the dipolar field, and SFD will be reduced.

These results are similar to the current granular perpendicular media with capped magnetic layers or the CGC media, where the continuous layers provide an exchange coupling between the grains which results in a reduction of SFD [48, 49]. It must be mentioned here that we are using the same materials for the capping layer with the same magnetization, unlike other reports which propose the use of a soft magnetic material [43, 44]. It has to be emphasized that the thickness and saturation magnetization of the capping layer need to be chosen for an optimized exchange coupling in order to obtain the narrowest SFD without increasing the

noise. In fact, CBPM2 sample with 25 bilayers (which had 13.4 nm continuous bilayers and hence a significantly larger exchange coupled) showed a very low coercivity of 2 kOe and the formation of clusters indicating the need for an optimized exchange coupling.

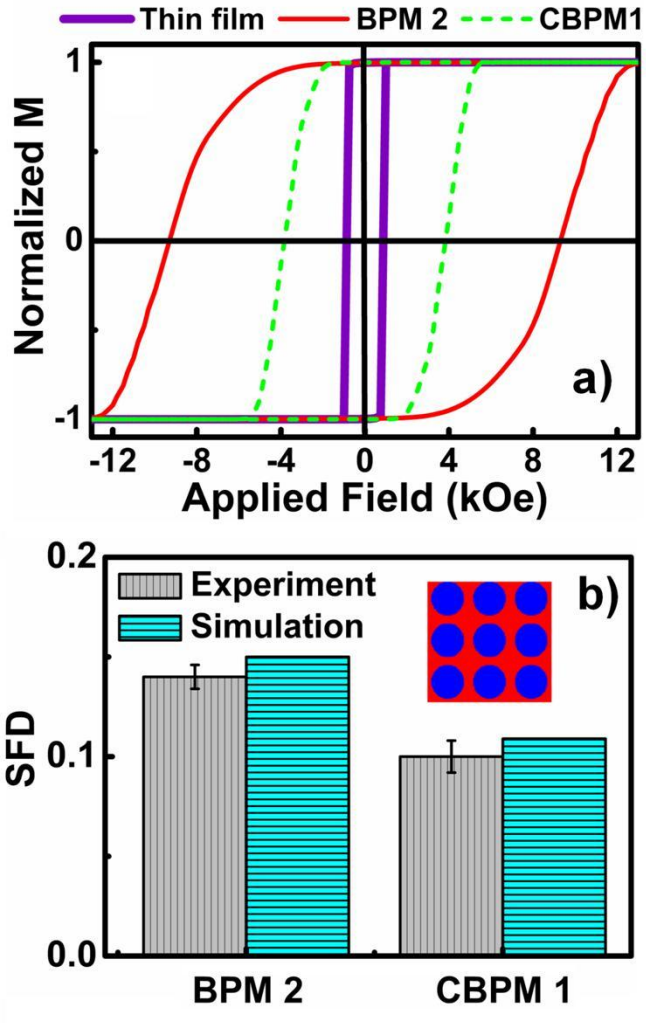

Figure 6.11. a) Simulated hysteresis loops of structures that represent BPM2, thin continuous film that represent the capping film and CBPM1, and b) simulated and experimental values of SFD of BPM2 and CBPM1.

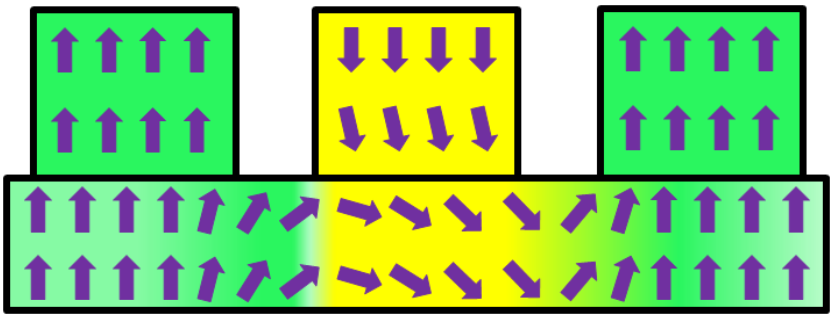

Figure 6.12. An illustration for compensation of dipolar interactions with lateral exchange coupling field in capped layer.

It mentioned earlier, the objective in this chapter is to tune the exchange coupling field simply by changing the thickness of the continuous layer with the same magnetization like in coupled granular/continuous (CGC) media. However, the difference between CGC media and our design is that the two layers in our media are of the same material. In addition, no exchange break layer is proposed in this scheme, but, an exchange break layer in continuous layer is another possible approach to fine tune the exchange coupling and to minimize the SFD. The exchange coupling is tuned by controlling the thickness of the layer itself. Optimizing the exchange coupling using other materials is also can be done for future work.

6.6 Planar Hall voltage (PHV)

As the films are made of Co/Pd multilayers, the continuous layer has a perpendicular anisotropy. In order to confirm the magnetization direction of capping layer, and Hall-voltage measurement can also provide information about the magnetization direction of capping layer, we extracted the in-plane loop from the planar Hall Voltage (PHV) as discussed in section (2.6.2) [50-51]. PHV loops for BPM1, BPM2, CBPM1 and CBPM2 are shown in figure 6.13.

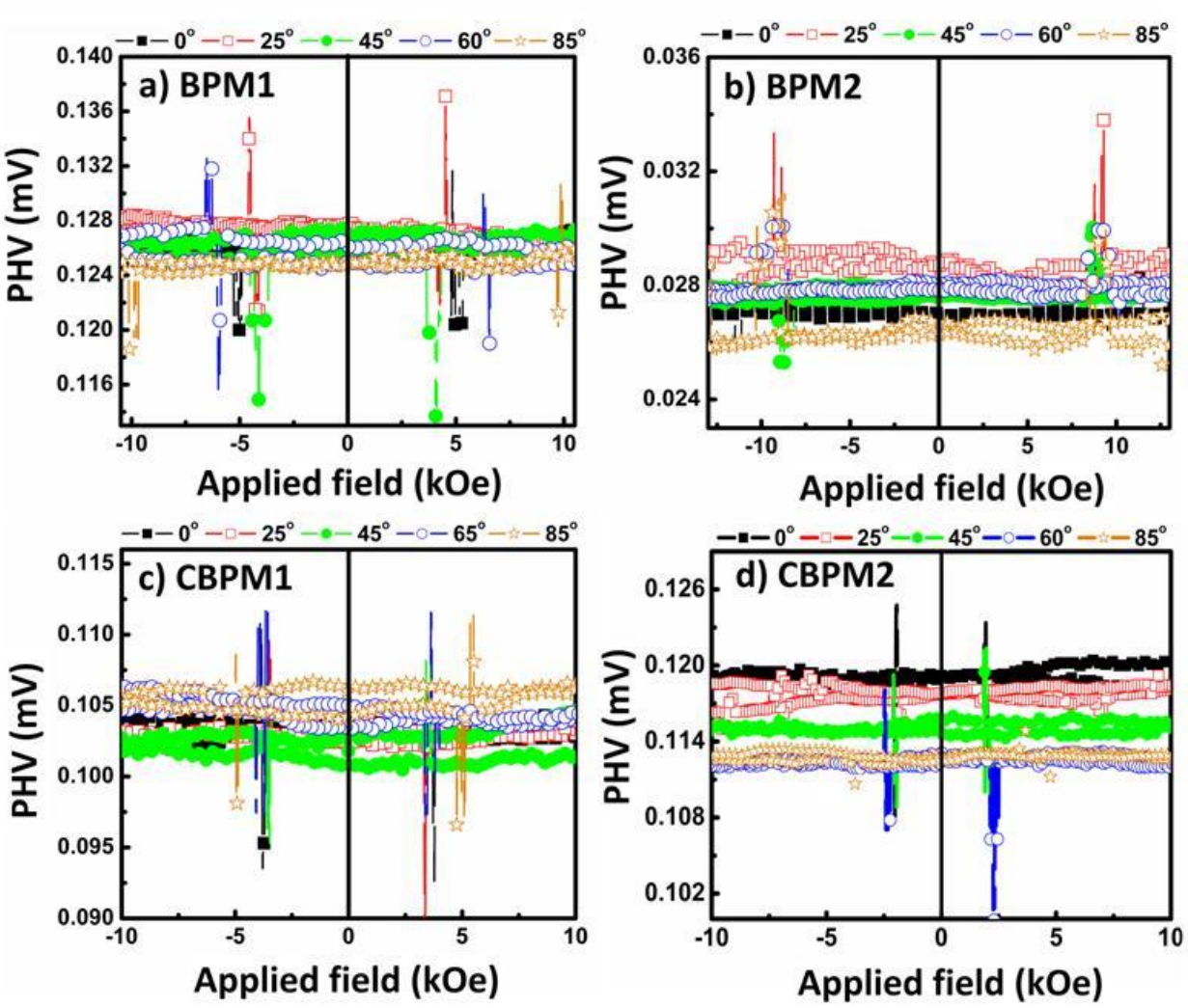

Figure 6.13. Planar Hall Voltage (PHV) loops for BPM and CBPM samples.

Each curve was measured for different angle α between the film-normal and applied magnetic field. It can be noticed from the PHV loops that there is no in-plane magnetization direction on capping layer for CBPM1 and CBPM2. The PHV results further confirm that the magnetization in the patterned and continuous region were aligned in perpendicular direction.

6.7 Thermal stability factor and the anisotropy field for BPM and CBPM

Although reduction of switching field and its distribution were achieved using our new scheme, there is still a need to evaluate thermal stability factor which has to be kept higher than 60. For this purpose, we measured the thermal stability factor and the anisotropy field from dynamic coercivity measurements. For this purpose, AHE was measured at different time-scales and a fit of the coercivity to the time-scale was made using Sharrock's equation [52]:

$$H_c = H_o[1-\frac{1}{\beta}\ln(\frac{f_o t}{\ln 2})]^{1/n} \qquad (6.1)$$

Where t is the hold time, $\beta(=K_uV/k_BT)$ is the thermal stability factor, the value of attempt frequency (f_o) is around 10^{11}-10^{12}Hz, and exponent n values to 3/2 are preferred for perpendicular recording media [53].

Figure 6.14 shows the stability factor (β) and anisotropy field ($H_o=H_k$) obtained from the fitting. It can be noticed that the value of H_k is 7 kOe, 12 kOe and 5.5 kOe and the estimated β is 82, 160 and 109 for patterned [$(Co/Pd)_5$], [$(Co/Pd)_{10}$) multilayer and CBPM1, respectively. As the thickness and the diameter of the dots are known, an estimate of K_u can be made from the values of β. However, fitting of Sharrock's equation involves two unknown parameters, f_o and n and the value of β is very sensitive to the value of n chosen and hence the K_u was found to be below 2×10^6 erg/cc for n=11, far below the values expected for Co/Pd multilayers.

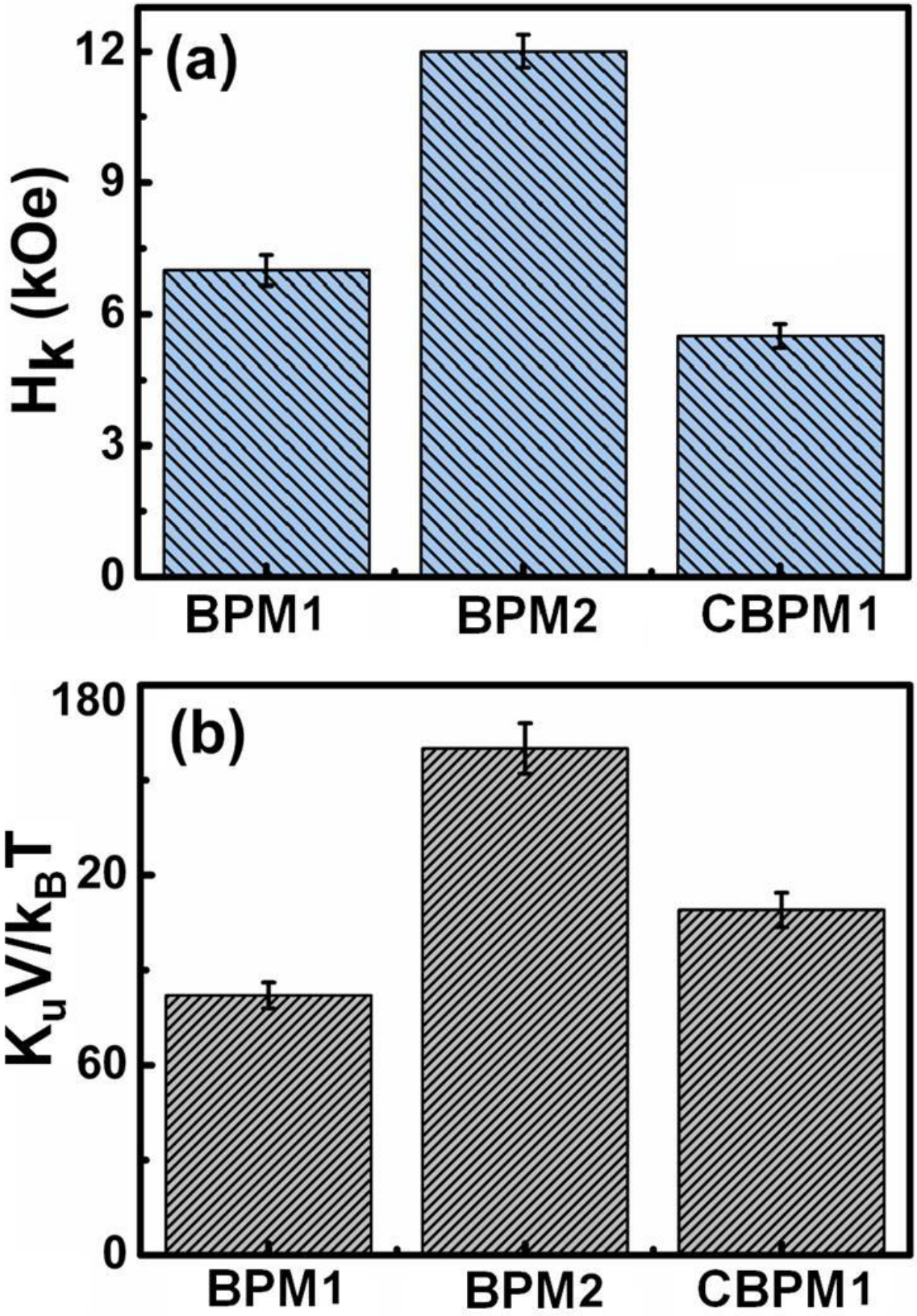

Figure 6.14.a) Anisotropy filed H_k, and b) stability factor ($\beta=K_uV/k_BT$) of conventional bit-patterned media (BPM1 and BPM2) and CBPM1.

Contrarily, the value of K_u can also be measured from the H_o values from the fitting, as H_o changes only a little with f_o or n. The values of K_u calculated from H_o using the formula, $K_u = M_s.H_o/2$, where M_s is saturation magnetization, were about 2×10^6 erg/cc for 5 bilayers and 3.8×10^6 erg/cc for 10 bilayers, within the reasonable values for Co/Pd multilayers. From these results, it can be understood that the increase of coercivity in media with 10 bilayers is due to an increase of K_u although the origins of this increase of K_u is not understood.

Summary

As a summary, conventional bit-patterned media as well as capped BPM were investigated experimentally using anomalous Hall effect measurements. The exchange coupling, provided by the thin continuous layer, was effective in reducing the switching field distribution and coercivity under optimized conditions. SFD increases and coercivity decreases for very high values of exchange coupling due to the formation of multi-domains. Besides reducing SFD, the CBPM also exhibit potential writability advantage at higher densities, indicating their potential application as bit-patterned media.

References

1. P. F. Carcia, A. D. Meinhaldt, and A. Suna, Appl. Phys. Lett.**47**, 178 (1985).
2. J. Moritz, B. Dieny, J. P. Nozières, R. J. M. van de Veerdonk, T. M.Crawford, D. Weller, and S. Landis, Appl. Phys. Lett. **86**, 063512 (2005).
3. T. Thomson, G. Hu, and B. D. Terris, Phys. Rev. Lett.**96**, 257204 (2006).
4. O. Hellwig, A. Berger, T. Thomson, E. Dobisz, Z. Z. Bandic, H. Yang, andD. S. Kercher, Appl. Phys. Lett. **90**, 162516 (2007).

5. J. M. Shaw, W. H. Rippard, S. E. Russek, T. Reith, and C. M. Falco, J.Appl. Phys. **101**, 023909 (2007).

6. C. E, V. Parekh, P. Ruchhoeft, S. Khizroev, and D. Litvinov, J. Appl. Phys.**103**, 063904 (2008).

7. D. Smith, V. Parekh, E. Chunsheng, S. Zhang, W. Donner, T. R. Lee, S.Khizroev, and D. Litvinov, J. Appl. Phys. **103**, 023920 (2008).

8. R. Sbiaa, K. O. Aung, S. N. Piramanayagam, E.-L.Tan, and R. Law, J.Appl. Phys. **105**, 073904 (2009).

9. F. Garcia, F. Fettar, S. Auffret, B. Rodmacq, and B. Dieny, J. Appl. Phys.**93**, 8397 (2003).

10. S. Mangin, D. Ravelosona, J. A. Katine, M. J. Carey, B. D. Terris, and E.E. Fullerton, Nat. Mater. **5**, 210 (2006).

11. R. Law, R. Sbiaa, T. Liew, and T. C. Chong, Appl. Phys. Lett. **91**, 242504 (2007).

12. J.-H. Park, C. Park, T. Jeong, M. T. Moneck, N. T. Nufer, and J.-G.Zhu,J. Appl. Phys. **103**, 07A917 (2008).

13. N. Thiyagarajah and S. Bae, J. Appl. Phys. **104**, 113906 (2008).

14. R. Law, E.-L. Tan, R. Sbiaa, T. Liew, and T. C. Chong, Appl. Phys. Lett.**94**, 062516 (2009).

15. X. T. G. Pokhil, J. Appl. Phys. **81**, 5035 (1997).

16. X. M. Cheng, V. I. Nikitenko, A. J. Shapiro, R. D. Shull, and C. L. Chien,J. Appl. Phys. **99**, 08C905 (2006).

17. G. N. Phillips, K. O'Grady, Q. Meng, and J. C. Lodder, IEEE Trans.Magn. **32**, 4070 (1996).

18. O. Hellwig, S. Maat, J. B. Kortright, and E. E. Fullerton, Phys. Rev. B **65**,144418 (2002).

19. M. Kisielewski, A. Maziewski, M. Tekielak, J. Ferré, S. Lemerle, V. Mathet,and C. Chappert, J. Magn. Magn.Mater.**260**, 231 (2003).

20. J. E. Davies, O. Hellwig, E. E. Fullerton, G. Denbeaux, J. B. Kortright,and K. Liu, Phys. Rev. B **70**, 224434 (2004).

21. J. W. Knepper and F. Y. Yang, Phys. Rev. B **71**, 224403 (2005).

22. R. Sbiaa, C. Z. Hua, S. N. Piramanayagam, R. Law, K. O. Aung, and N.Thiyagarajah, J. Appl. Phys. **106**, 023906 (2009).

23. C. M. Günther, F. Radu, A. Menzel, S. Eisebitt, W. F. Schlotter, R. Rick,J. Lüning, and O. Hellwig, Appl. Phys. Lett. **93**, 072505 (2008).

24. R. Sbiaa, E. L. Tan, K. O. Aung, S. K. Wong, K. Srinivasan, and S. N.Piramanayagam, IEEE Trans. Magn. **45**, 828 (2009).

25. C. Kittel, Phys. Rev. **70**, 965 (1946).

26. K. Janicka, J. D. Burton, and E. Y. Tsymbal, J. Appl. Phys. **101**, 113921 (2007).

27. B. Kaplan and G. A. Gehring, J. Magn.Magn.Mater.**128**, 111 (1993).

28. R. Sbiaa, Z. Bilin, M. Ranjbar, H. K. Tan, S. J. Wong, S. N. Piramanayagam, and T. C. Chong, J. Appl. Phys. **107**, 103901 (2010).

29. S. N. Piramanayagam, J. Appl. Phys. **102**, 011301 (2007).

30. D. Weller, L. Folks, M. Best, E. E. Fullerton, B. D. Terris, G. J. Kusinski, K. M. Krishnan, and G. Thomas, J. Appl. Phys. **89**, 7525 (2001).

31. J.U. Thiele, S. Maat, and E. E. Fullerton, Appl. Phys. Lett. **82**, 2859 (2003).

32. B. D. Terris, M. Albrecht, G. Hu, T. Thomson, and C. T. Rettner, IEEE Trans. Magn. **41**, 2822 (2005).

33. J. M. Shaw, W. H. Rippard, S. E. Russek, T. Reith, and C. M. Falco, J. Appl. Phy. **101**, 023909 (2007).

34. R. L. White and R. F. W. Pease, IEEE Trans. Magn. **33**, 990 (1997).

35. O. Hellwig, J. K. Bosworth, E. Dobisz, D. Kercher, T. Hauet, G. Zeltzer, J. D. Risner-Jamtgaard, D. Yaney, and R. Ruiz, Appl. Phys. Lett. **96**, 052511 (2010).

36. P. W. Nutter, I. T. Ntokas, B. K. Middleton, and D. T. Wilton, IEEE Trans.Magn.**41**, 3214 (2005).

37. A. Moser, O. Hellwig, D. Kercher, and E. Dobisz, Appl. Phys. Lett. **91**, 162502 (2007).

38. S. N. Piramanayagam, K. O. Aung, S. Deng, and R. Sbiaa, J. Appl. Phys. **105**, 07C118 (2009).

39. M. Ranjbar, S. N. Piramanayagam, D. Suzi, K. O. Aung, R. Sbiaa, Y. S. Key, S. K. Wong, and T. C. Chong, IEEE Trans. Magn, **46**, 1787 (2010).

40. T. Thomson, G. Hu, and B. D. Terris, Phys. Rev. Lett.**96**, 257204 (2006).

41. R. Sbiaa, K. O. Aung, S. N. Piramanayagam, E. L. Tan, and R. Law, J. Appl. Phys. **105**, 073904 (2009).

42. S. Li, B. Livshitz, N. H. Bertram, A. Inomata, E. E. Fullerton, and V. Lomakin, J. Appl. Phys., **105**, 07C121 (2009).

43. M. V. Lubarda, S. Li, B. Livshitz, E. E. Fullerton, and V. Lomakin, IEEE Trans. Magn., **47**, 18 (2011).

44. M. V. Lubarda, S. Li, B. Livshitz, E. E. Fullerton, and V. Lomakin, Appl. Phys. Lett**. 98**, 012513 (2011).

45. S. N. Piramanayagam, H. B. Zhao, J. Z. Shi, and C. S. Mah, Appl. Phys. Lett. **88**, 092506 (2006).

46. J. W. Lau, R. D. McMichael, S. H. Chung, J. O. Rantschler, V. Parekh, and D. Litvinov, Appl. Phys. Lett., **92**, 012506 (2008).

47. B. D. Terris and T. Thomson, J. Phys. D: Appl. Phy. **38**, R199 (2005).

48. Y. Sonobe, D. Weller, Y. Ikeda, M. Schabes, K. Takano, G. Zeltzer, B.K. Yen, M.E. Best, S.J. Greaves,

49. B.R. Acharya, M. Zheng, G. Choe, M. Yu, P. Gill and E.N. Abarra, IEEE Trans. Magn. **41**, 3145 (2005).

50. S. Das, S. Kong, and S. Nakagawa, J. Appl. Phys. **93**, 6772 (2003).

51. S. K. Wong, K. Srinivasan, R. Sbiaa, R. Law, E. L. Tan, and S. N. Piramanayagam, IEEE Trans. Magn. **46**, 2409 (2010).

52. M. P. Sharrock, J. Appl. Phys. **76**, 6413 (1994).

53. S.N. Piramanayagam, and K.Srinivasan, J. Magn. Magn.Mater, **321**, 485 (2009).

Chapter 7. Conclusions

7.1 Summary of this thesis

The primary aim of this dissertation is to understand and reduce the switching field distributions (SFDs) of patterned perpendicular magnetic islands from a data storage perspective. For this purpose, Antiferromagnetically coupled (AFC) patterned media and capped bit patterned media (CBPM) were investigated as two novel pathways to reduce the dipolar interactions and to minimize the SFDs. Our approaches to investigate the SFD of patterned media were based on experimental methods, systematic modeling and simulations.

In this thesis, several methods have been used to fabricate patterned islands. The patterned islands were fabricated by Electron beam lithography (EBL) and Nano imprint lithography (NIL) methods. In order to characterize the switching mechanism of magnetic dots, we employed the Magnetic force microscopy (MFM) method, Alternating gradient magnetometer (AGM), and Anomalous Hall Effect (AHE) measurements.

The deposition of thin films, fabrication of patterned islands and characterization methods were described in chapter 2. MFM was utilized for investigating the domain pattern of an island for measuring the switching field distribution of patterned dots. On the other hand AGM was used to measure the full M-H loops of patterned media fabricated by NIL. In addition the full hysteresis loops of capped bit patterned media over a small area were measured using AHE. We have proposed that MFM using tips with perpendicular magnetic anisotropy is a suitable technique to improve the resolution.

In chapters 3, 4 and 5 we have described our investigations to reduce the SFD based on AFC patterned media. The main criteria to achieve AFC patterned media is the coercivity of stabilizing layer should be smaller than exchange coupling field after patterning. Hence, at

this condition the anti-parallel state can be achieved at remanent state. Since the dipolar interaction is proportional to net magnetization remanent moment, the dipolar interaction can be reduced by achieving the anti-parallel state. Therefore, AFC patterned media can help to minimize the SFDs.

In chapter 3, we tried to understand quantitatively the effect of dipolar interactions on SFDs of conventional and staggered patterned configurations based on systematic modeling, simulations and experimental methods. Although the staggered BPM have several advantages and it can help to increase the width of the reader and writer head in actual recording, it was observed that the SFD of staggered patterned media is larger than the conventional patterned island. The reason for having wider SFD in staggered patterned media was larger dipolar interaction. Therefore, AFC patterned media is proposed to reduce the dipolar interaction and minimize the SFD.

In chapter 4, the effect of coercivity of stabilizing layer in AFC patterned media is studied to achieve the anti-parallel state at remanent state. The anti-parallel stat at remanent state can reduce the net magnetization moment and the SFD can be minimized. For this purpose, in the first part of this chapter $CoCrSiO_2$ thin film layers as a stabilizing layer with different granularity were sputtered on top of the recording layer and 0.8 nm thick Ru layer. The patterned islands were fabricated using EBL and the SFD curves were measured by counting the reversal magnetic dot with using MFM images. We have expected that the AFC patterned media with stabilizing layer which is sputtered at higher pressure have lower SFD because of inducing superparamagnetic domains. Therefore the coercivity of stabilizing layer could be smaller than the exchange coupling field after pattering. However, the result was in contrast with our prediction. The smaller SFD curves observed for the AFC structures with stabilizing layer when it was sputtered at lower pressure. We realized that the difference could be due to the use of CoCrPt:Oxide layers for patterned media. Therefore in the final part of this chapter

other types of AFC patterned media were fabricated with low and high magnetic anisotropy constants for stabilizing layers. Moreover, Co/Pd multilayers or CoPt films without oxygen were used as the main recording layer. It was observed that the AFC patterned media with lower anisotropy constant can provide the criteria for AFC patterned media to reduce the SFD. However in order to further understand the effect of these samples; it would be nice to take full M-H loops of AFC samples for future studies. In addition, several configurations for AFC structures can be studied for more analysis. Such as keep increasing thickness of the recording layer and stabilizing layer with the same ratio to achieve the same remanent moment.

In chapter 5, the new kinds of AFC structures with low and high exchange coupling fields and their influences were described on SFD of patterned nanostructures. Spin reorientation transition from in plane to out of plane direction with employing AFC concept could help to induce different kinds of AFC structures.

In the first part of this chapter, the Co/Pd multilayers with 10 repeats were fabricated and antiferromagnetically coupled with $(Co_t/Pd)_3$ as AFC samples with low exchange coupling field. The thickness of Co layer was changed from 0.4 nm to 1.2 nm. The patterned nanostructures were fabricated by nano imprint lithography over a large area. Full M-H loops of those nanostructures were measured with AGM and AFC configuration in magnetic nanotsrutures were observed when the Co thickness was 1 nm. Another interesting result was the observation of perpendicular magnetic anisotropy for Co/Pd multilayers when the Co sublayers thickness was 1 nm.

In the next part of this chapter, a new type AFC structures with high exchange coupling fields was sputtered at room temperature. The $(Co/Pd)_{\times 15}$ multi layers were coupled with thin

Co layer and the thickness of Co was varied from 0.6 nm to 2.4 nm. The exchange field was reduced from 15 kOe to 8.5 kOe for 0.75 nm and 1.2 nm, respectively.

The origin of exchange field was categorized in three regions. In the first region when the Co layer thickness was between 0.75 nm to 0.9 nm, interface magnetic anisotropy between the Co layer and Co/Pd multilayers was the main reason to induce the high exchange coupling fields. In the second region when the Co layer thickness was between 0.9 nm to 1.2 nm, the AFC was induced by spin reorientation from in plane to out of plane. However in the third region after 1.2 nm thick Co layer, the spin reorientation was not observed. At this range of Co thickness the bulk anisotropy overcomes the interface anisotropy.

In addition the SFD of magnetic nanostructures for those samples was studied in this chapter. The smallest SFD was observed for the AFC pattern structures with high exchange coupling filed close to 15 kOe. These observations are significant for patterned media and spintronics devices.

Finally in chapter 6, Capped bit patterned media was investigated based on simulation and experimental results to reduce the SFD of patterned dots. The full hysteresis loops of capped bit patterned media were studied with anomalous Hall Effect measurements. It was observed that the SFD can be reduced when the hard patterned magnetic island coupled with a thin film layer. The thin film layer material was the same as patterned islands. It was concluded that optimum exchange field between the thin film and magnetic bits can help to reduce the SFD. The reduction in SFD is explained by compensation of dipolar interaction with exchange coupling field. However, it is necessary to study the effect of different kinds of thin layer such as soft layer and exchange breaking layer on SFD.

7.2 Suggested Future Work

Based on the understanding supported by this dissertation, future work can focus on investigating the magnetic properties of bit patterned media at much higher densities than what we have studied. At higher densities, the role of magnetostatic interaction will be even stronger and hence, the methods we proposed might be more useful in that regime. In addition, most of our studies were based on MFM, and hence we could not carry out the thermal stability investigations. This is one area where further attention can be paid. In addition, a dynamic study on the reversal mechanism of patterned dots and nucleation mapping on different patterned size are worthy investigating. Moreover, the switching field distribution patterned media with pitch size of smaller than 15 nm is still unknown. Given the potential coherent rotation based on S-W model, the smaller pitch and dot diameter might be more subject to the edge damage, which have not been studied to be a clear reason in the widen switching field distribution for this technology.

In spite of recent progress in areal density with current perpendicular magnetic recording, there is still one important question. The question is how far perpendicular magnetic recording technology can augment the areal density. As is mentioned in the first chapter, the superparamagnetic effect is the extreme limitation of current perpendicular magnetic recording technology as the areal density range becomes more than 2 Tbit/in^2. A lot of researchers are working to optimize the parameters for bit patterned media. However, it is necessary to look at also BPM technologies for areal densities more than 10 Tbit/in^2 .This density corresponds to an island dimension of 4 nm and a period of 8 nm in both the down track and cross track directions. For patterned media to become an economically viable alternative, means to fabricate large area patterns of such high density at reasonable costs have to be devised. Nano imprint lithography with a proper master mold and combination of

diblock copolymers with conventional lithography techniques make a promise in this regard. But still a lot needs to be done to reach the goal.